Electronic Supplementary Material (ESI) for New Journal of Chemistry.

Supporting Information for

Alkali Metal Complex–Mediated Ring-opening Polymerization of *rac-LA*, ε-Caprolactone, and δ-Valerolactone

Adimulam Harinath, Jayeeta Bhattcharjee, Alok Sarkar and Tarun K. Panda*

Department of Chemistry, Indian Institute of Technology Hyderabad, Kandi, Sangareddy, 502285, Telangana, India. Fax: + 91(40) 2301 6032; Tel: + 91(40) 2301 6036; E-mail: tpanda@iith.ac.in

Table of Contents

29. Figure FS28: ^{1}H NMR spectra of complex **5b**.
30. Figure FS29: ^{31}P NMR spectra of complex **5b**.
31. Figure FS30: ^{13}C NMR spectra of complex **5b.**
32. Kinetic studies.
33. Characterization of polymers.

Table TS1. Crystallographic data and refinement parameters of **1-H**, **2-H**, **3b**, **4a**, and **4b**.

Crystal Parameters	**1-H**	**2-H**	**3b.THF**	**4a**	**4b**
CCDC No.	1849552	1849551	1849553	1849554	1849555
Empirical formula	$C_{18}H_{15}FNPSe$	$C_{18}H_{15}N_2O_2PSe$	$C_{30}H_{38}LiN_2O_5PSe$	$C_{30}H_{38}FNNaO_3PSe$	$C_{30}H_{38}N_2NaO_5PSe$
Formula weight	374.24	401.25	623.49	612.53	639.54
T (K)	293(2) K	293(2) K	150(2) K	150(2) K	150(2) K
λ (Å)	1.54184 Å	1.54184 Å	1.54184 Å	0.71073 Å	1.54184 Å
Crystal system	Monoclinic	Monoclinic	Monoclinic	Monoclinic	Orthorhombic
Space group	$P\,2_1/c$	$C2/c$	$P\,2_1/c$	$P\,2_1$	P bca
a(Å)	9.9310(5)	27.298(3)	10.3315(9)	9.9424(17)	17.2014(7)
b (Å)	16.1798(5)	9.3728(5)	18.068(2)	15.5693(7)	17.4404(7)
c(Å)	13.6047(7)	16.0877(15)	18.204(2)	10.617(5)	20.4846(17)
α (°)	90	90	90	90	90
β (°)	130.222(3)	122.050(13)	113.795(8)	113.65(4)	90
γ (°)	90	90	90	90	90
V(Å^3)	1669.13(14)	3488.7(5)	3109.3(6)	1505.4(8)	6145.4(4)
Z	4	8	4	2	8
D_{calc} g cm^{-3}	1.489	1.528	1.332	1.351	1.382
μ (mm^{-1})	3.997	3.890	1.298	1.352	2.618
F(000)	752	1616.0	1296	636	2656
Theta range for data collection	5.060 to 70.258 deg	3.82 to 70.76 deg	3.02 to 29.11 deg	3.349 to 28.948 deg	4.21 to 70.57 deg
Limiting indices	-8<=h<=12, -19<=k<=18, -16<=l<=13	-30 ≤ h ≤ 33, -8 ≤ k ≤ 11, -19 ≤ l ≤ 19	--13<=h<=13, -23<=k<=24, -22<=l<=20.	-12<=h<=13, -19<=k<=18, -13<=l<=9	-20 ≤ h ≤ 19, -21 ≤ k ≤ 21, -18 ≤ l ≤ 24
Reflections collected / unique	7494/ 3126 [R(int) = 0.0226]	7342 / 3298 [R(int) = 0.0307]	14754 / 7134 [R(int) = 0.0368]	6394 / 5152 [R(int) = 0.0202]	28196 / 5806 [R(int) = 0.0714]
Completeness to theta	99.8 %	98.1 %	99.8 %	99.7%	98.7 %
Absorption corraction	Multi-scan	Multi-scan	Multi-scan	Multi-scan	Multi-scan

Max. and min. transmission	1.00000 and 0.60794	1.00000 and 0.30530	1.00000 and 0.90361	1.00000 and 0.91034	1.00000 and 0.38059
Refinement method	Full-matrix least-squares on F^2	Full-matrix least-squares on F^2	Full-matrix least-squares on F^2	Full-matrix least-squares on F^2	Full-matrix least-squares on F^2
Data /restraints / parameters	3126 / 0 / 200	3298 / 0 / 217	7134/0/361	5152 / 203 / 436	5806/ 0 / 362
Goodness-of-fit on F^2	1.072	1.023	1.065	1.080	1.062
Final R indices [I>2sigma(I)]	*R*1 = 0.0345, *wR*2 = 0.0949	*R*1 = 0.0385, *wR*2 = 0.0987	*R*1 = 0.0487, *wR*2 = 0.1101	*R*1 = 0.0358, *wR*2 = 0.0878	*R*1 = 0.0672, *wR*2 = 0.1807
R indices (all data)	*R*1 = 0.0365, *wR*2 = 0.0968	*R*1 = 0.0480, *wR*2 = 0.1057	*R*1 = 0.0670, *wR*2 = 0.1202	*R*1 = 0.0401, *wR*2 = 0.0912	*R*1 = 0.0846, *wR*2 = 0.2104
Flack parameter	-	-	-	-0.002(12)	-
Largest diff. peak and hole	0.343 and -0.623 e.Å^{-3}	0.265 and -0.576 e. Å^{-3}	0.546 and -0.451 e. Å^{-3}	0.832 and -0.865 e. Å^{-3}	0.691 and -1.176 e. Å^{-3}

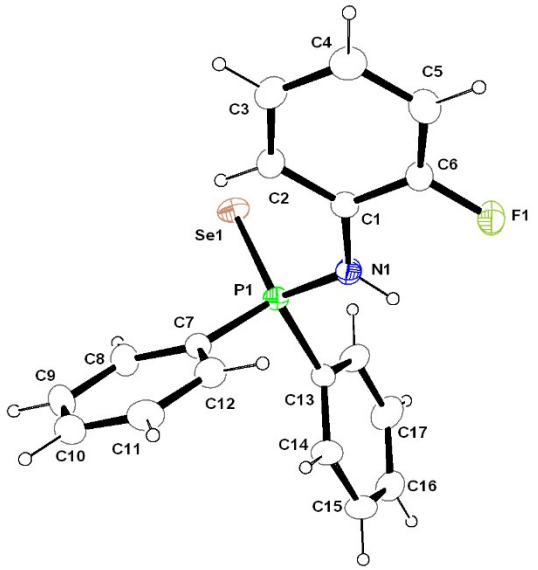

Figure FS1. Molecular solid-state structure of **1-H**. Selected bond lengths (Å) and angles (º) are: P1–Se1 2.1047(5), P1–N1 1.6779(17), P1–C7 1.811(2), F1–C6 1.365(2), N1–C1 1.408(3), P1–C13 1.815(2), C5–C6 1.368(3), N1–P1–Se1 116.13(7), C13–P1–Se1 113.25(7), C7–P1–Se1 113.53(7), N1–P1–C7 104.64(10), C7–P1–C13 106.45(9), F1–C6–C5 119.91(19).

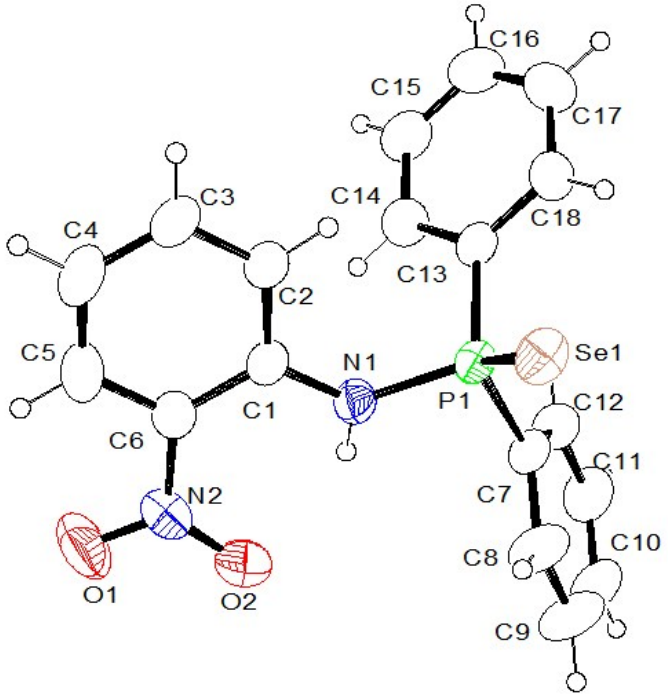

Figure FS2. Molecular solid-state structure of **2-H**. Selected bond lengths (Å) and angles (º) are: P1–Se1 2.0948(8), P1–N1 1.682(2), P1–C13 1.806(3), O1–N2 1.217(2), N2–O2 1.231(4), N1–C1 1.387(3), C6–N2 1.454(4), C5–C6 1.388(4), N1–P1–Se1 114.58(9), C13–P1–Se1 113.06(9), C7–P1–Se1 114.58(9), C13–P1–C7 108.19(13), N2–P1–C13 105.69(12), N1–P1–C7 98.67(12).

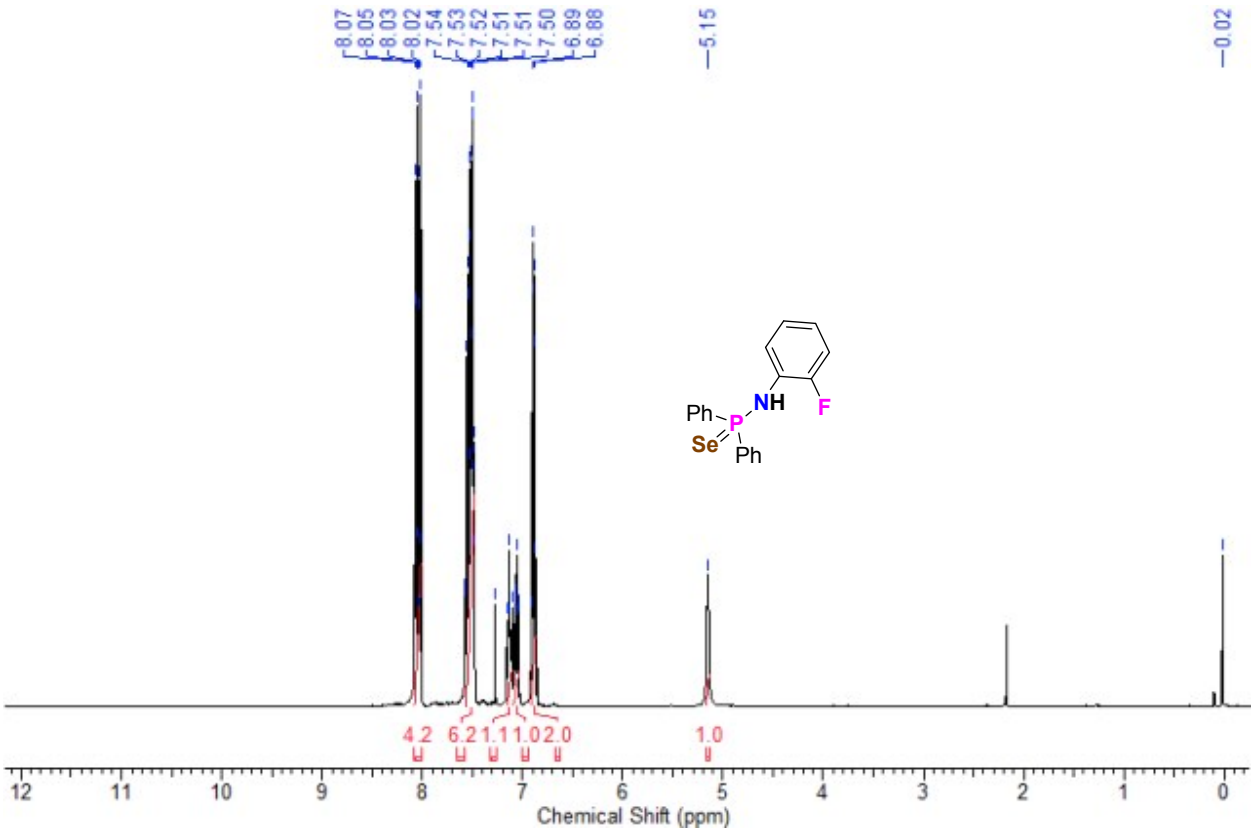

Figure FS3: ^{1}H NMR spectra of complex **1-H.**

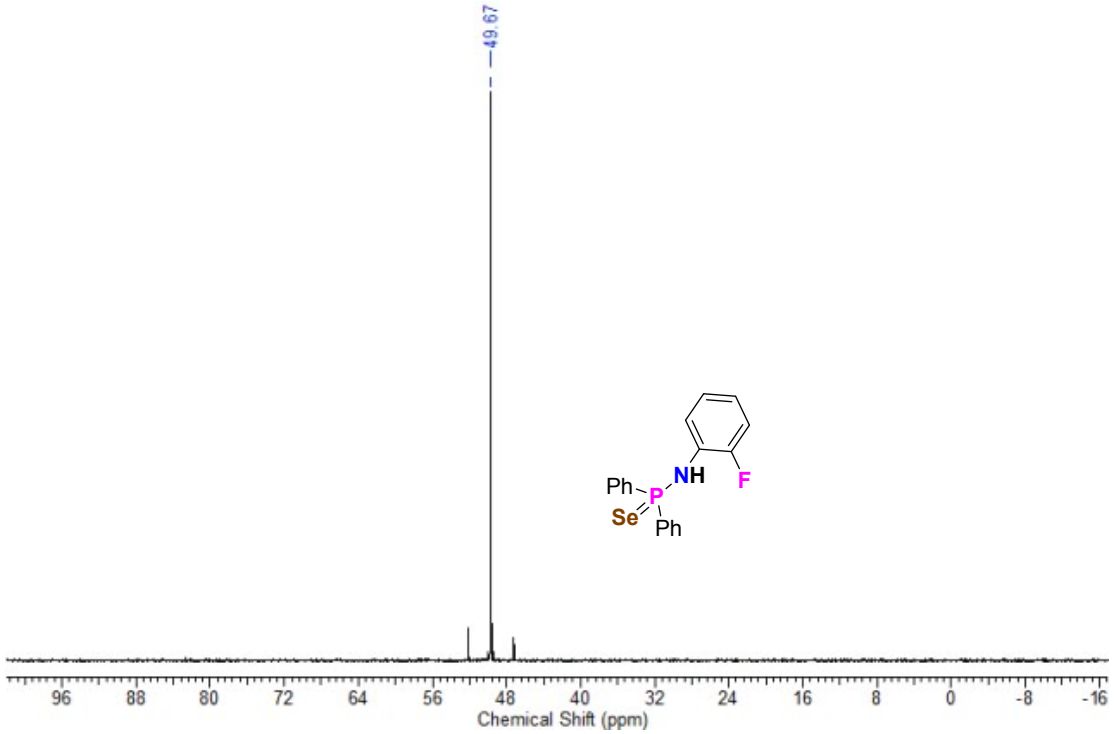

Figure FS4: ^{31}P NMR spectra of complex **1-H.**

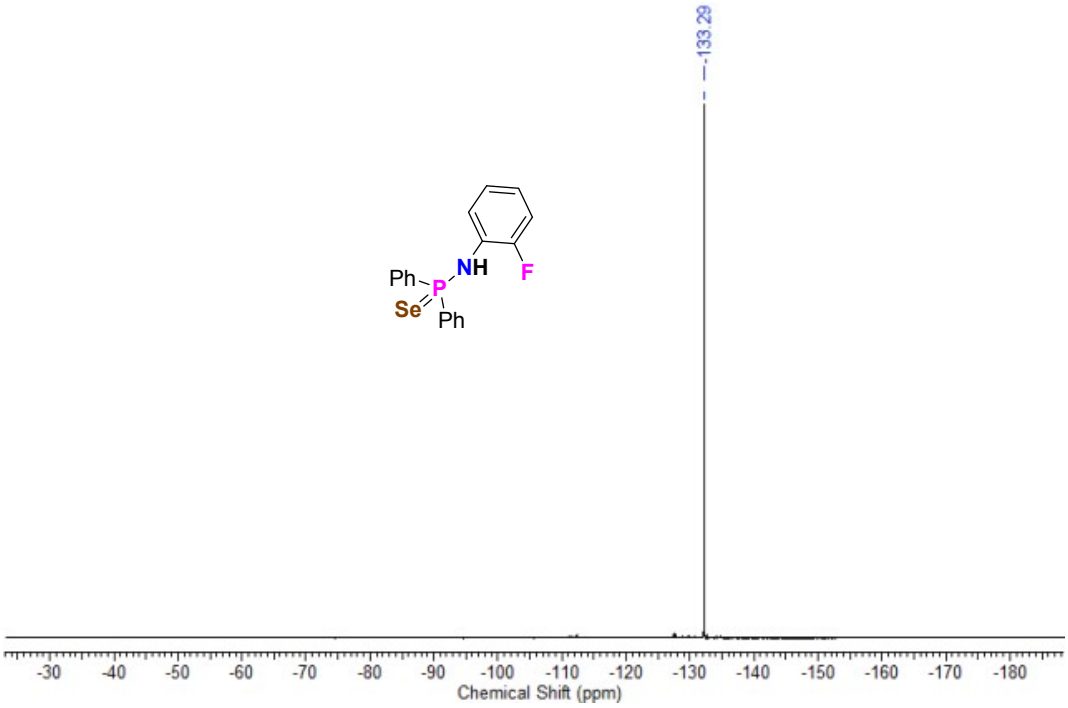

Figure FS5: ^{19}F NMR spectra of complex **1-H.**

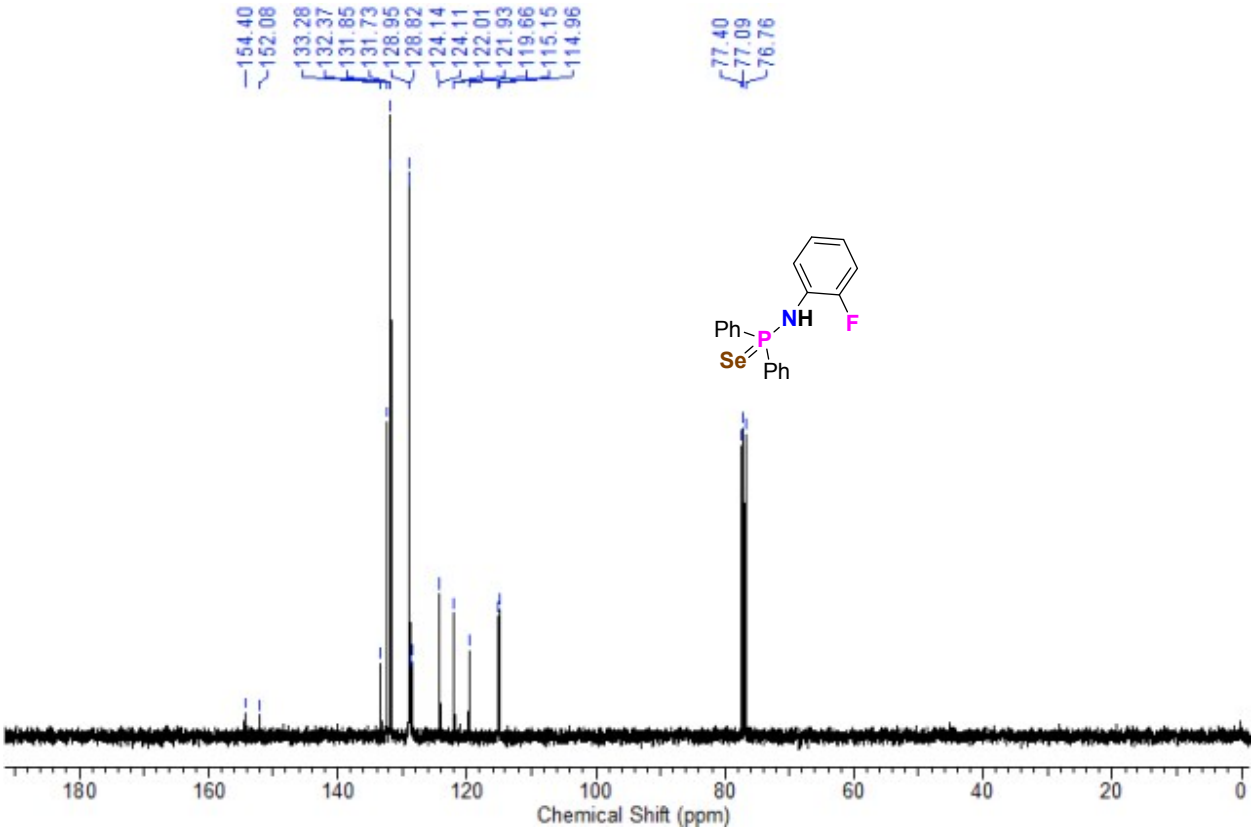

Figure FS6: ^{13}C NMR spectra of complex **1-H.**

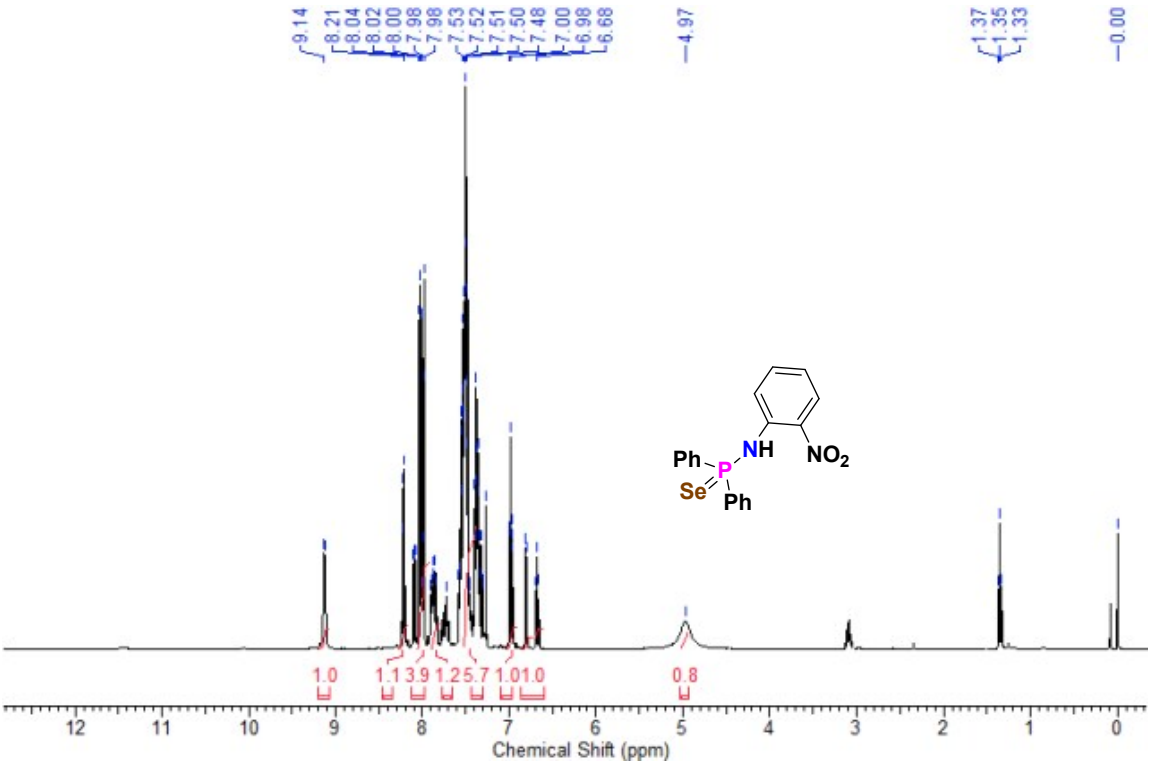

Figure FS7: ^{1}H NMR spectra of complex **2-H.**

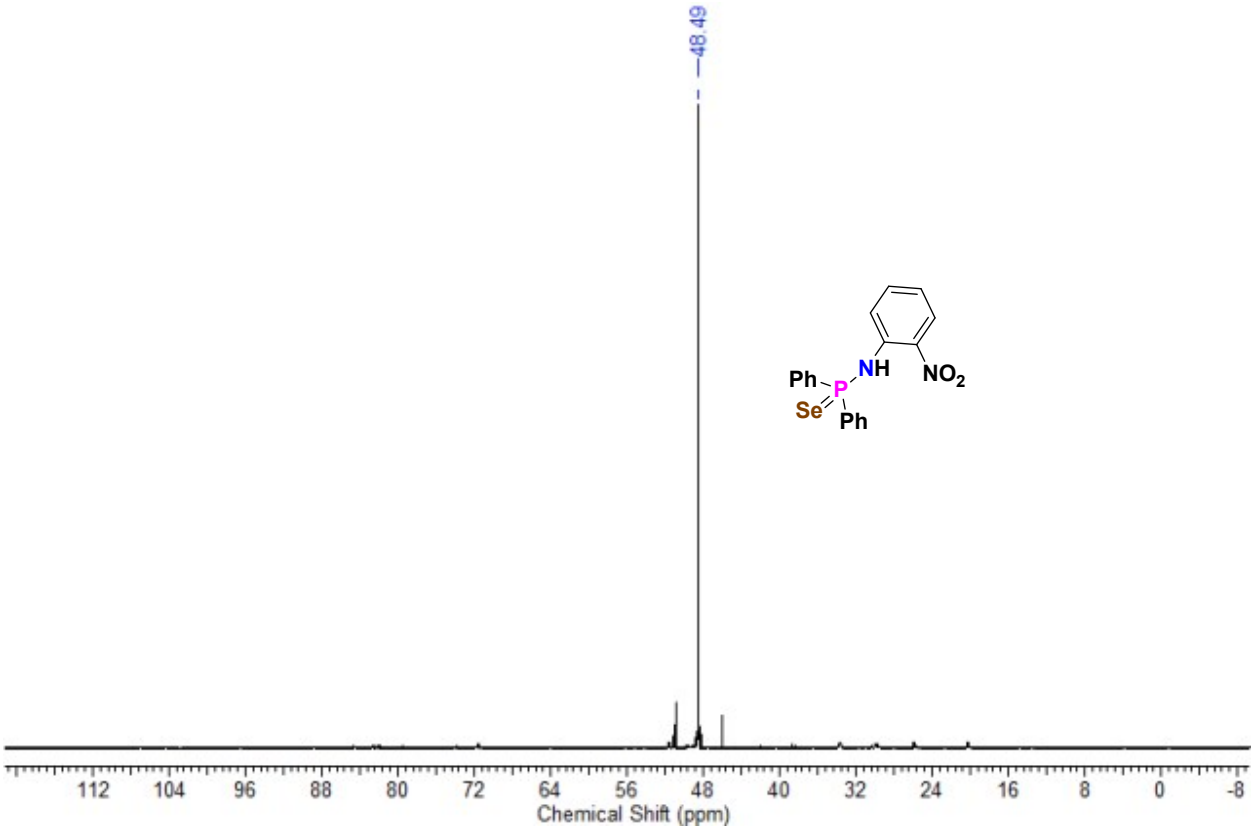

Figure FS8: ^{31}P NMR spectra of complex **2-H**.

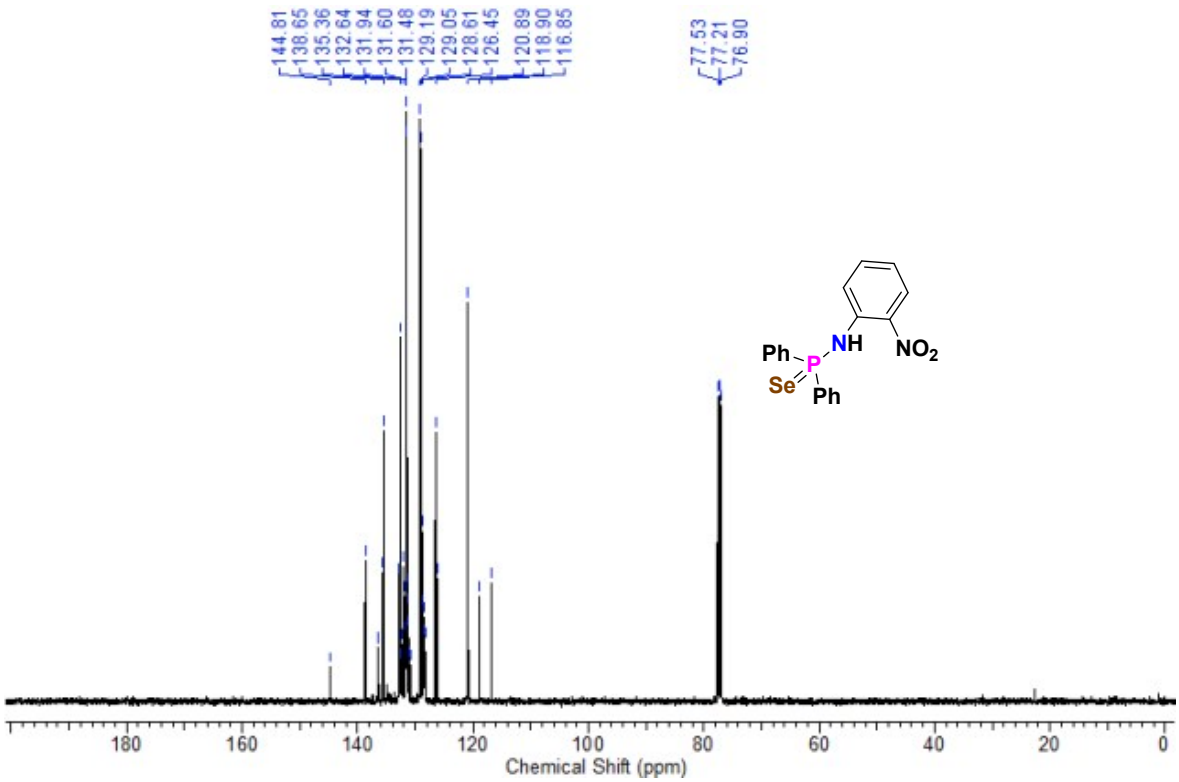

Figure FS9: ^{13}C NMR spectra of complex **2-H.**

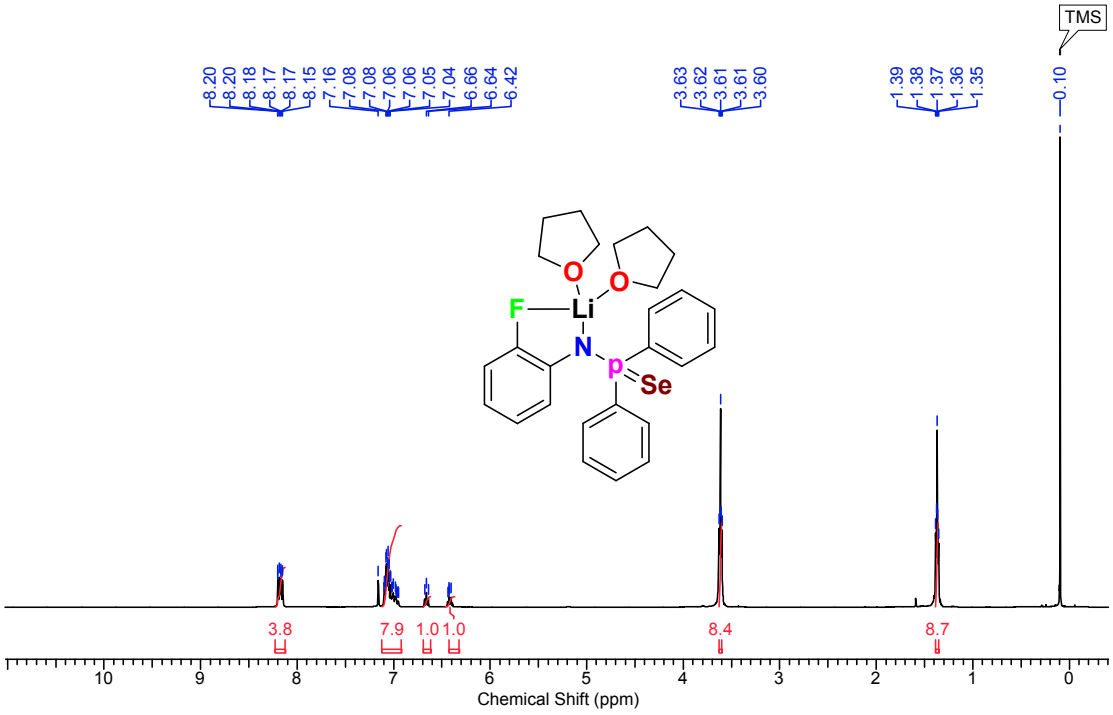

Figure FS10: ^{1}H NMR spectra of complex **3a**.

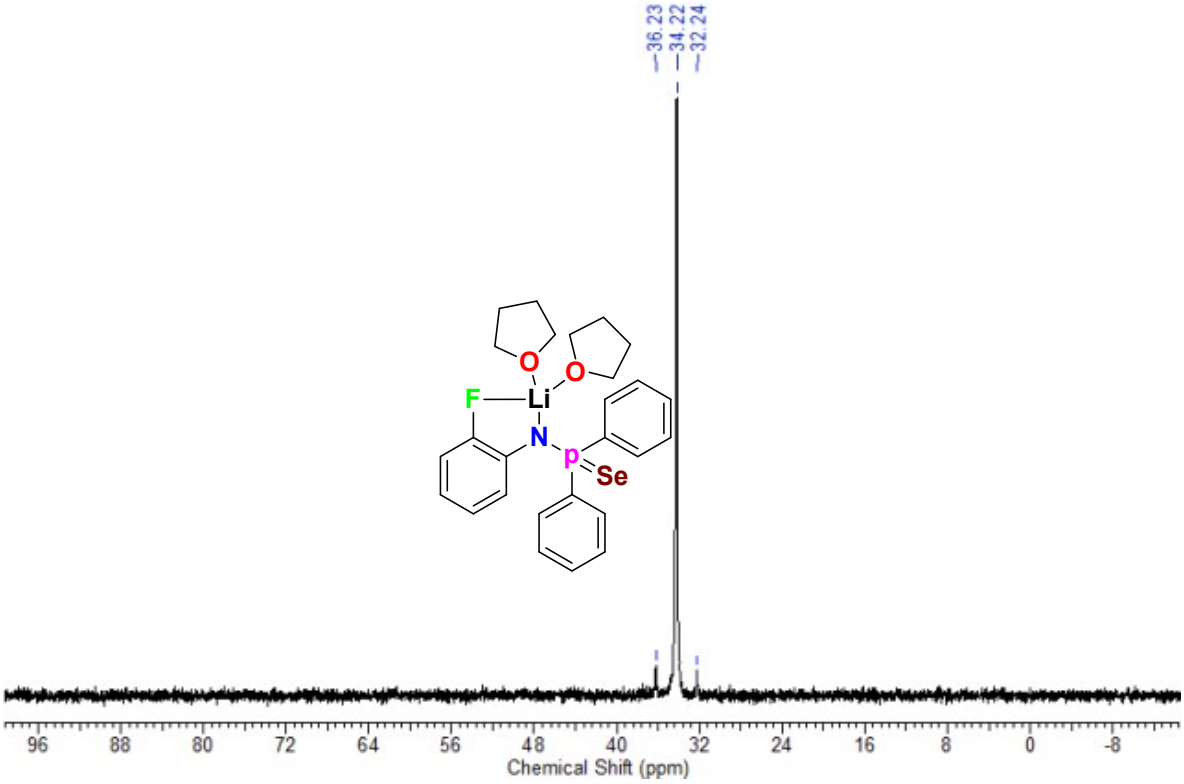

Figure FS11: ^{31}P NMR spectra of complex **3a**.

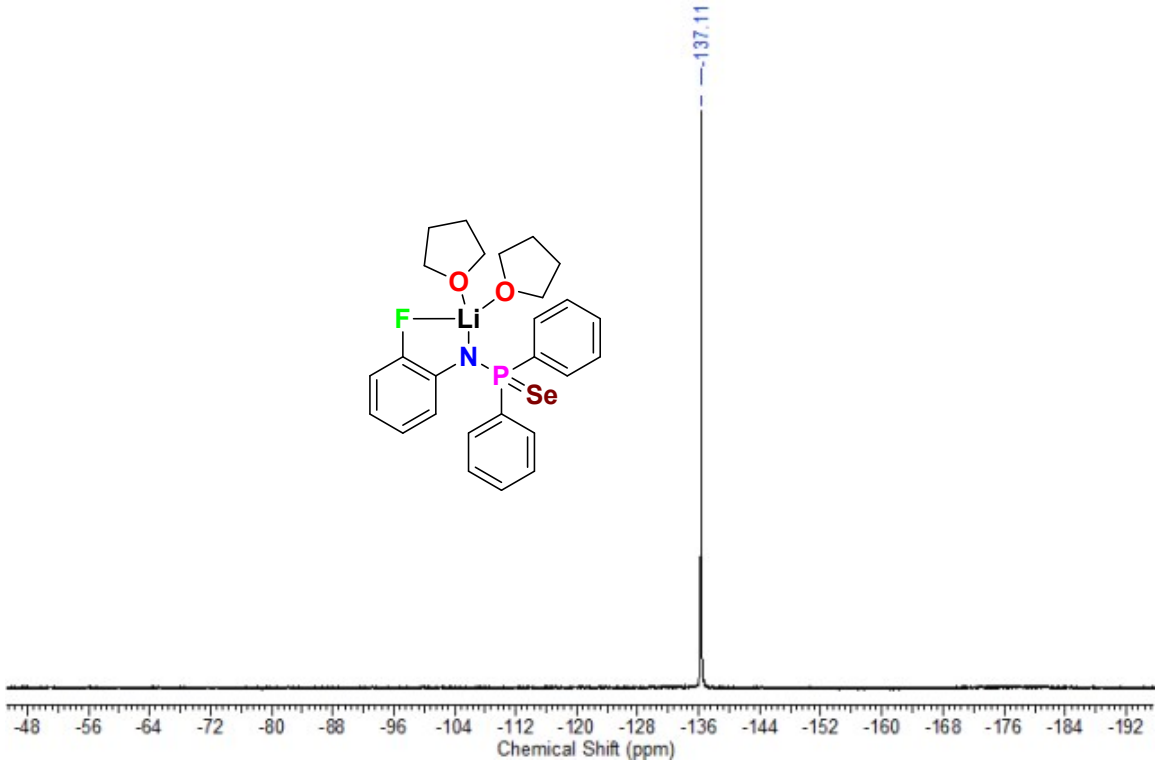

Figure FS12: ^{19}F NMR spectra of complex **3a.**

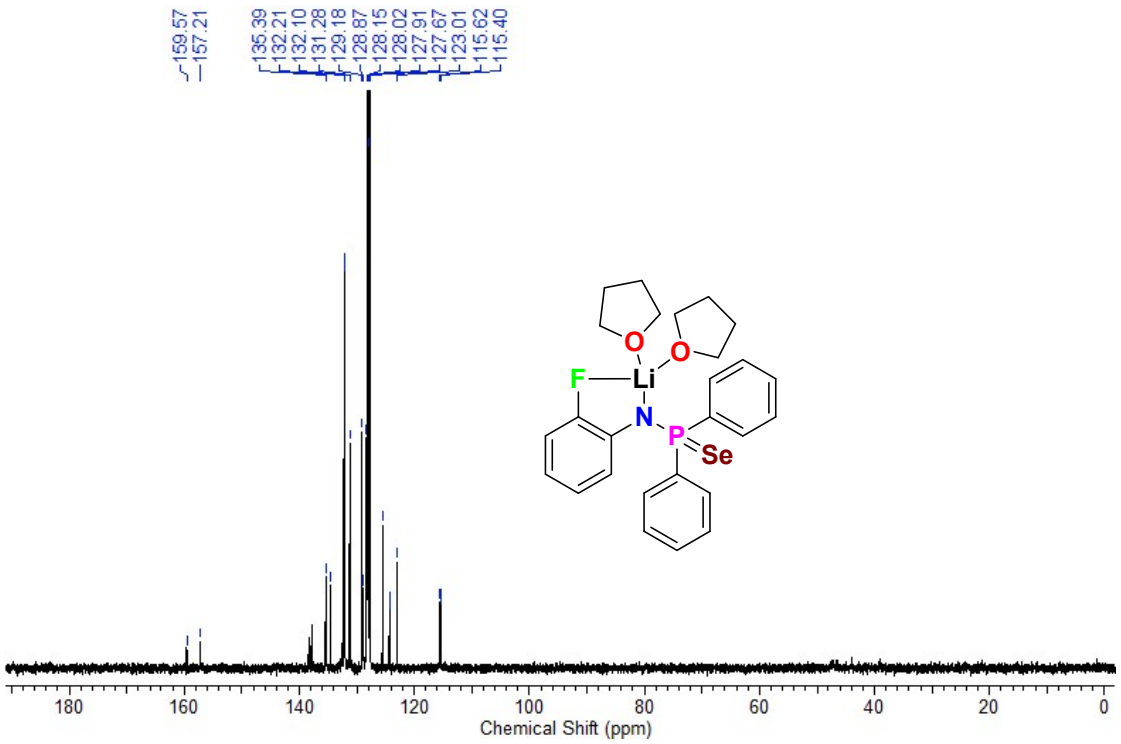

Figure FS13: ^{13}C NMR spectra of complex **3a.**

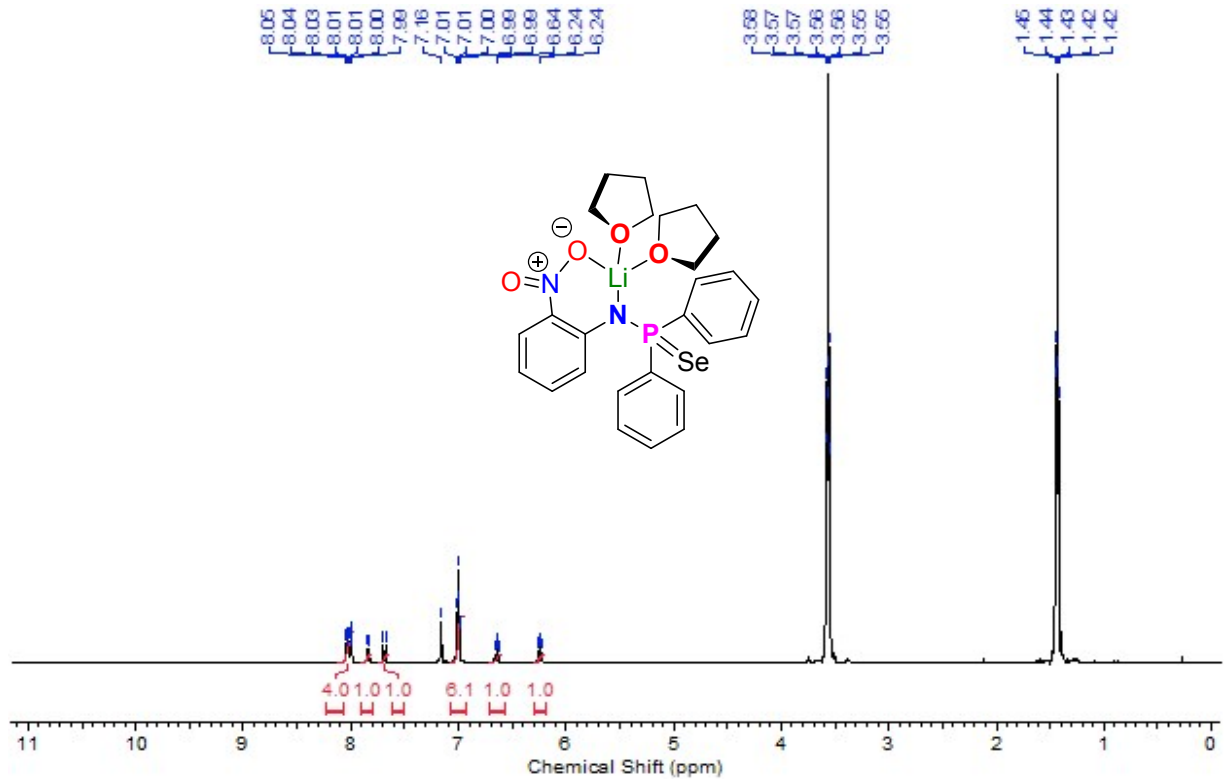

Figure FS14: ^{1}H NMR spectra of complex **3b.**

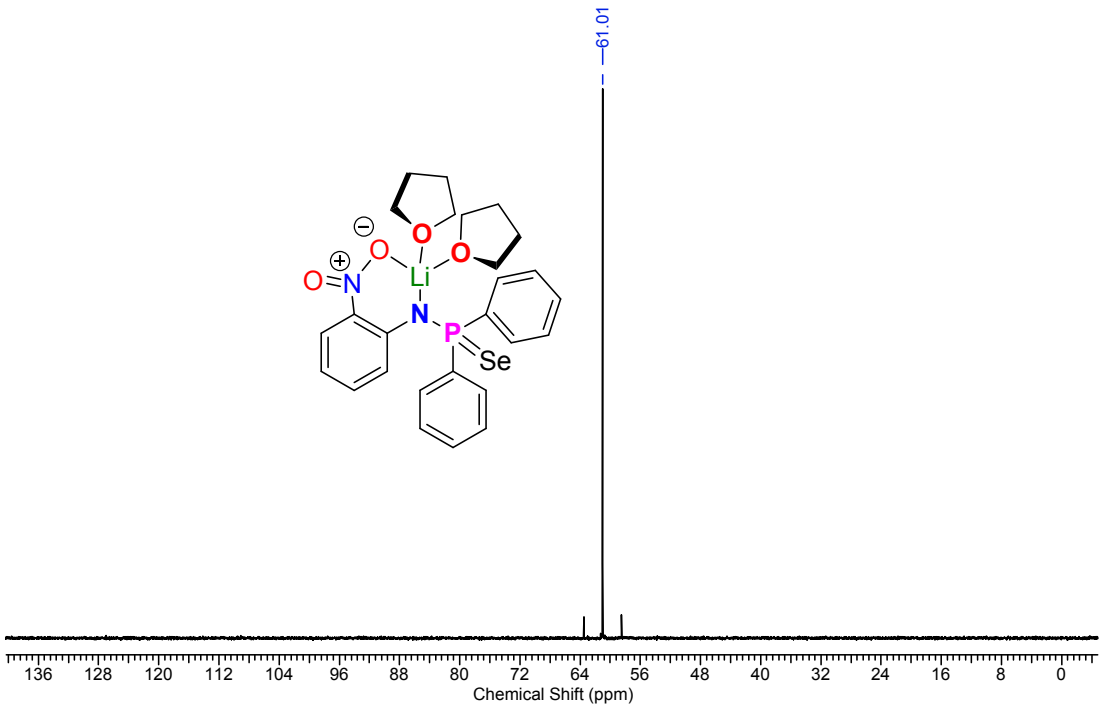

Figure FS15: ^{31}P NMR spectra of complex **3b.**

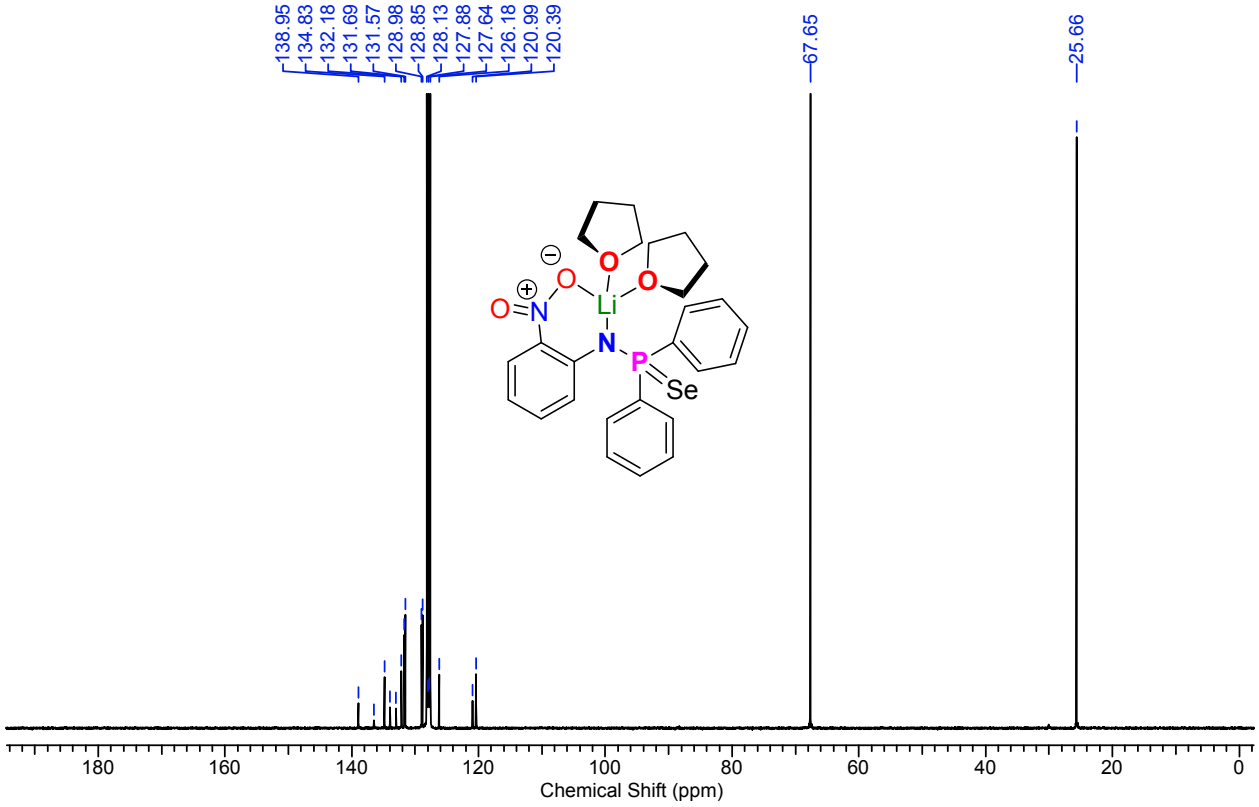

Figure FS16: ^{13}C NMR spectra of complex **3b.**

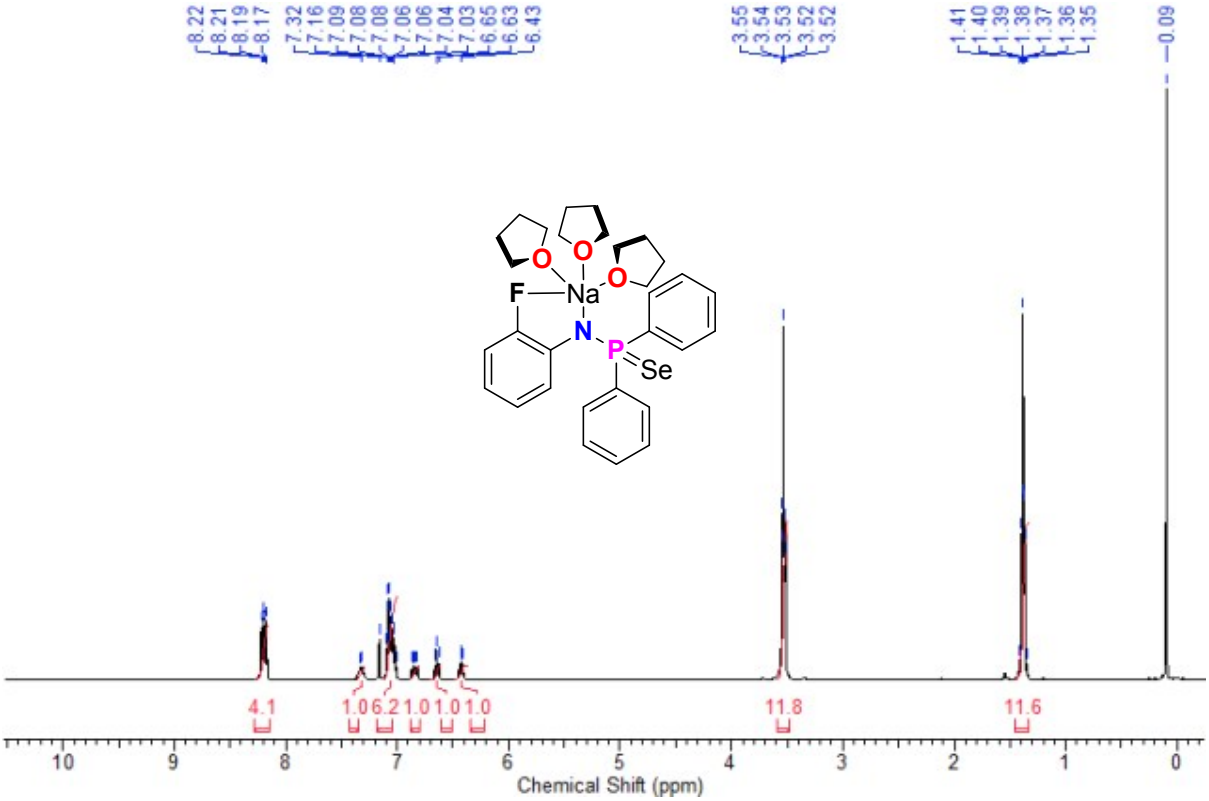

Figure FS17: ^{1}H NMR spectra of complex **4a**.

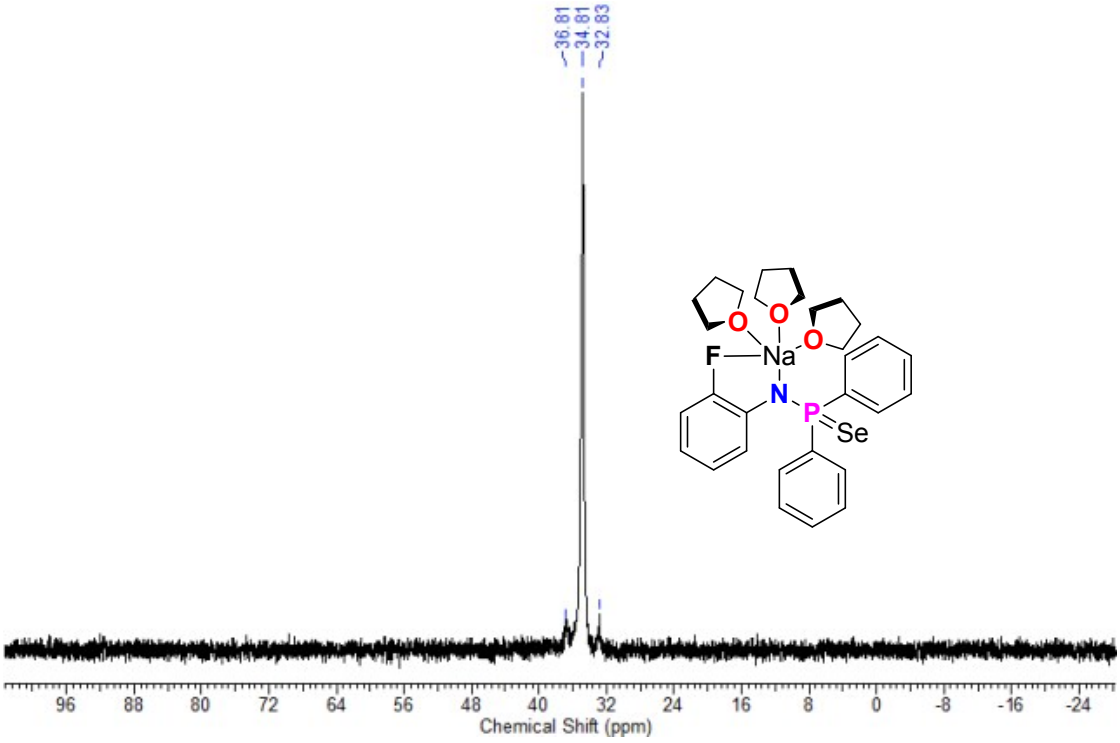

Figure FS18: ^{31}P NMR spectra of complex **4a**.

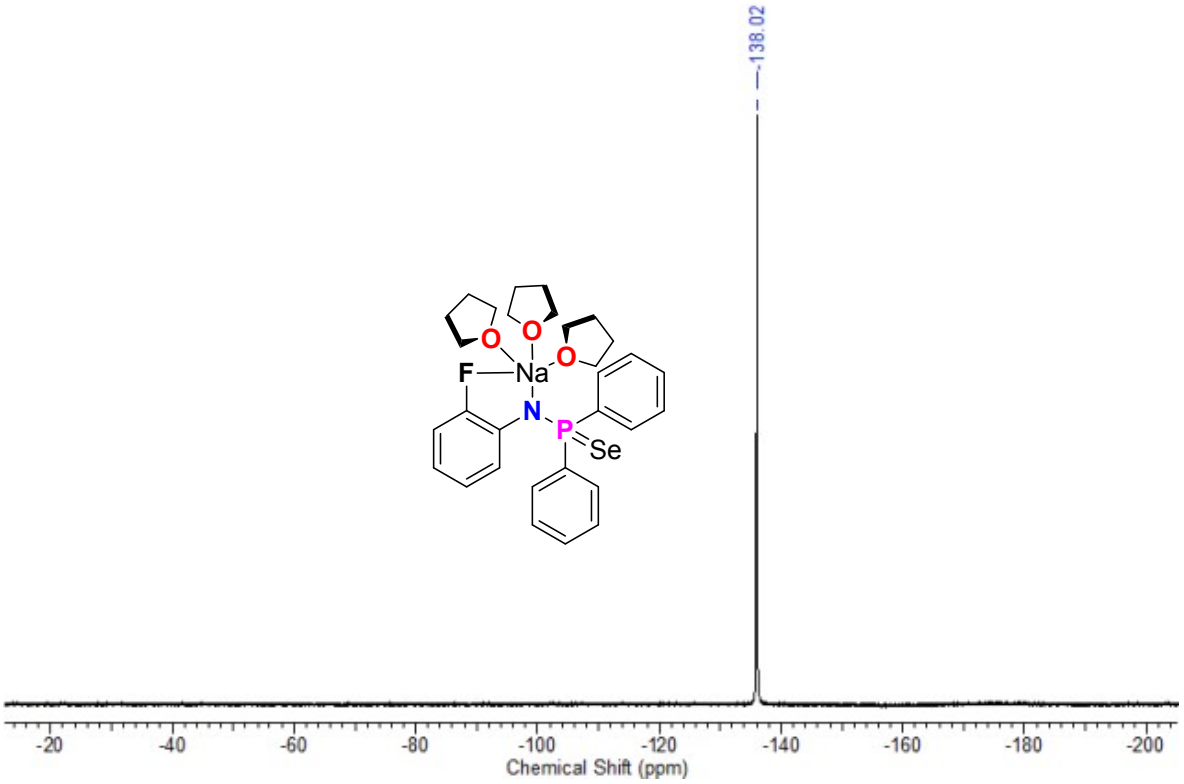

Figure FS19: ^{19}F NMR spectra of complex **4a.**

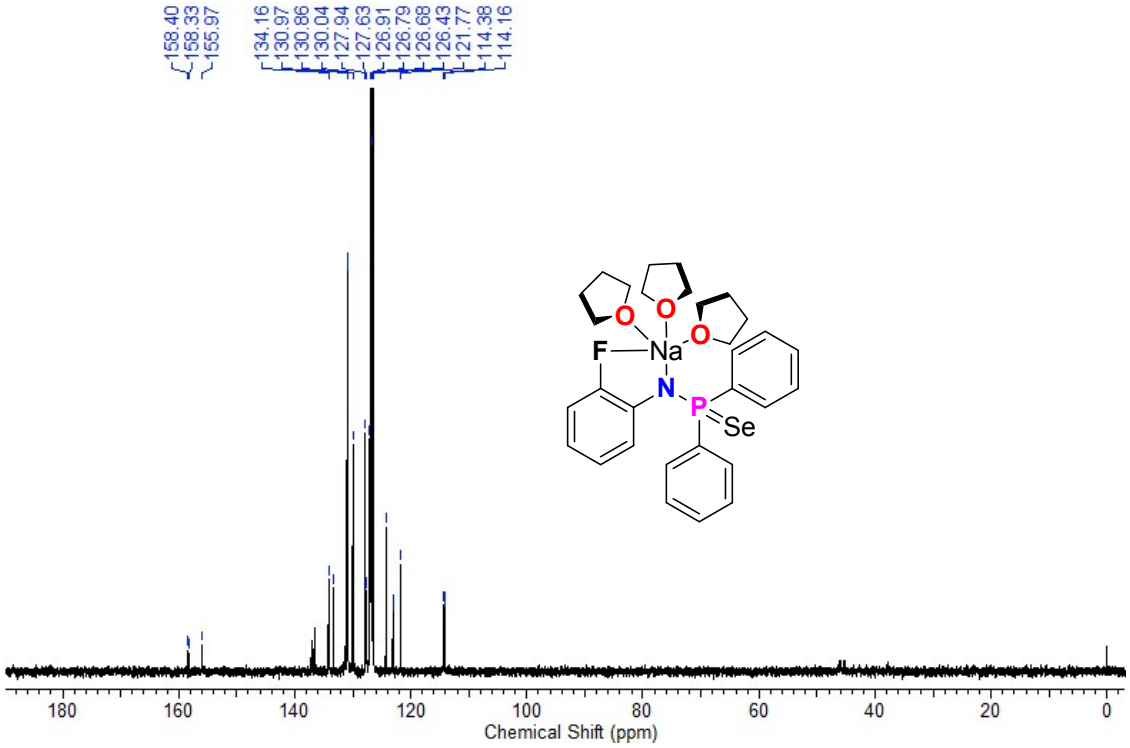

Figure FS20: ^{13}C NMR spectra of complex **4a.**

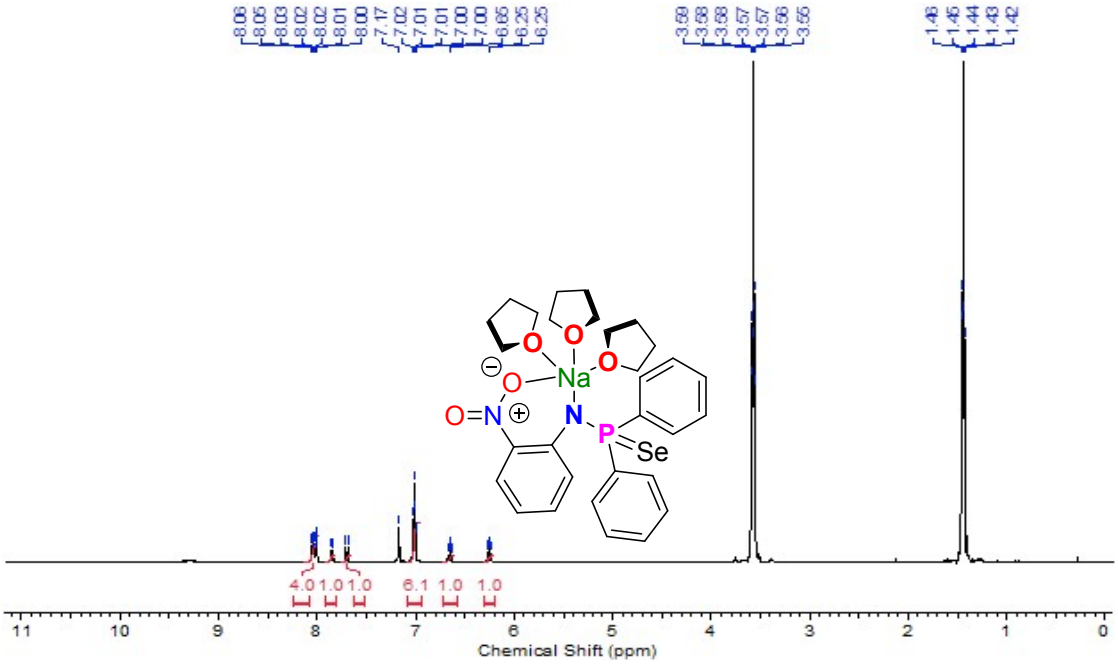

Figure FS21: ^{1}H NMR spectra of complex **4b**.

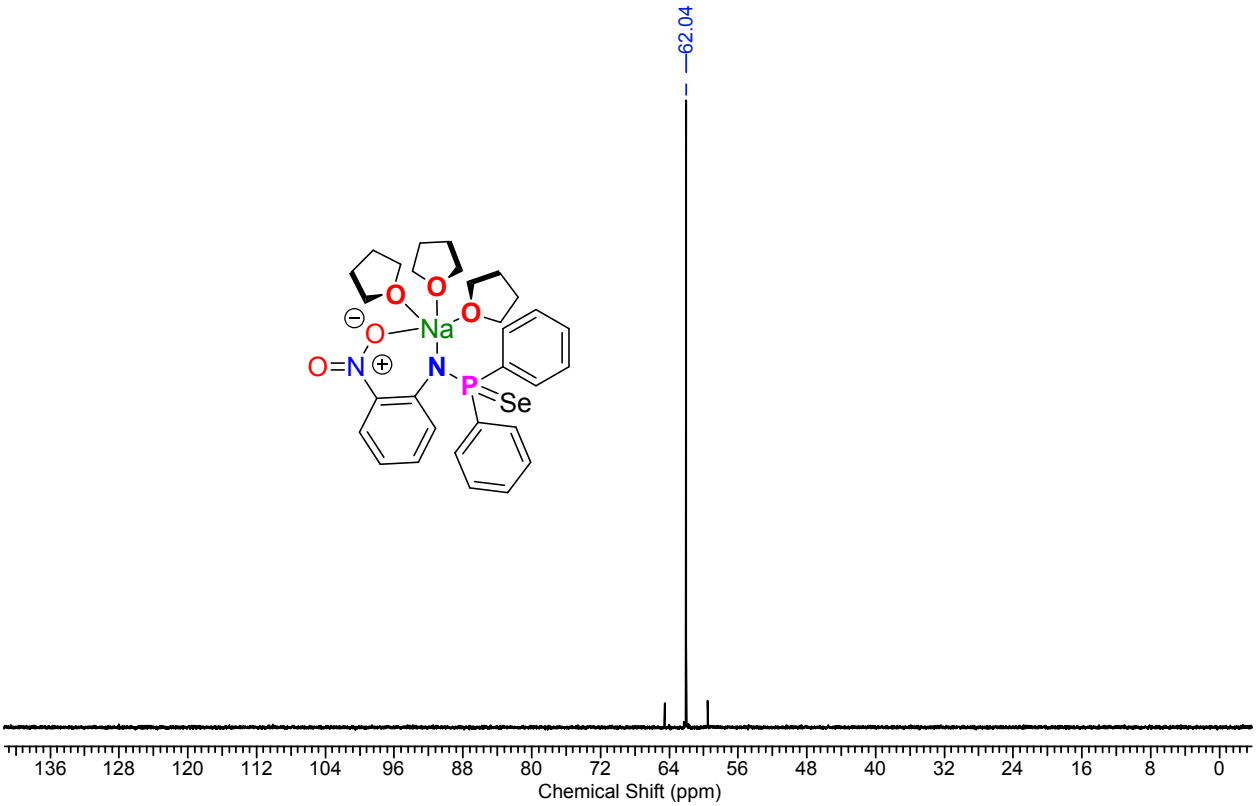

Figure FS22: ^{19}F NMR spectra of complex **4b.**

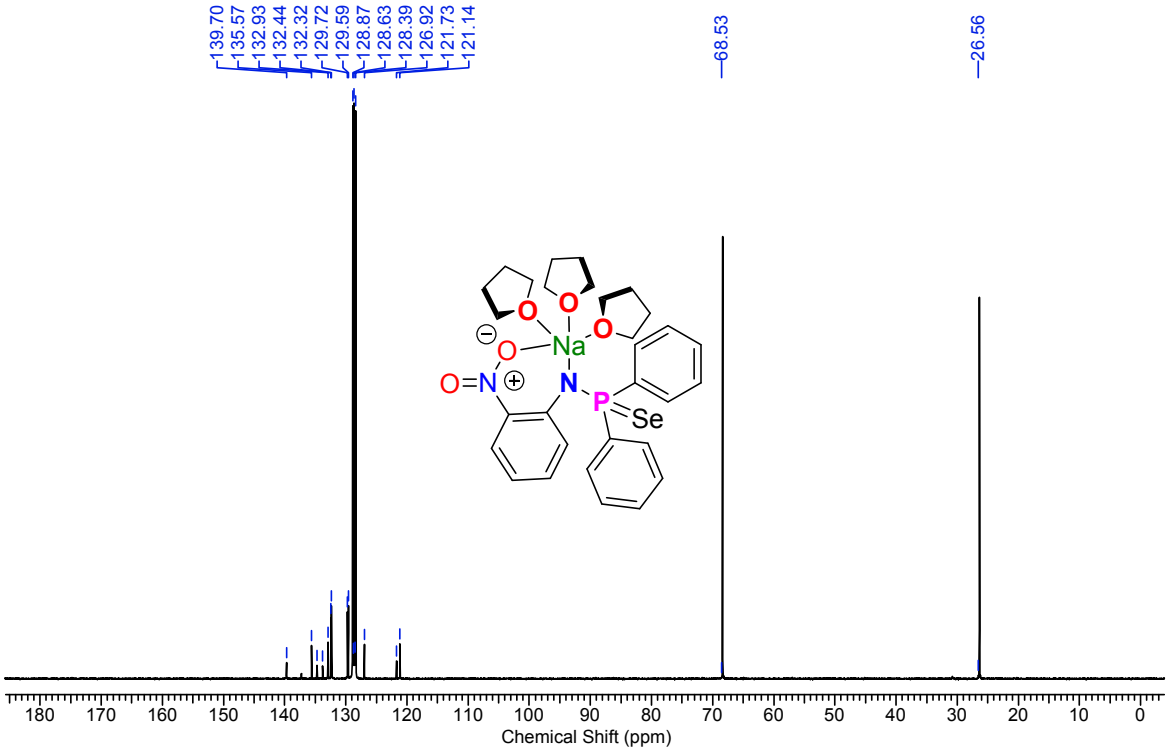

Figure FS23: ^{13}C NMR spectra of complex **4b.**

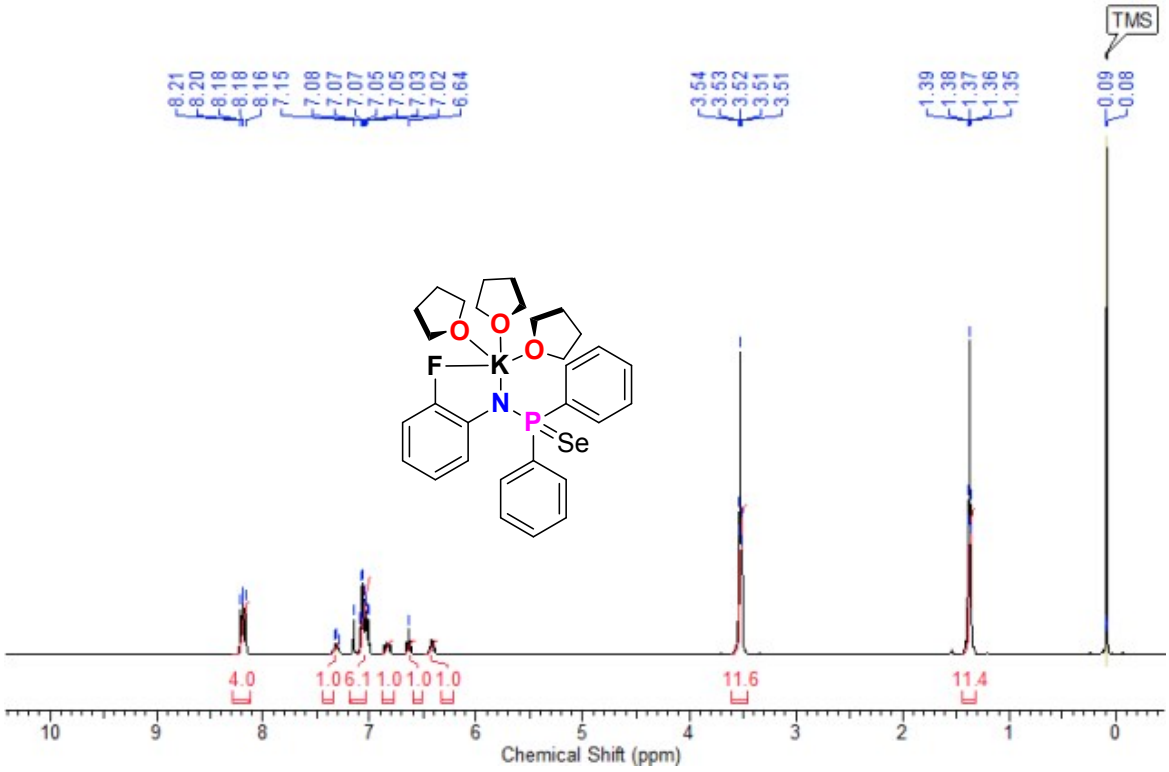

Figure FS24: ^{1}H NMR spectra of complex **5a**.

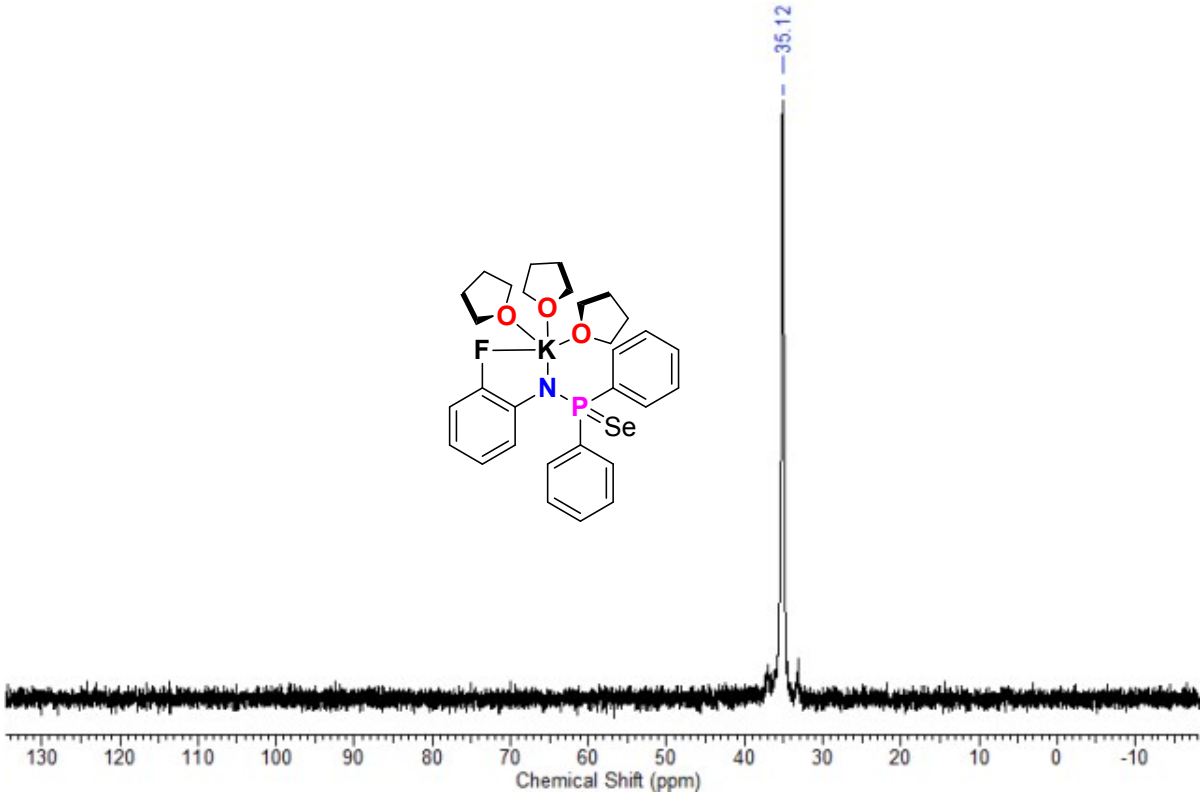

Figure FS25: ^{31}P NMR spectra of complex **5a**.

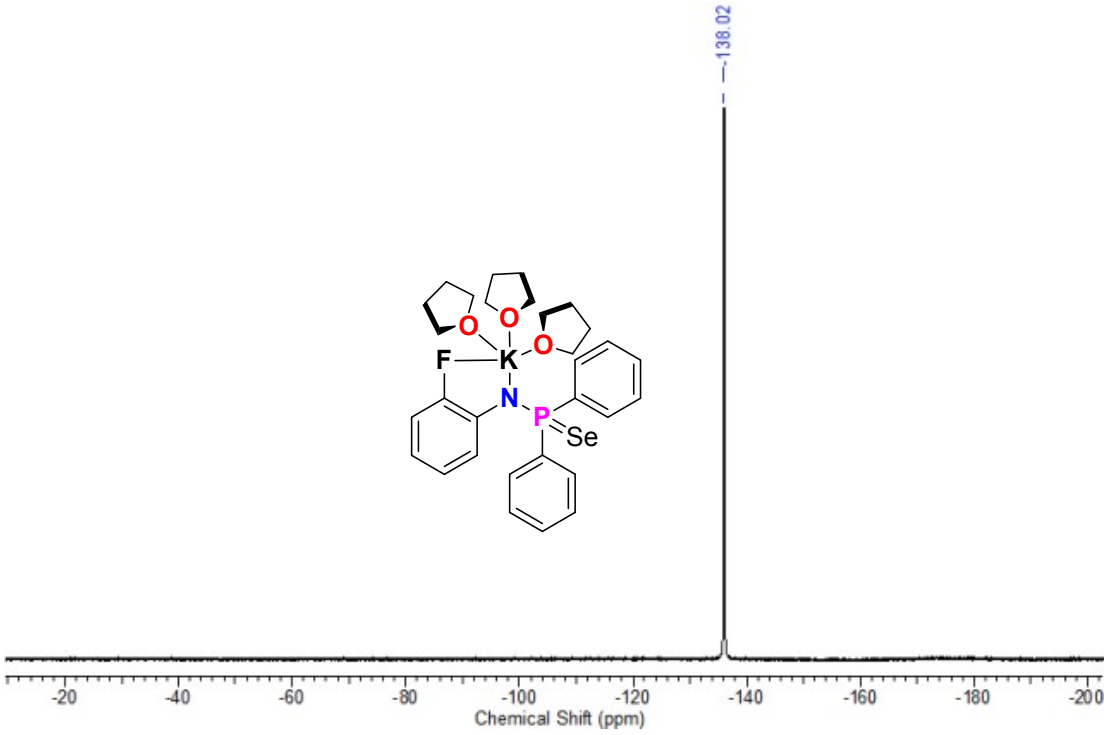

Figure FS26: ^{19}F NMR spectra of complex **5a.**

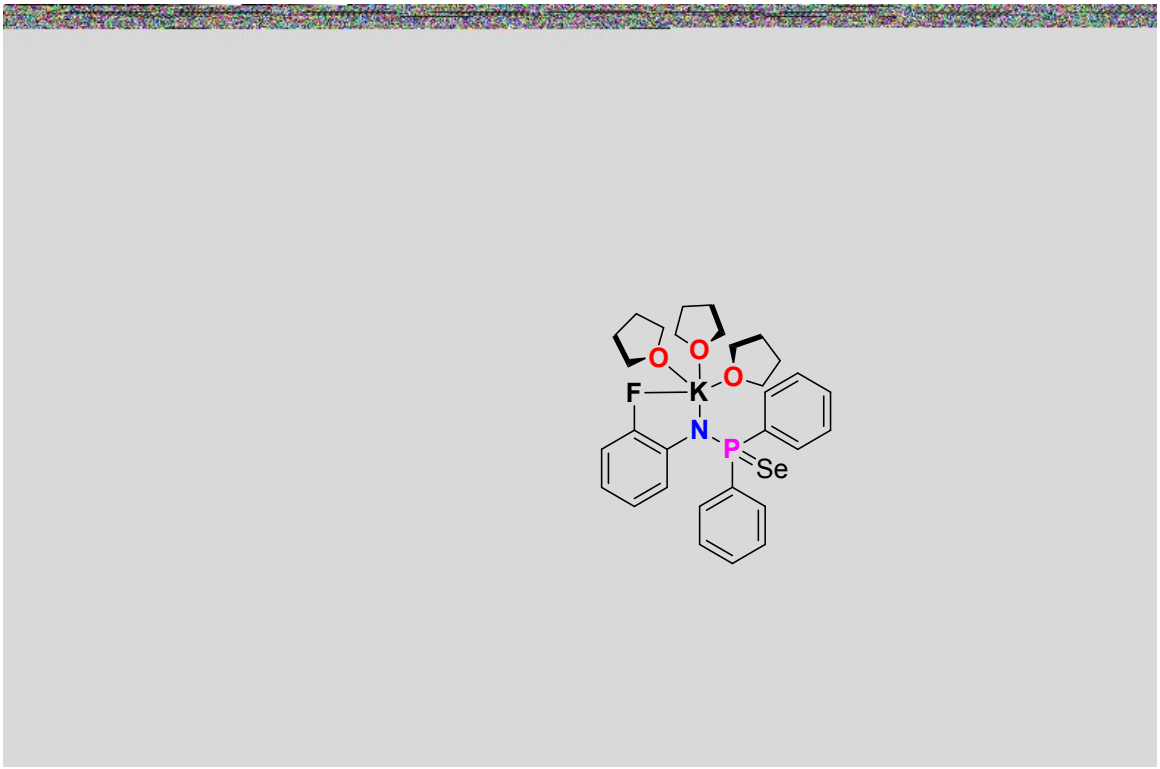

Figure FS27: ^{13}C NMR spectra of complex **5a.**

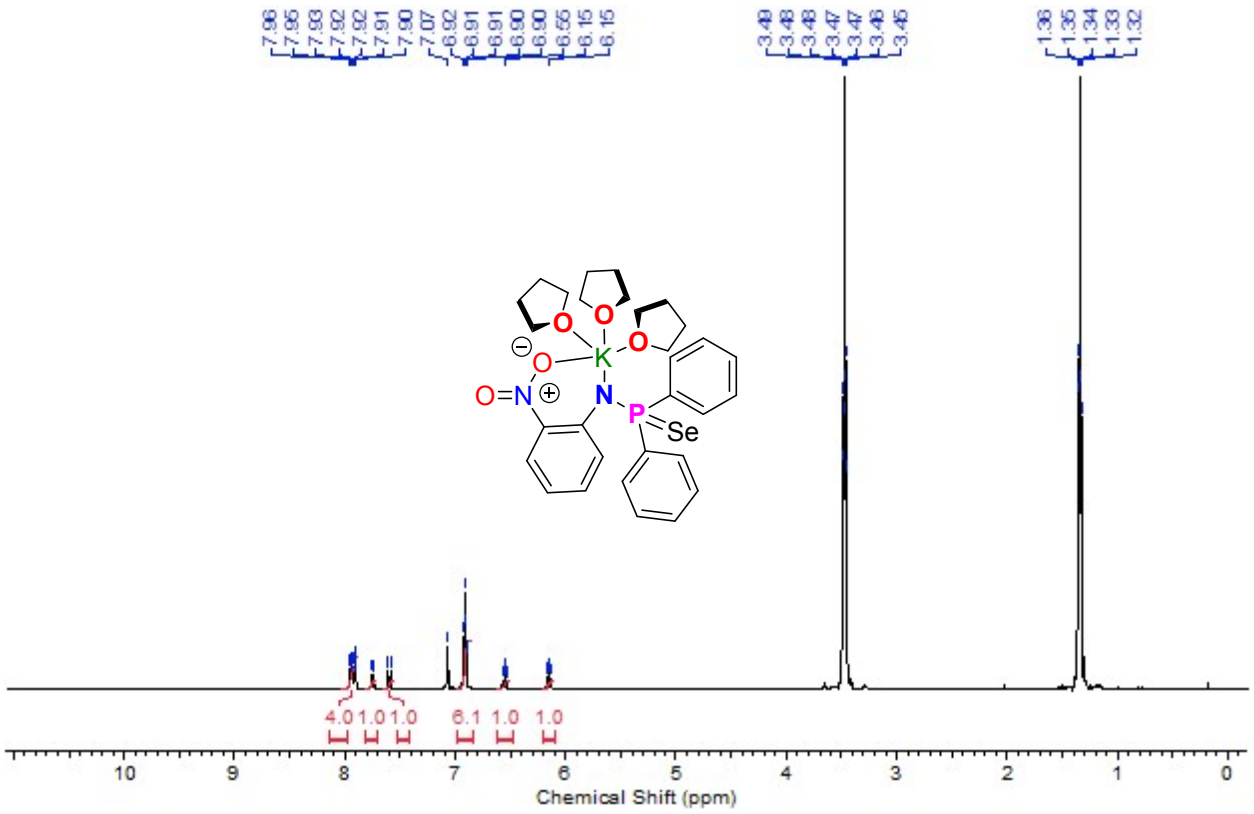

Figure FS28: ^{1}H NMR spectra of complex **5b**.

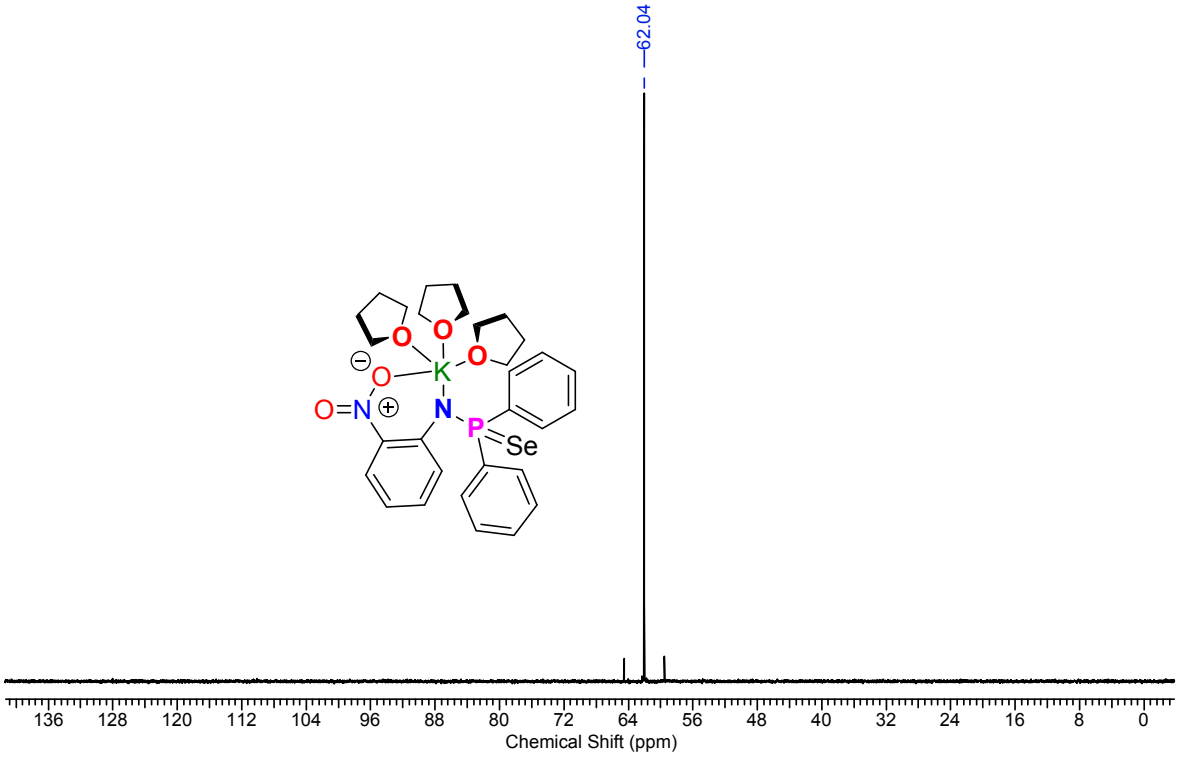

Figure FS29: ^{31}P NMR spectra of complex **5b**.

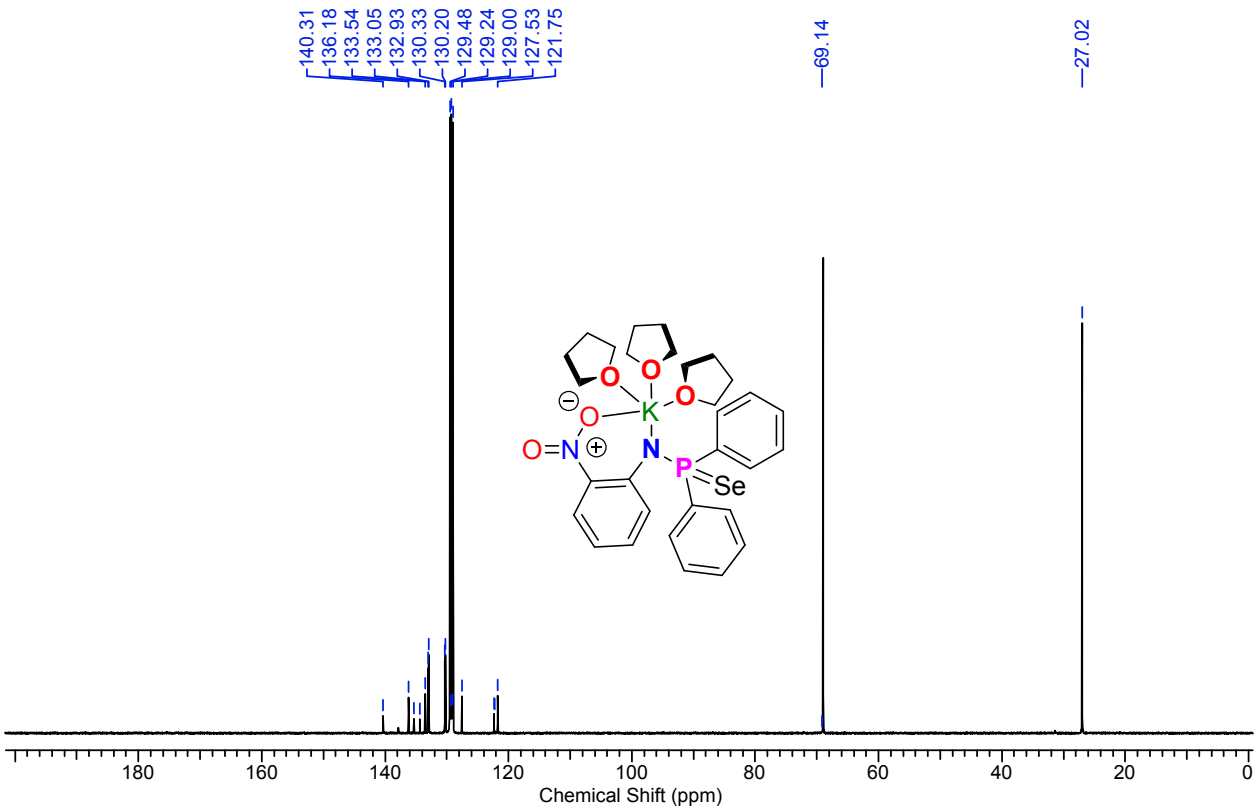

Figure FS30: ^{13}C NMR spectra of complex **5b**

rac-LA Polymerization
Kinetics Data

Typical polymerization of *rac*-lactide.

rac-LA (0.288 g, 2.0 mmol) was added to a solution of **4a,b-5a,b** (0.02 mmol) in toluene (1 mL, Table 1 entry 6). After the solution was stirred at room temperature for 30 min to 2 hour depends on nature of initiator, the reaction was then quenched by the addition of a drop of 2(N) HCl and methanol. Then the solution was concentrated under vacuum, and the polymer was recrystallized from dichloromethane and hexane. The final polymer was then dried under vacuum to constant weight.

Details of the Kinetics Study for *rac*–LA Polymerization

[K(THF)$_3$(Ph$_2$P(Se)N(2-(F)-C$_4$H$_4$)] (5a) as a catalyst.

A typical kinetics study was conducted to establish the reaction order with respect to monomer and [K(THF)$_3$(Ph$_2$P-(Se)N(2-(F)-C$_4$H$_4$)] (**5a**) as catalyst. For LA polymerization, *rac* – LA (0.228 g, 2.0 mmol) was added to a solution of **5a** (0.01, 0.02, 0.03, 0.04, 0.05 M) in $CDCl_3$ (1 mL), respectively. The solution was set in the NMR tube at 25^{o}C.At the indicated time intervals; the tube was analyzed by ^1H NMR. The *rac*-LA concentration [LA] was determined by integrating the quartet methine peak of LA at 5.01 ppm and broad singlet methine peak at 5.09-5.20 ppm. As expected, plots of $[LA]_0/[LA]$ vs. time for a wide range of **5a** are linear indicating the usual first order dependence on monomer concentration (Figure FS31). Thus, the rate expression can be written as $-d[LA]/dt = K_{kpp}[La]^1K(THF)_3(Ph_2P\text{-}(Se)N(2\text{-}(F)\text{-}C_4H_4)]^x = k[LA]^1$,

where $k_{obs} = k_{app}[K(THF)_3(Ph_2P\text{-}(Se)N(2\text{-}(F)\text{-}C_4H_4)]^x$. A plot of $\ln(k_{obs})$ vs. $\ln[K(THF)_3(Ph_2P\text{-}(Se)N(2\text{-}(F)\text{-}C_4H_4)]$ (Figure FS32, Table TS2) is linear, indicating the order of $[K(THF)_3(Ph_2P\text{-}(Se)N(2\text{-}(F)\text{-}C_4H_4)]$ is (x = 0.95 or 1) and k_{app} which is 0.882 $M^{-1}m^{-1}$.($\ln k_{app}$ = -0.126).

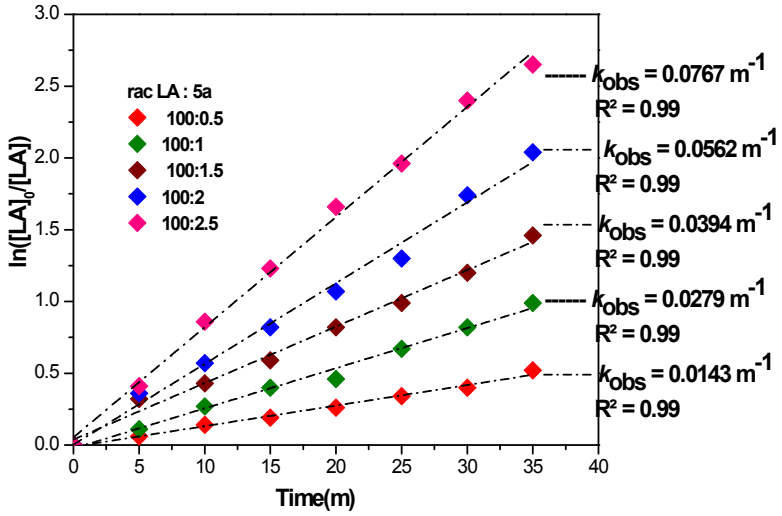

Figure FS31. First order kinetics plots for *rac* LA polymerizations with time in $CDCl_3$ (1 mL) with different concentration of $[K(THF)_3(Ph_2P\text{-}(Se)N(2\text{-}(F)\text{-}C_4H_4)]$ (**5a**) at 25°C.

Table TS2. Kinetics plots of $\ln k_{obs}$ vs $\ln[K(THF)_3(Ph_2P\text{-}(Se)N(2\text{-}(F)\text{-}C_4H_4)]$ / ln(**5a**) for the polymerization of rac-LA with [LA] = 2.0 M in $CDCl_3$ (1 mL) at 25°C.

S.NO.	$[K(THF)_3(Ph_2P\text{-}(Se)N(2\text{-}(F)\text{-}C_4H_4)]$ (**5a**) (M)	ln k_{obs} (Mm^{-1})
1	-4.6	-4.25
2	-3.912	-3.57
3	-3.506	-3.23
4	-3.218	-2.88
5	-2.813	-2.57

Table TS3. Kinetics plots of k_{obs} vs $[K(THF)_3(Ph_2P\text{-}(Se)N(2\text{-}(F)\text{-}C_4H_4)]$ (**5a**) for the polymerization of *rac*-LA with [LA] = 2.0 M in $CDCl_3$ (1 mL) at 25°C.

S. NO.	$[K(THF)_3(Ph_2P\text{-}(Se)N(2\text{-}(F)\text{-}C_4H_4)]$ (**5a**) (M)	k_{obs} (Mm^{-1})

1	0	0
2	0.01	0.0143
3	0.02	0.0279
4	0.03	0.0394
5	0.04	0.0562
6	0.05	0.0767

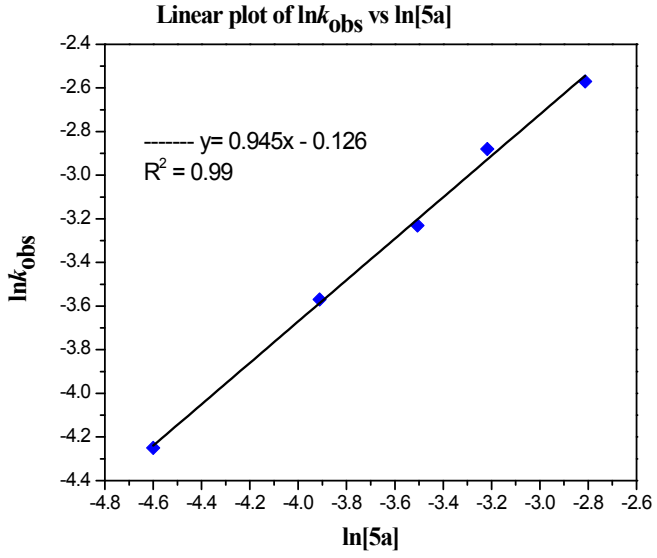

Figure FS32. Kinetics plots of ln k_{obs} vs ln[K(THF)$_3$(Ph$_2$P-(Se)N(2-(F)-C$_4$H$_4$)] / ln (**5a**) for the polymerization of *rac*-LA with [LA] = 2.0 M in $CDCl_3$ (1 mL) at 25^{o}C.

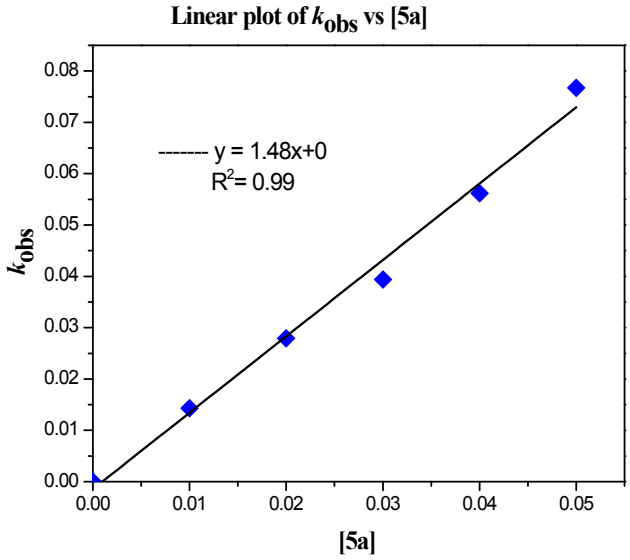

Figure FS33. Kinetics plots of k_{obs} vs [K(THF)$_3$(Ph$_2$P-(Se)N(2-(F)-C$_4$H$_4$)] (**5a**) for the polymerization of rac-LA with [LA] = 2.0 M in $CDCl_3$ (1 mL) at 25^{o}C.

$$\text{Rate of the reaction} = -d[\text{LA}]/dt = 0.882\ [\text{La}]^1[\text{K(THF)}_3(\text{Ph}_2\text{P-(Se)N(2-(F)-C}_4\text{H}_4)]^1$$

[K(THF)$_3$(Ph$_2$P-(Se)N(2-(NO$_2$)-C$_4$H$_4$)] (5b) as a catalyst.

A typical kinetics study was conducted to establish the reaction order with respect to monomer and [K(THF)$_3$(Ph$_2$P-(Se)N(2-(NO$_2$)-C$_4$H$_4$)] (**5b**) as catalyst. For LA polymerization, *rac* – LA (0.228 g, 2.0 mmol) was added to a solution of **5b** (0.01, 0.02, 0.03, 0.04, 0.05 M) in $CDCl_3$ (1 mL), respectively. The solution was set in the NMR tube at 25^{o}C.At the indicated time intervals; the tube was analyzed by ^{1}H NMR. The rac-LA concentration [LA] was determined by integrating the quartet methine peak of LA at 5.01 ppm and broad singlet methine peak at 5.09-5.20 ppm. As expected, plots of $[LA]_0/[LA]$ vs. time for a wide range of **5b** are linear indicating the usual first order dependence on monomer concentration (Figure FS34). Thus, the rate expression can be written as $-d[\text{LA}]/dt = K_{kpp}[\text{La}]^1[\text{K(THF)}_3(\text{Ph}_2\text{P-(Se)N(2-(NO}_2\text{)-C}_4\text{H}_4)]^x = k[\text{LA}]^1$, where $kobs = k_{app}[\text{K(THF)}_3(\text{Ph}_2\text{P-(Se)N(2-(NO}_2\text{)-C}_4\text{H}_4)]^x$. A plot of ln(*kobs*) vs. ln[K(THF)$_3$(Ph$_2$P-(Se)N(2-(NO$_2$)-C$_4$H$_4$)] (Figure FS35, Table TS4) is linear, indicating the order of [K(THF)$_3$(Ph$_2$P-(Se)N(2-(NO$_2$)-C$_4$H$_4$)] is (x = 0.82 or 1) and k_{app} which is 0.755 $M^{-1}m^{-1}$.($\ln k_{app}$ = -0.28).

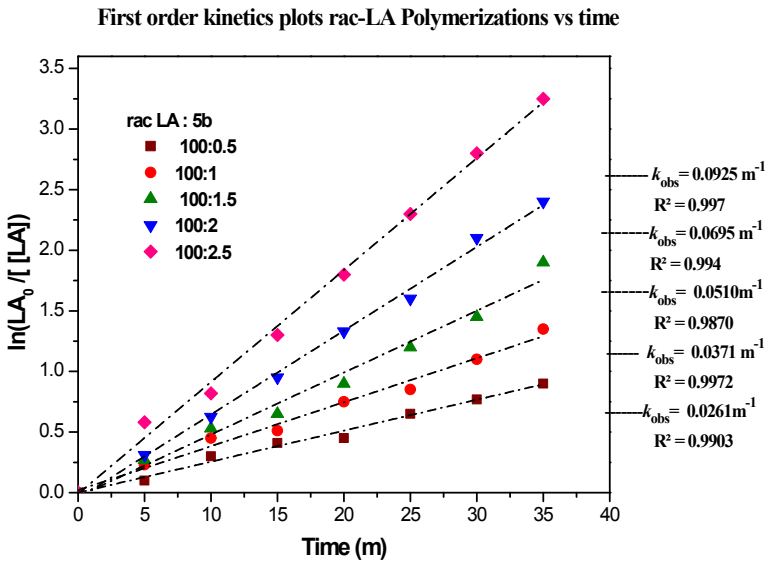

Figure FS34. First order kinetics plots for rac LA polymerizations with time in $CDCl_3$ (1 mL) with different concentration of [K(THF)$_3$(Ph$_2$P-(Se)N(2-(NO$_2$)-C$_4$H$_4$)] (**5b**) at 25^{o}C.

Table TS4. Kinetics plots of lnk_{obs} vs ln[K(THF)$_3$(Ph$_2$P-(Se)N(2-(NO$_2$)-C$_4$H$_4$)]/ln(**5b**) for the polymerization of *rac*-LA with [LA] = 2.0 M in $CDCl_3$ (1 mL) at 25^{o}C.

S.NO.	ln[K(THF)$_3$(Ph$_2$P-(Se)N(2-(NO$_2$)-C$_4$H$_4$)] (**5b**) (M)	ln k_{obs} (Mm^{-1})
1	-4.6	-3.66
2	-3.912	-3.32
3	-3.506	-2.97
4	-3.218	-2.67
5	-2.813	-2.38

Table TS5. Kinetics plots of k_{obs} vs [K(THF)$_3$(Ph$_2$P-(Se)N(2-(NO$_2$)-C$_4$H$_4$)] (**5b**) for the polymerization of *rac*-LA with [LA] = 2.0 M in $CDCl_3$ (1 mL) at 25^{o}C.

S. NO.	[K(THF)$_3$(Ph$_2$P-(Se)N(2-(NO$_2$)-C$_4$H$_4$)] (**5b**) (M)	k_{obs} (Mm^{-1})
1	0	0
2	0.01	0.0256
3	0.02	0.036

4	0.03	0.051
5	0.04	0.069
6	0.05	0.092

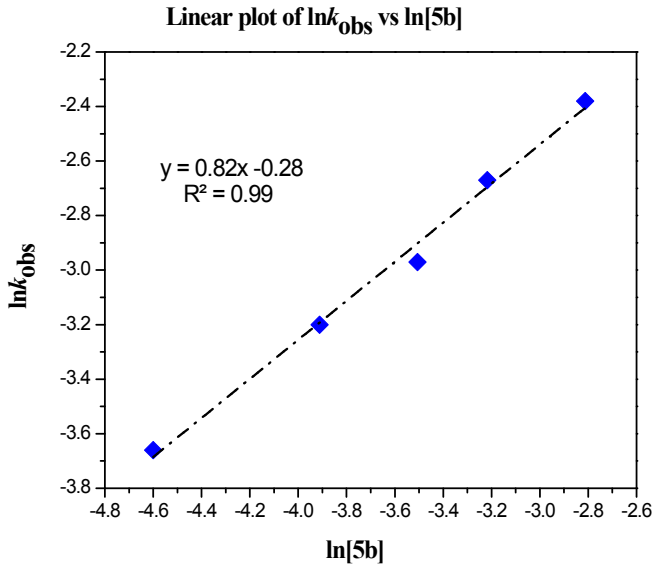

Figure FS35. Kinetics plots of ln k_{obs} vs ln[K(THF)$_3$(Ph$_2$P-(Se)N(2-(NO$_2$)-C$_4$H$_4$)]/ ln (**5b**) for the polymerization of *rac*-LA with [LA] = 2.0 M in $CDCl_3$ (1 mL) at 25^{o}C.

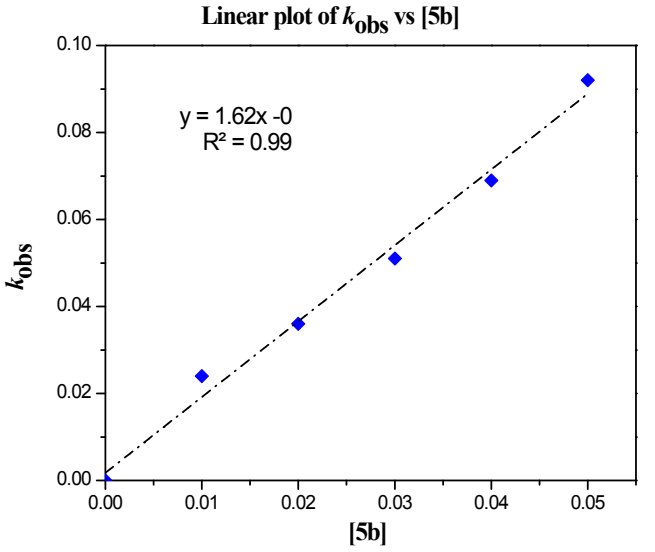

Figure FS36. Kinetics plots of k_{obs} vs [K(THF)$_3$(Ph$_2$P-(Se)N(2-(NO$_2$)-C$_4$H$_4$)] (**5b**) for the polymerization of rac-LA with [LA] = 2.0 M in $CDCl_3$ (1 mL) at 25^{o}C.

Rate of the reaction = $-d[LA]/dt = 0.755\ [La]^1[K(THF)_3(Ph_2P\text{-}(Se)N(2\text{-}(NO_2)\text{-}C_4H_4)]^1$.

[Na(THF)$_3$(Ph$_2$P-(Se)N(2-(F)-C$_4$H$_4$)] (4a) as a catalyst.

A typical kinetics study was conducted to establish the reaction order with respect to monomer and [Na(THF)$_3$(Ph$_2$P-(Se)N(2-(F)-C$_4$H$_4$)] (**4a**) as catalyst. For LA polymerization, *rac* – LA (0.228 g, 2.0 mmol) was added to a solution of **4a** (0.01, 0.02, 0.03, 0.04, 0.05 M) in $CDCl_3$ (1 mL), respectively. The solution was set in the NMR tube at 25^{o}C.At the indicated time intervals; the tube was analyzed by ^{1}H NMR. The rac-LA concentration [LA] was determined by integrating the quartet methine peak of LA at 5.01 ppm and broad singlet methine peak at 5.09-5.20 ppm. As expected, plots of $[LA]_0/[LA]$ vs. time for a wide range of **4a** are linear indicating the usual first order dependence on monomer concentration (Figure FS37). Thus, the rate expression can be written as $-d[LA]/dt = K_{kpp}[La]^1[Na(THF)_3(Ph_2P\text{-}(Se)N(2\text{-}(F)\text{-}C_4H_4)]^x = k[LA]^1$, where $kobs = k_{app}[Na(THF)_3(Ph_2P\text{-}(Se)N(2\text{-}(F)\text{-}C_4H_4)]^x$. A plot of ln(*kobs*) vs. ln[Na(THF)$_3$(Ph$_2$P-(Se)N(2-(F)-C$_4$H$_4$)] (Figure FS38, Table TS6) is linear, indicating the order of [Na(THF)$_3$(Ph$_2$P-(Se)N(2-(F)-C$_4$H$_4$)] is (x = 0.99 or 1) and k_{app} which is 0.619 $M^{-1}m^{-1}$.($\ln k_{app}$ = -0.479).

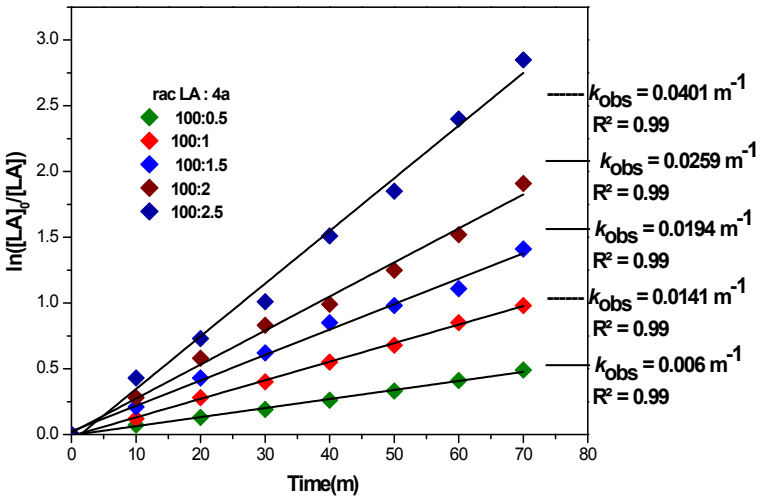

Figure FS37. First order kinetics plots for *rac* LA polymerizations with time in $CDCl_3$ (1 mL) with different concentration of [Na(THF)$_3$(Ph$_2$P-(Se)N(2-(F)-C$_4$H$_4$)] (**4a**) at 25^{o}C.

Table TS6. Kinetics plots of lnk_{obs} vs ln[Na(THF)$_3$(Ph$_2$P-(Se)N(2-(F)-C$_4$H$_4$)] / ln(**4a**) for the polymerization of rac-LA with [LA] = 2.0 M in $CDCl_3$ (1 mL) at 25^{o}C.

S.NO.	[Na(THF)$_3$(Ph$_2$P-(Se)N(2-(F)-C$_4$H$_4$)] (**4a**) (M)	ln k_{obs} (Mm^{-1})
1	-4.6	-5.12

2	-3.912	-4.26
3	-3.506	-3.94
4	-3.218	-3.65
5	-2.813	-3.34

Table TS7. Kinetics plots of k_{obs} vs [Na(THF)$_3$(Ph$_2$P-(Se)N(2-(F)-C$_4$H$_4$)] (**4a**) for the polymerization of *rac*-LA with [LA] = 2.0 M in $CDCl_3$ (1 mL) at 25^{o}C.

S. NO.	[Na(THF)$_3$(Ph$_2$P-(Se)N(2-(F)-C$_4$H$_4$)] (**4a**) (M)	k_{obs} (Mm^{-1})
1	0	0
2	0.01	0.006
3	0.02	0.0141
4	0.03	0.0194
5	0.04	0.0259
6	0.05	0.0351

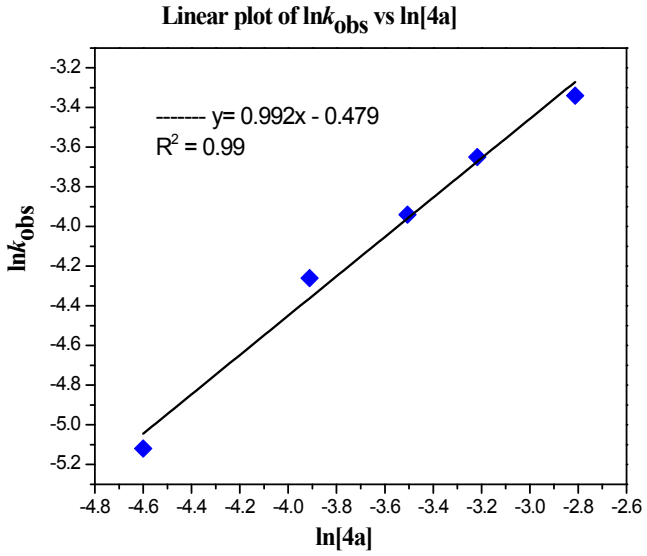

Figure FS38. Kinetics plots of ln k_{obs} vs ln[K(THF)$_3$(Ph$_2$P-(Se)N(2-(F)-C$_4$H$_4$)] / ln (**4a**) for the polymerization of *rac*-LA with [LA] = 2.0 M in $CDCl_3$ (1 mL) at 25^{o}C.

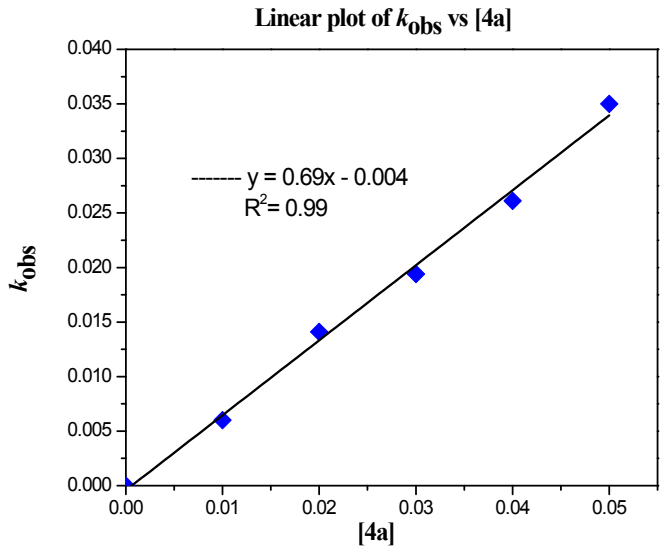

Figure FS39. Kinetics plots of k_{obs} vs [Na(THF)$_3$(Ph$_2$P-(Se)N(2-(F)-C$_4$H$_4$)] (**4a**) for the polymerization of rac-LA with [LA] = 2.0 M in $CDCl_3$ (1 mL) at 25^{o}C.

Rate of the reaction = $-d$[LA]/dt = 0.619 [La]^1[Na(THF)$_3$(Ph$_2$P-(Se)N(2-(F)-C$_4$H$_4$)]^1.

[Na(THF)$_3$(Ph$_2$P-(Se)N(2-(NO$_2$)-C$_4$H$_4$)] (4b) as a catalyst.

A typical kinetics study was conducted to establish the reaction order with respect to monomer and [Na(THF)$_3$(Ph$_2$P-(Se)N(2-(NO$_2$)-C$_4$H$_4$)] (**4b**) as catalyst. For LA polymerization, *rac* – LA (0.228 g, 2.0 mmol) was added to a solution of **4b** (0.01, 0.02, 0.03, 0.04, 0.05 M) in $CDCl_3$ (1 mL), respectively. The solution was set in the NMR tube at 25^{o}C.At the indicated time intervals; the tube was analyzed by ^{1}H NMR. The *rac*-LA concentration [LA] was determined by integrating the quartet methine peak of LA at 5.01 ppm and broad singlet methine peak at 5.09-5.20 ppm. As expected, plots of [LA]$_0$/[LA] vs. time for a wide range of **4b** are linear indicating the usual first order dependence on monomer concentration (Figure FS40). Thus, the rate expression can be written as $-d$[LA]/dt = K_{kpp}[La]^1[Na(THF)$_3$(Ph$_2$P-(Se)N(2-(NO$_2$)-C$_4$H$_4$)]^x = k[LA]^1, where $kobs$ = k_{app}[Na(THF)$_3$(Ph$_2$P-(Se)N(2-(NO$_2$)-C$_4$H$_4$)]^x. A plot of ln($kobs$) vs. ln[Na(THF)$_3$(Ph$_2$P-(Se)N(2-(NO$_2$)-C$_4$H$_4$)] (Figure FS41, Table TS8) is linear, indicating the order of [Na(THF)$_3$(Ph$_2$P-(Se)N(2-(NO$_2$)-C$_4$H$_4$)] is (x = 0.82 or 1) and k_{app} which is 0.755 M^{-1}m^{-1}.(lnk_{app} = -0.28).

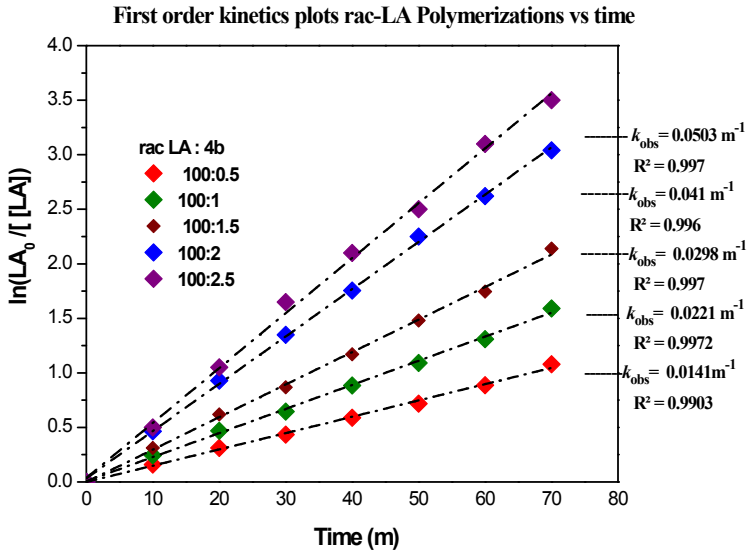

Figure FS40. First order kinetics plots for *rac* LA polymerizations with time in $CDCl_3$ (1 mL) with different concentration of [Na(THF)$_3$(Ph$_2$P-(Se)N(2-(NO$_2$)-C$_4$H$_4$)] (**4b**) at 25^{o}C.

Table TS8. Kinetics plots of lnk_{obs} vs ln[Na(THF)$_3$(Ph$_2$P-(Se)N(2-(NO$_2$)-C$_4$H$_4$)]/ln(**4b**) for the polymerization of rac-LA with [LA] = 2.0 M in $CDCl_3$ (1 mL) at 25^{o}C.

S.NO.	[Na(THF)$_3$(Ph$_2$P-(Se)N(2-(NO$_2$)-C$_4$H$_4$)] (**4b**) (M)	ln k_{obs} (Mm^{-1})
1	-4.6	-4.26
2	-3.912	-3.812
3	-3.506	-3.513
4	-3.218	-3.19
5	-2.813	-2.99

Table TS9. Kinetics plots of k_{obs} vs [Na(THF)$_3$(Ph$_2$P-(Se)N(2-(NO$_2$)-C$_4$H$_4$)] (**4b**) for the polymerization of *rac*-LA with [LA] = 2.0 M in $CDCl_3$ (1 mL) at 25^{o}C.

S. NO.	[Na(THF)$_3$(Ph$_2$P-(Se)N(2-(NO$_2$)-C$_4$H$_4$)] (**4b**) (M)	k_{obs} (Mm^{-1})
1	0	0
2	0.01	0.0141
3	0.02	0.0221

4	0.03	0.0298
5	0.04	0.041
6	0.05	0.0503

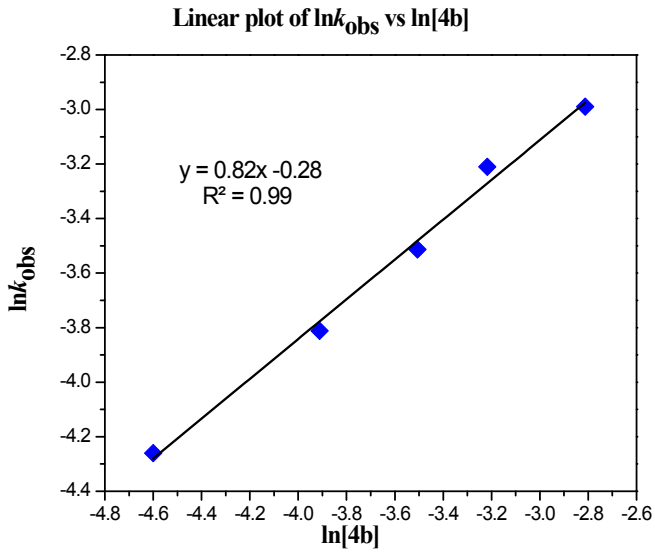

Figure FS41. Kinetics plots of ln k_{obs} vs ln[Na(THF)$_3$(Ph$_2$P-(Se)N(2-(NO$_2$)-C$_4$H$_4$)]/ ln (**4b**) for the polymerization of rac-LA with [LA] = 2.0 M in $CDCl_3$ (1 mL) at 25^{o}C.

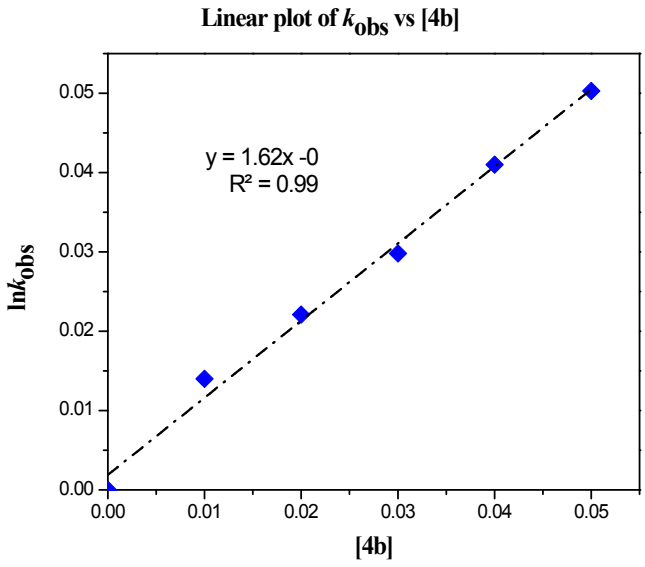

Figure FS42. Kinetics plots of k_{obs} vs [Na(THF)$_3$(Ph$_2$P-(Se)N(2-(NO$_2$)-C$_4$H$_4$)] (**4b**) for the polymerization of *rac*-LA with [LA] = 2.0 M in $CDCl_3$ (1 mL) at 25^{o}C.

Rate of the reaction = $-d$[LA]/dt = 0.755 [La]^1[Na(THF)$_3$(Ph$_2$P-(Se)N(2-(NO$_2$)-C$_4$H$_4$)]^1.

S.No	Catalyst	*rac*-LA : catalyst	k_{obs} in (Mm^{-1})
1	[Na(THF)$_3$(Ph$_2$P-(Se)N(2-(F)-C$_4$H$_4$)](**4a**)	100:0.5	0.006
2	[Na(THF)$_3$(Ph$_2$P-(Se)N(2-(NO$_2$)-C$_4$H$_4$)](**4b**)	100:0.5	0.0141
3	[K(THF)$_3$(Ph$_2$P-(Se)N(2-(F)-C$_4$H$_4$)] (**5a**)	100:0.5	0.0143
4	[K(THF)$_3$(Ph$_2$P-(Se)N(2-(NO$_2$)-C$_4$H$_4$)] (**5b**)	100:0.5	0.0256
5	[Na(THF)$_3$(Ph$_2$P-(Se)N(2-(F)-C$_4$H$_4$)](**4a**)	100:1	0.0141
6	[Na(THF)$_3$(Ph$_2$P-(Se)N(2-(NO$_2$)-C$_4$H$_4$)](**4b**)	100:1	0.0221
7	[K(THF)$_3$(Ph$_2$P-(Se)N(2-(F)-C$_4$H$_4$)] (**5a**)	100:1	0.0279
8	[K(THF)$_3$(Ph$_2$P-(Se)N(2-(NO$_2$)-C$_4$H$_4$)] (**5b**)	100:1	0.036

Table TS10: Comparison of rate constants for polymerization of *rac*-LA with various concentration of [Na(THF)$_3$(Ph$_2$P-(Se)N(2-(F)-C$_4$H$_4$)](**4a**), [Na(THF)$_3$(Ph$_2$P-(Se)N(2-(NO$_2$)-C$_4$H$_4$)] (**4b**), [K(THF)$_3$(Ph$_2$P-(Se)N(2-(F)-C$_4$H$_4$)] (**5a**), [K(THF)$_3$(Ph$_2$P-(Se)N(2-(NO$_2$)-C$_4$H$_4$)] (**5b**) as a catalyst.

9	$[Na(THF)_3(Ph_2P\text{-}(Se)N(2\text{-}(F)\text{-}C_4H_4)]$(**4a**)	100:1.5	0.0194
10	$[Na(THF)_3(Ph_2P\text{-}(Se)N(2\text{-}(NO_2)\text{-}C_4H_4)]$(**4b**)	100:1.5	0.0298
11	$[K(THF)_3(Ph_2P\text{-}(Se)N(2\text{-}(F)\text{-}C_4H_4)]$ (**5a**)	100:1.5	0.0394
12	$[K(THF)_3(Ph_2P\text{-}(Se)N(2\text{-}(NO_2)\text{-}C_4H_4)]$ (**5b**)	100:1.5	0.051
13	$[Na(THF)_3(Ph_2P\text{-}(Se)N(2\text{-}(F)\text{-}C_4H_4)]$(**4a**)	100:2	0.0259
14	$[Na(THF)_3(Ph_2P\text{-}(Se)N(2\text{-}(NO_2)\text{-}C_4H_4)]$(**4b**)	100:2	0.041
15	$[K(THF)_3(Ph_2P\text{-}(Se)N(2\text{-}(F)\text{-}C_4H_4)]$ (**5a**)	100:2	0.0562
16	$[K(THF)_3(Ph_2P\text{-}(Se)N(2\text{-}(NO_2)\text{-}C_4H_4)]$ (**5b**)	100:2	0.069
17	$[Na(THF)_3(Ph_2P\text{-}(Se)N(2\text{-}(F)\text{-}C_4H_4)]$(**4a**)	100:2	0.0351
18	$[Na(THF)_3(Ph_2P\text{-}(Se)N(2\text{-}(NO_2)\text{-}C_4H_4)]$(**4b**)	100:2	0.0503
19	$[K(THF)_3(Ph_2P\text{-}(Se)N(2\text{-}(F)\text{-}C_4H_4)]$ (**5a**)	100:2.5	0.0767
20	$[K(THF)_3(Ph_2P\text{-}(Se)N(2\text{-}(NO_2)\text{-}C_4H_4)]$ (**5b**)	100:2.5	0.092
All reactions were carried out with 100 equiv. of monomer (2 M) in $CDCl_3$ at 25ºC and followed to 99% conversion by ^1H NMR spectroscopy.			

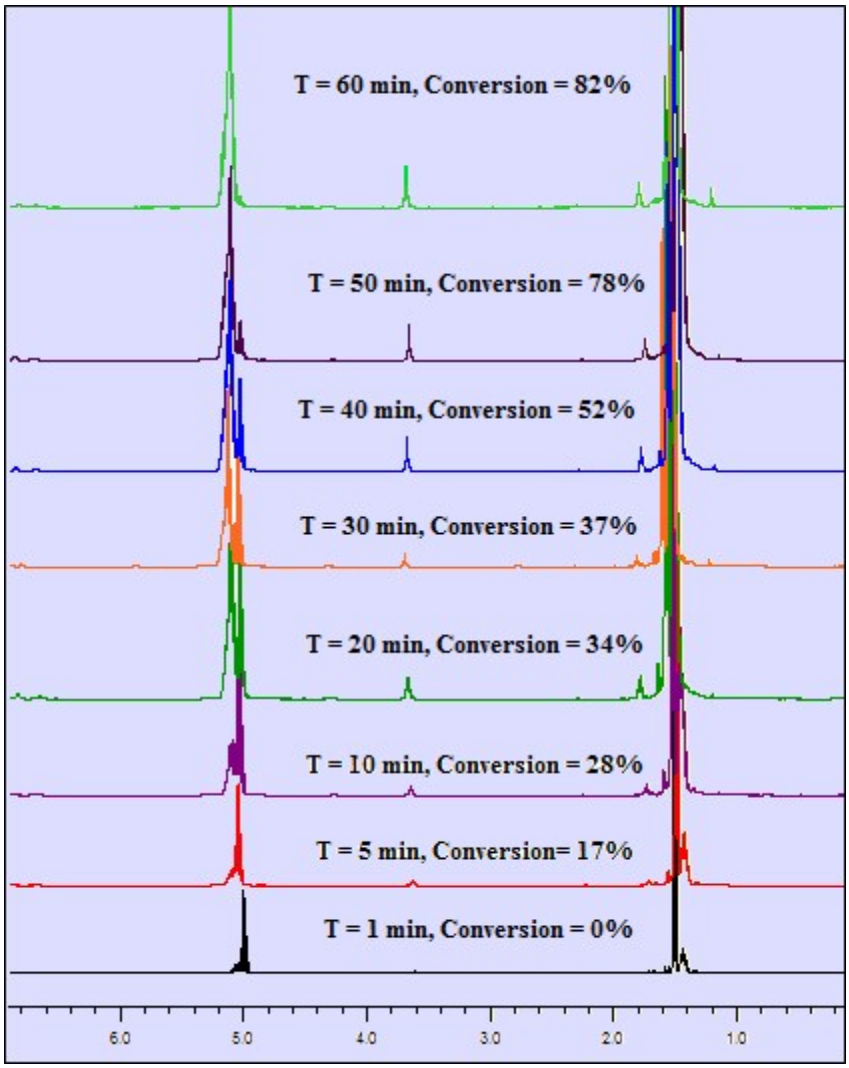

Figure FS43. Stack of ^{1}H NMR spectra for the kinetic study of the polymerization of 400 eq. of *rac*-LA using **5b**. Conditions: [rac-LA] = 2M, $CDCl_3$, 25^{o}C.

Kinetics study in presence of benzyl alcohol as external initiator.

[K(THF)$_3$(Ph$_2$P-(Se)N(2-(NO$_2$)-C$_4$H$_4$)] (5b) as a catalyst in presence of BnOH.

A typical kinetics study was conducted to establish the reaction order with respect monomer [K(THF)$_3$(Ph$_2$P-(Se)N(2-(NO$_2$)-C$_4$H$_4$)] (**5b**) and benzyl alcohol . For LA polymerization, rac – LA

(0.228 g, 2.0 mmol) and benzyl alcohol (0.02 mmol) was added to a solution of **5b** (0.01, 0.02, 0.03, 0.04, 0.05 M) in $CDCl_3$ (1 mL), respectively. The solution was set in the NMR tube at 25°C.At the indicated time intervals; the tube was analyzed by ^1H NMR. The rac-LA concentration [LA] was determined by integrating the quartet methine peak of LA at 5.01 ppm and broad singlet methine peak at 5.09-5.20 ppm. As expected, plots of $[LA]_0/[LA]$ vs. time for a wide range of **5b** are linear indicating the usual first order dependence on monomer concentration (Figure FS44). Thus, the rate expression can be written as $-d[LA]/dt = k_{app}[La]^1[K(THF)_3(Ph_2P\text{-}(Se)N(2\text{-}(NO_2)\text{-}C_4H_4)]^x = k_{obs}[LA]^1$, where $k_{obs} = k_{app}[K(THF)_3(Ph_2P\text{-}(Se)N(2\text{-}(F)C_4H_4)]^x$. A plot of $\ln(k_{obs})$ vs. $\ln[K(THF)_3(Ph_2P\text{-}(Se)N(2\text{-}(NO_2)\text{-}C_4H_4)]$ (Figure FS 45) is linear, indicating the order of $[K(THF)_3(Ph_2P\text{-}(Se)N(2\text{-}(NO_2)\text{-}C_4H_4)]$ is (x = 0.82) . From the kinetics data it clearly indicated that there was no change in values for rate constant for the ROP of rac-LA catalyzed by **5a** in presence of benzyl alcohol.(Figure FS44-FS46).

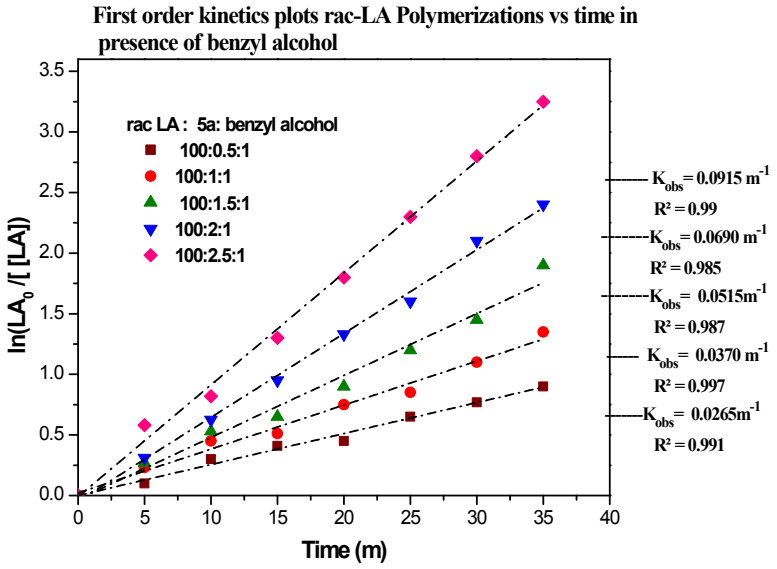

Figure FS44. First order kinetics plots for rac LA polymerizations with time in $CDCl_3$ (1 mL) with different concentration of $[K(THF)_3(Ph_2P\text{-}(Se)N(2\text{-}(NO_2)\text{-}C_4H_4)]$ (**5b**) at 25°C having having *rac* – LA (0.228 g, 2.0 mmol) and benzyl alcohol (0.01 mmol).

Table TS11. Kinetics plots of $\ln k_{obs}$ vs $\ln[K(THF)_3(Ph_2P\text{-}(Se)N(2\text{-}(NO_2)\text{-}C_4H_4)]/\ln$(**5b**) for the polymerization of rac-LA with [LA] = 2.0 M in $CDCl_3$ (1 mL) at 25°C.

S.NO.	$\ln[K(THF)_3(Ph_2P\text{-}(Se)N(2\text{-}(NO_2)\text{-}C_4H_4)]$ /ln(**5b**) (M)	$\ln k_{obs}$ (Mm^{-1})
1	-4.6	-3.63

2	-3.912	-3.30
3	-3.506	-2.97
4	-3.218	-2.67
5	-2.813	-2.39

Table TS12. Kinetics plots of k_{obs} [K(THF)$_3$(Ph$_2$P-(Se)N(2-(NO$_2$)-C$_4$H$_4$)] (**5b**) for the polymerization of rac-LA with [LA] = 2.0 M in $CDCl_3$ (1 mL) at 25^{o}C.

S. NO.	[K(THF)$_3$(Ph$_2$P-(Se)N(2-(NO$_2$)-C$_4$H$_4$)] (**5b**) (M)	k_{obs} (Mm^{-1})
1	0	0
2	0.01	0.0265
3	0.02	0.0370
4	0.03	0.0515
5	0.04	0.0690
6	0.05	0.0915

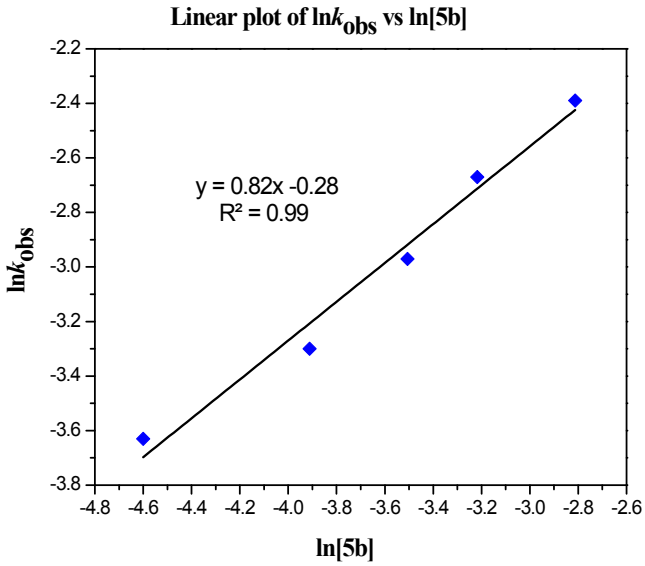

Figure FS45. Kinetics plots of ln k_{obs} vs ln[K(THF)$_3$(Ph$_2$P-(Se)N(2-(NO$_2$)-C$_4$H$_4$)]/ ln (**5b**) for the polymerization of *rac*-LA with [LA] = 2.0 M in $CDCl_3$ (1 mL) at 25^{o}C.

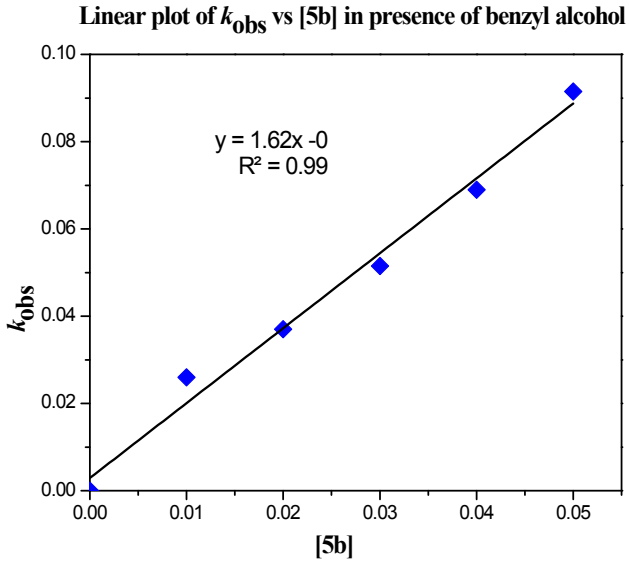

Figure FS46. Kinetics plots of k_{obs} vs [K(THF)$_3$(Ph$_2$P-(Se)N(2-(NO$_2$)-C$_4$H$_4$)] (**5b**) for the polymerization of rac-LA with [LA] = 2.0 M in $CDCl_3$ (1 mL) at 25^{o}C.

Rate of the reaction = $-d[LA]/dt = 0.755\ [La]^1[K(THF)_3(Ph_2P\text{-}(Se)N(2\text{-}(NO_2)\text{-}C_4H_4)]^1$.

Several reactions were conducted varying the concentration of benzyl alcohol (0.01, 0.02, 0.04. 0.08, 0.1 M) in wide range and keeping the concentration of catalyst **5b (**0.02M**)** and rac-LA (0.228 g, 2.0 mmol) constant. The plot of $[LA]_0/[LA]$ vs. time for a wide range of **5b** are linear indicating the usual first order dependence on monomer concentration (Figure FS47) but in all cases the value of rate constant kobs remain same. This lack of dependence on benzylalcohol concentration confirms its zero-order contribution to the rate law (Figure FS547-49). So Kinetics study prove that polymerization reaction does not depends on external initiator and our catalyst itself act as an initiator for ROP of *rac*-LA.

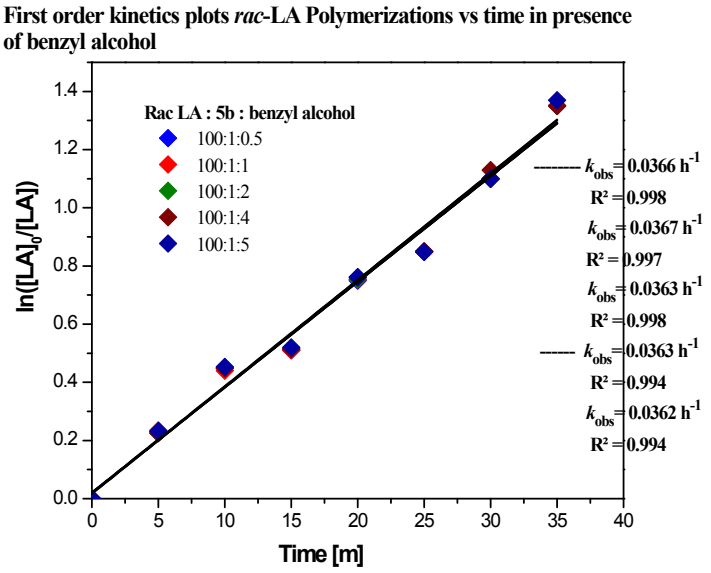

Figure FS47. First order kinetics plots for rac- LA polymerizations with time in $CDCl_3$ (1 mL) with different concentration of Benzyl alcohol at 25°C having rac – LA (0.228 g, 2.0 mmol) and $[K(THF)_3(Ph_2P\text{-}(Se)N(2\text{-}(NO_2)\text{-}C_4H_4)]$ (**5b**) (0.02 mmol).

Table TS13. Kinetics plots of $\ln k_{obs}$ vs ln[benzyl alcohol] for the polymerization of *rac*-LA with [LA] = 2.0 M and $[K(THF)_3(Ph_2P\text{-}(Se)N(2\text{-}(NO_2)\text{-}C_4H_4)]$ (**5b**) (0.02 mmol) in $CDCl_3$ (1 mL) at 25°C.

S.NO.	ln Benzyl alcohol(M)	ln k_{obs} (Mh^{-1})
1	-4.60	-3.315
2	-3.91	-3.32
3	-3.21	-3.32
4	-2.52	-3.30
5	-2.30	-3.31

Table TS14. Kinetics plots of k_{obs} vs [benzyl alcohol] for the polymerization of *rac*-LA with [LA] = 2.0 M and $[K(THF)_3(Ph_2P\text{-}(Se)N(2\text{-}(NO_2)\text{-}C_4H_4)]$ (**5b**) (0.02 mmol) in $CDCl_3$ (1 mL) at 25°C.

S.NO.	Benzyl alcohol(M)	k_{obs} (Mh^{-1})
1	0.01	0.0362
2	0.02	0.0363
3	0.04	0.0363
4	0.08	0.0367
5	0.1	0.0366

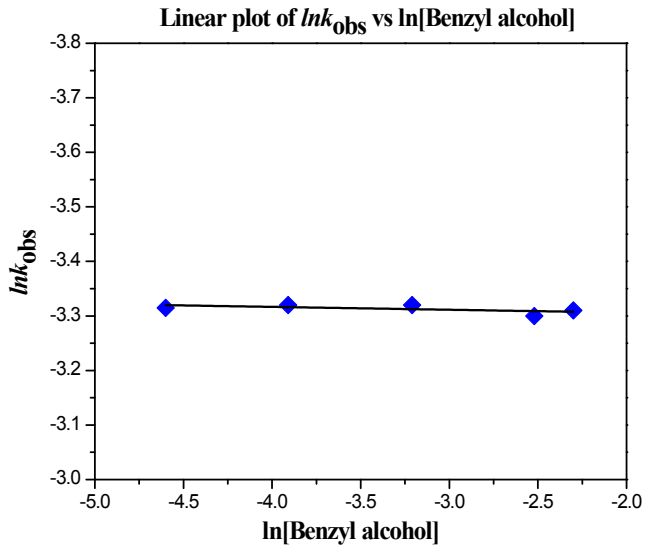

Figure FS48. Kinetics plots of ln k_{obs} vs ln[benzyl alcohol] for the polymerization of *rac*-LA with [LA] = 2.0 M and $[K(THF)_3(Ph_2P\text{-}(Se)N(2\text{-}(NO_2)\text{-}C_4H_4)]$ (**5b**) (0.02 mmol) in $CDCl_3$ (1 mL) at 25°C.

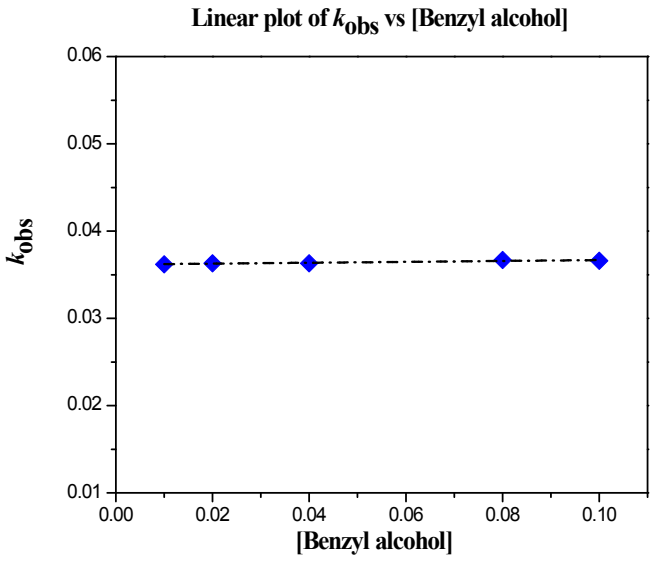

Figure FS49. Kinetics plots of k_{obs} vs [benzyl alcohol] for the polymerization of rac-LA with [LA] = 2.0 M and $[K(THF)_3(Ph_2P\text{-}(Se)N(2\text{-}(NO_2)\text{-}C_4H_4)]$ (**5b**) (0.02 mmol) in $CDCl_3$ (1 mL) at 25°C.

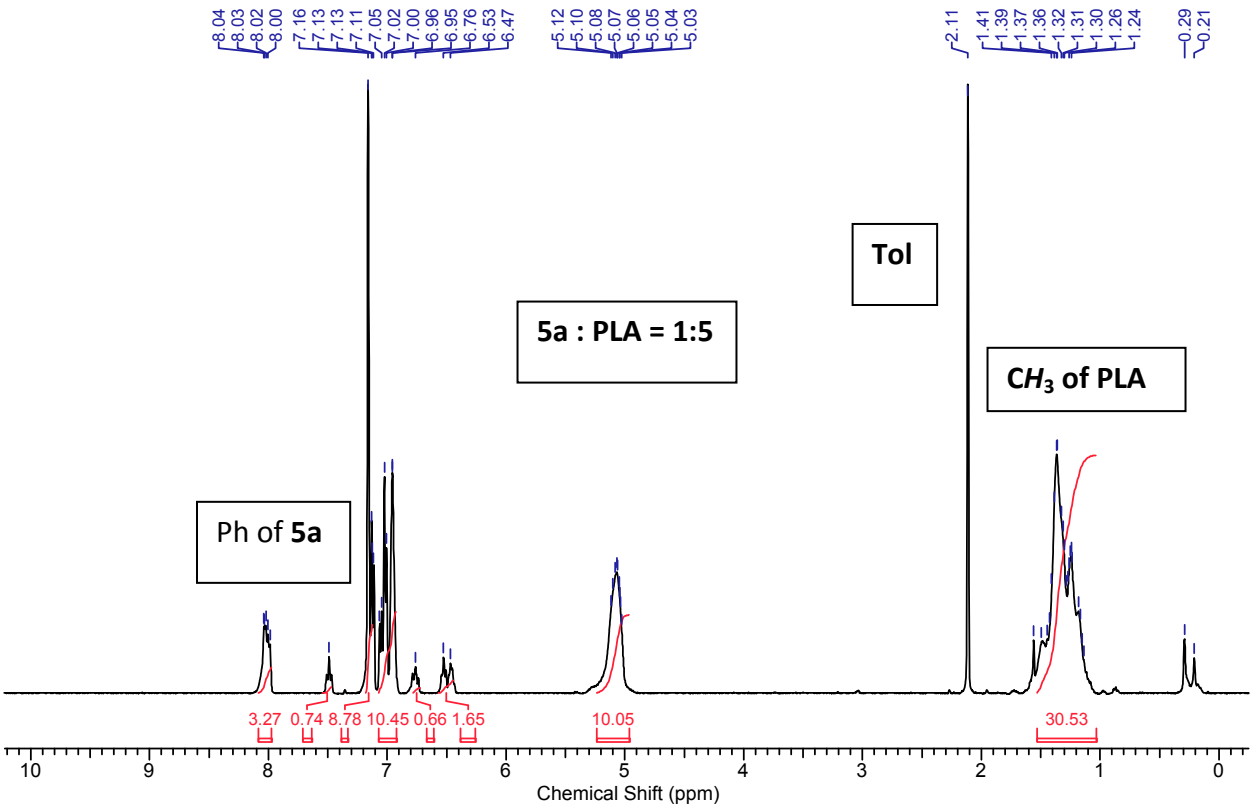

Figure FS50. ^{1}H NMR spectrum in C_6D_6 for *rac*-LA catalyzed by (**5a**) having (*rac*-LA : 5a = 5:1 ratio). Catalyst is present in equivalent amount with polymer moiety, which prove that catalyst itself initiate the polymerization process.

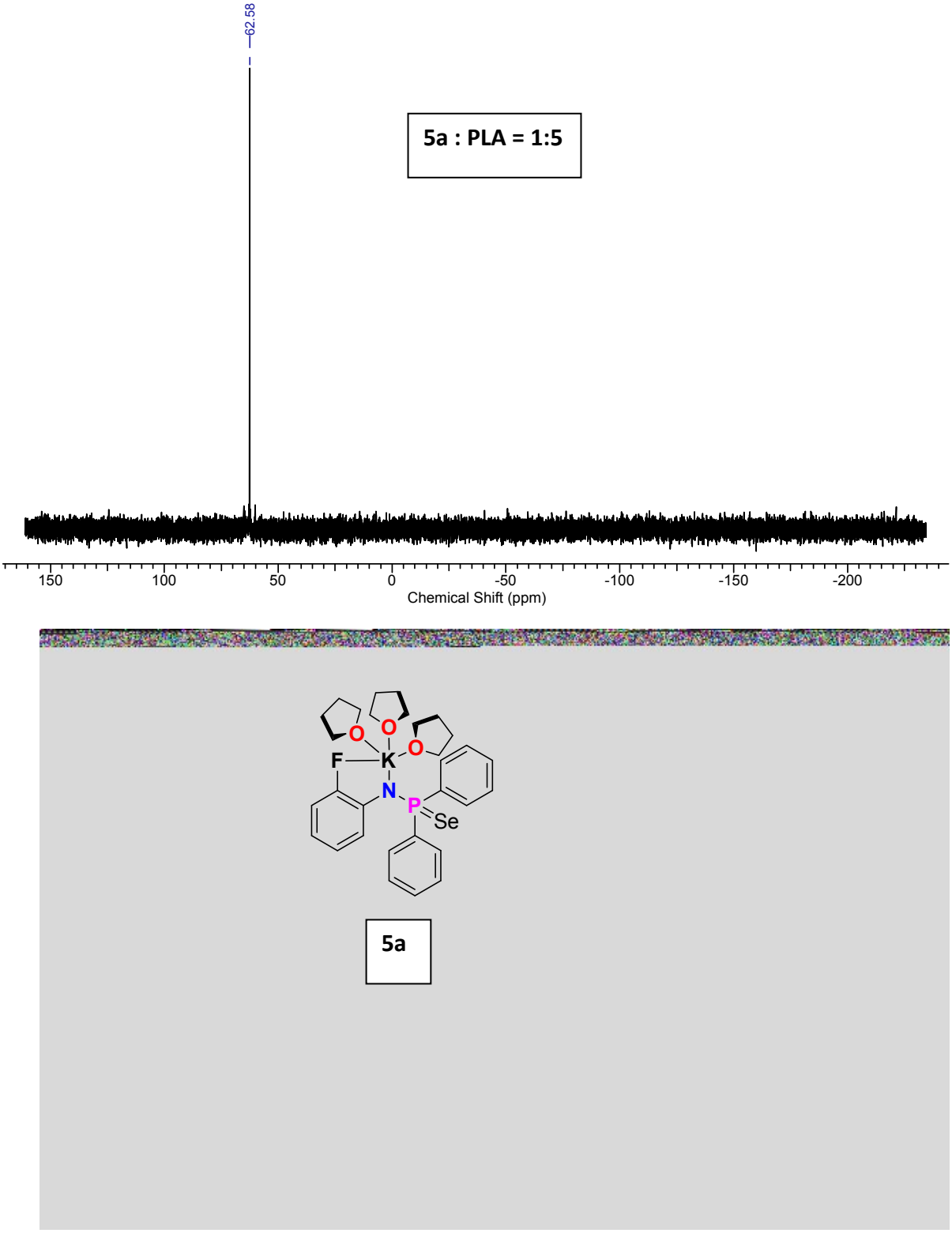

Figure FS51. ^{31}P NMR spectrum in C_6D_6 for rac-LA catalyzed by (**5a**) having (*rac*-LA : 5a = 5:1 ratio) along with Alkali metal complexe **5a**. The former peak is indicating the formation new selenium-carbon bond during the ring opening of the *rac*-LA initiated by potassium complex **5a** which is different than that of complex **5a**.

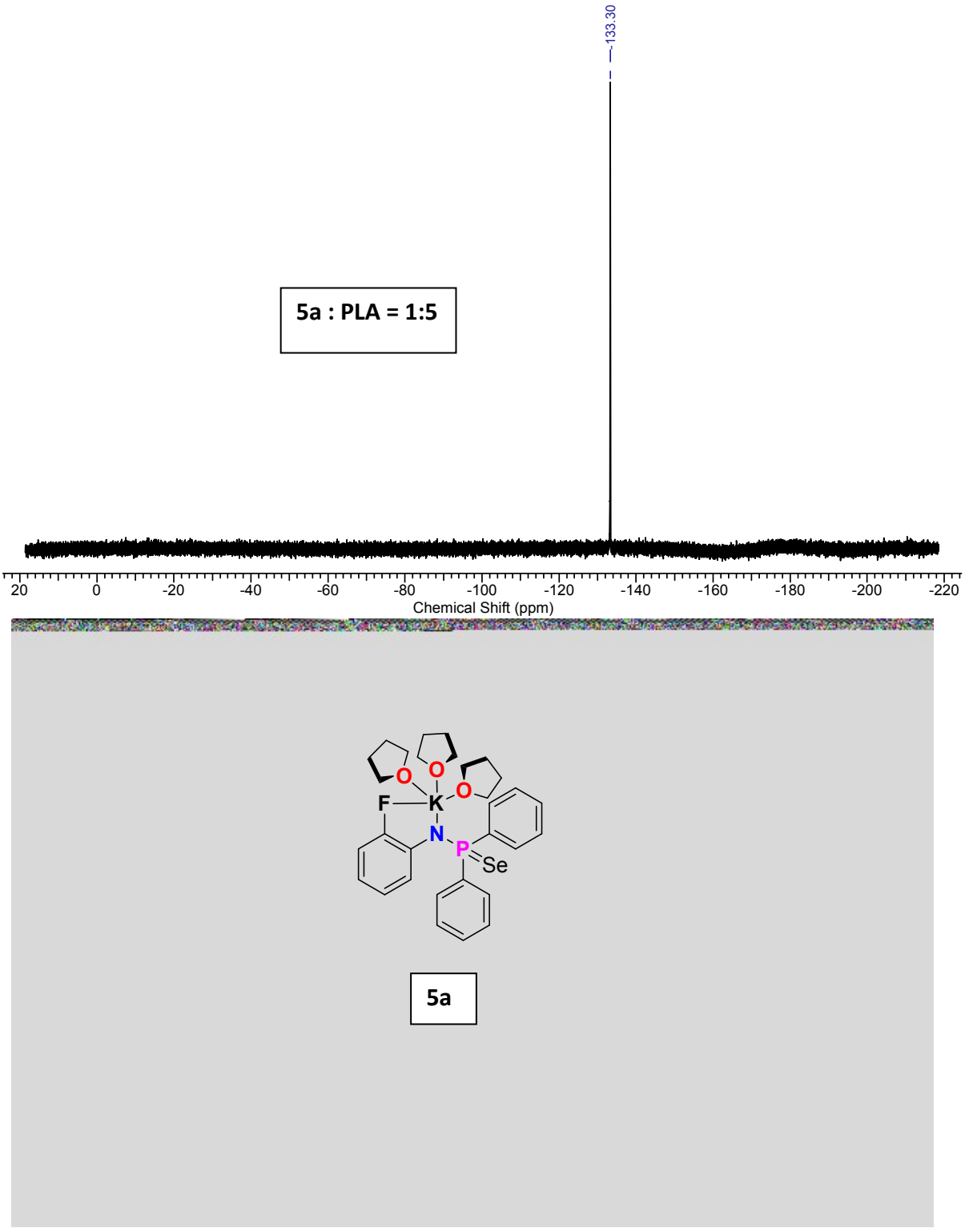

Figure FS52: ^{19}F NMR spectra in C_6D_6 for *rac*-LA catalyzed by (**5a**) having (*rac*-LA : 5a = 5:1 ratio) along with Alkali metal complexe **5a**. The former peak is indicating the formation new selenium-carbon bond during the ring opening of the *rac*-LA initiated by potassium complex **5a** which is different than the complex **5a**.

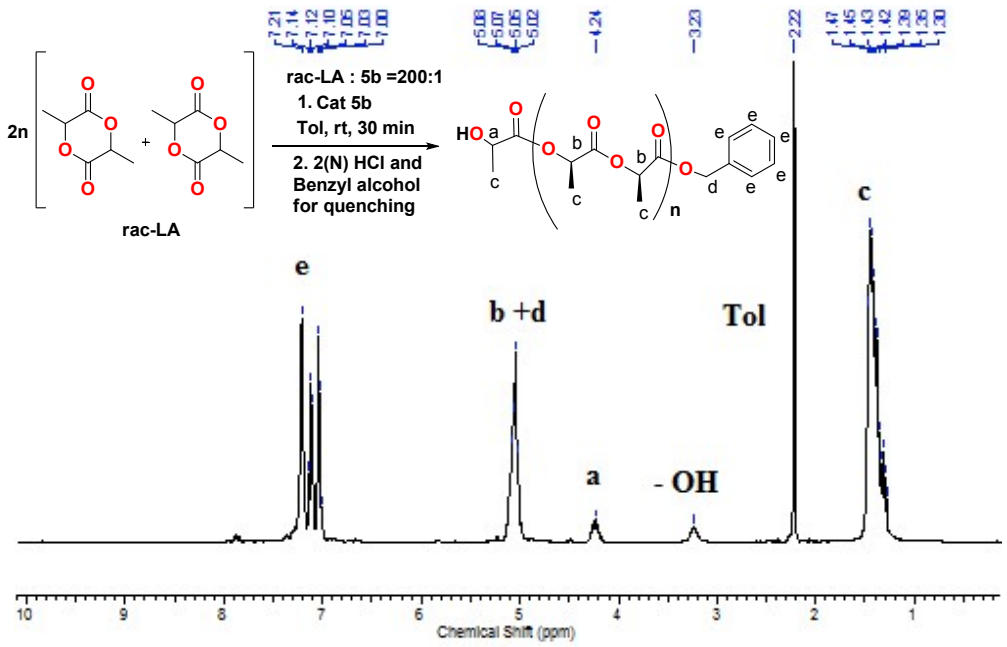

Figure FS53. ^{1}H NMR spectrum of PLA prepared by catalyst **5b** in presence of benzylalcohol as a as well as terminator ($[LA]_0/[M]_0$ = 100:1).

Characterization Data

Calculation of P_r / P_m Values

Several mechanisms have been well established for the ROP of lactide including anionic, pseudo-anionic (general base catalysis), coordination–insertion ROP and monomer-activated mechanism. In all cases, stereocontrol can be realized by two different mechanisms, chain end control and enantiomorphic site control. In a chain end controlled mechanism, the chirality of the propagating chain end bound to the catalyst determines the chirality of the next monomer to be inserted; this is generally associated with hindered and achiral catalyst systems so chirality of the polymer depends upon on the chirality of the monomer. In case of Enantiomorphic site control, chirality of the polymer demonstrated depends on the chirality of the catalyst, and not the chain end, dictates the chirality of the next insertion. Due to the significant steric bulk of the phosphoimino ligands and the achiral natures of the alkaline earth metal based complexes they used in this manuscript, these catalysts are usually considered to be capable of stereocontrol in the polymerization of *rac*-lactide via a chain end control mechanism and a Bernoullian statistics mode was usually employed to calculate P_m / P_r values. P_m / P_r is the probability of mesomeric / racemic linkages between monomer units determined from the methine region of the homonuclear decoupled ^{1}H NMR spectrum. P_r can also be expressed in terms of the enchainment rate constants: $P_r = k_{R/SS}/(k_{R/SS}+k_{R/RR}) = k_{S/RR}/(k_{S/RR}+k_{S/SS})$. The expressions for the tetrad concentrations in terms of P_r, assuming Bernoullian statistics and the absence of transesterification, are as follows:

tetrad Probability(*rac*-lactide)

[*mmm*] $P_m^2 + (1-P_m)P_m/2$
[*mmr*] $(1-P_m)P_m/2$
[*rmm*] $(1-P_m)P_m/2$
[*rmr*] $(1-P_m)^2/2$
[*rrr*] 0
[*rrm*] 0
[*mrr*] 0
[*mrm*] $[(1-P_m)^2 + (1-P_m)P_m]/2$

Most stereoselective ROP of *rac*-lactide in literatures involve only one single-site catalyst and the calculation of P_m / P_r usually use single-state statistic model even if in the case when *rac*-catalysts were used in ROP of *rac*-lactide.

Details characterization data of Isotatic PLA formed by catalyst by (4b) at 90% conversion at 25 °C in toluene. (PLA: 4b = 300: 0.01 having Mn = 37.4 KDa, Mw = 54.7 KDa and PDI = 1.46).

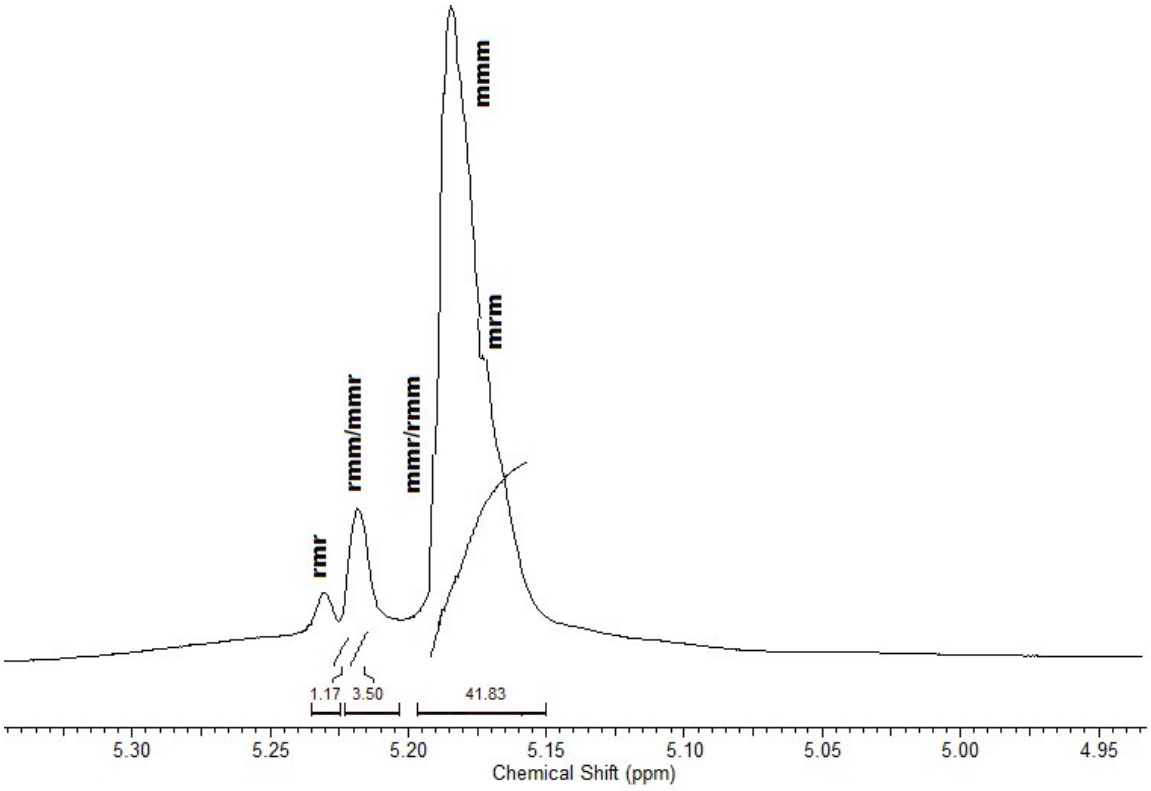

Figure FS54. $^1H\{^1H\}$ NMR spectra ($CDCl_3$, 25 °C) of methine regions for ROP of rac-LA

Analysis

Equations used:

[mmm] = $(Pm)^2 + Pr\ Pm/2$
[mmr] = $Pr\ Pm/2$
[rmm] = $Pr\ Pm/2$
[rmr] = $(Pr)^2/2$
[mrm] = $((Pr)^2 + PrPm)/2$

$Pr = \sqrt{(1.17/1.17+3.50+41.83)} = 0.22$

$Pm = 2\ (3.99/55.89) / 0.189 = 0.69$

*Effectively only these two equations are used in the calculations as the other peaks cannot be accurately integrated.

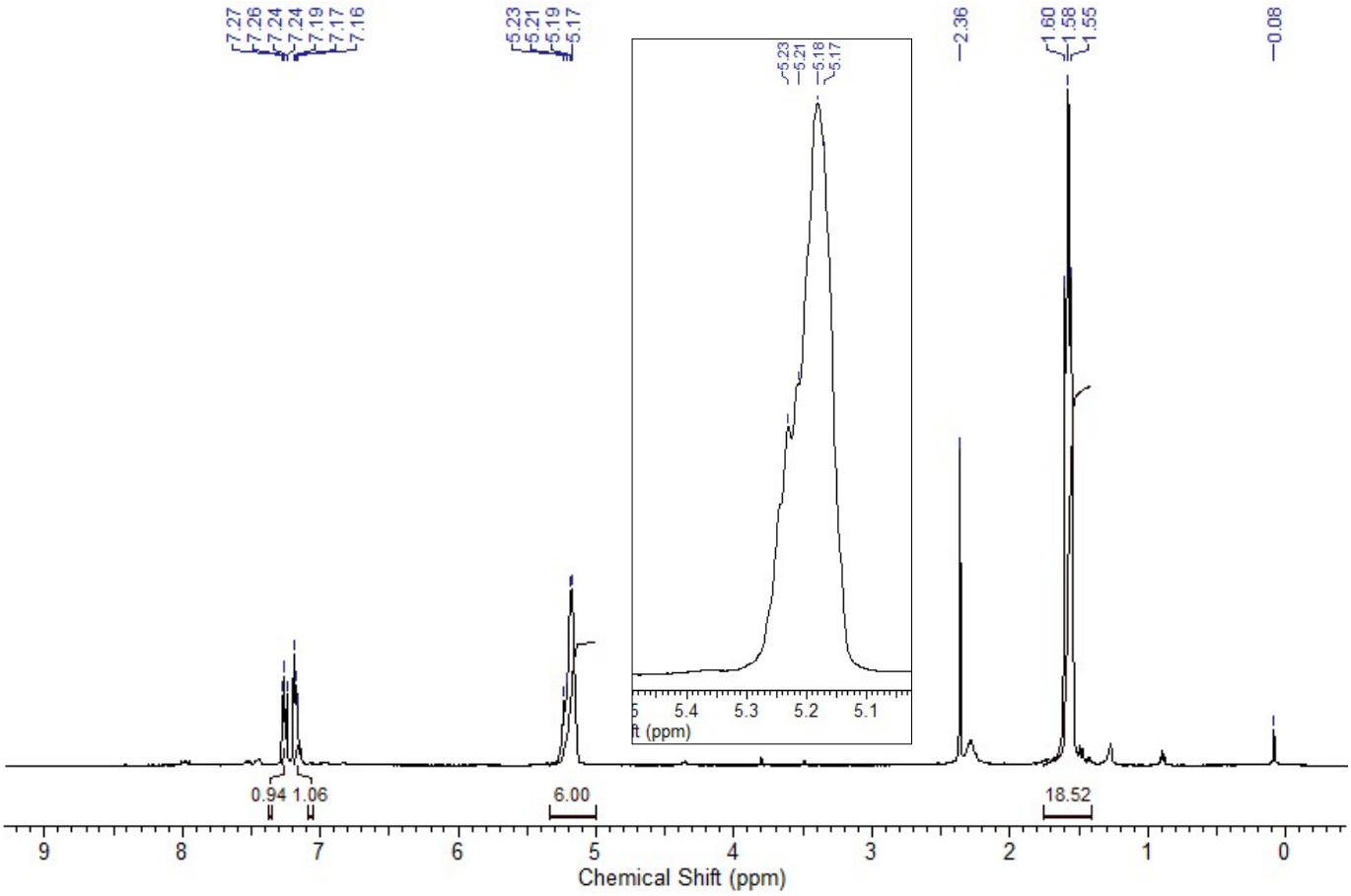

Figure FS55. ^{1}H NMR spectra ($CDCl_3$, 25 °C) of methine regions for ROP of rac-LA.

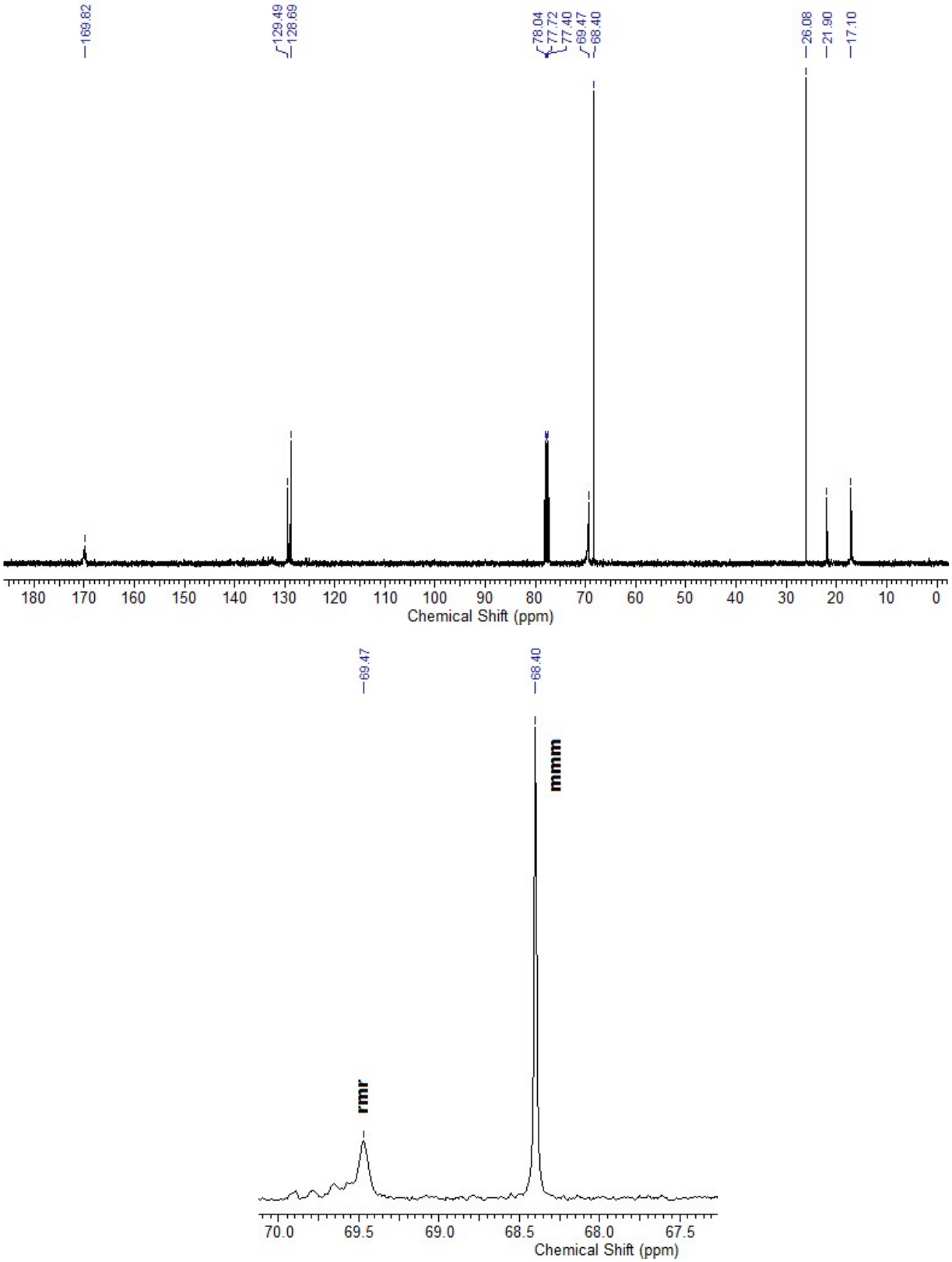

Figure FS56. ^{13}C NMR spectra ($CDCl_3$, 25 °C) of methine regions for ROP of rac-LA.

Details characterization data of Isotatic PLA formed by catalyst by (4b) at 95% conversion at 25 °C in toluene. (PLA: 4b = 100: 0.01 having Mn = 13.6 KDa, Mw = 19.1 KDa and PDI = 1.39).

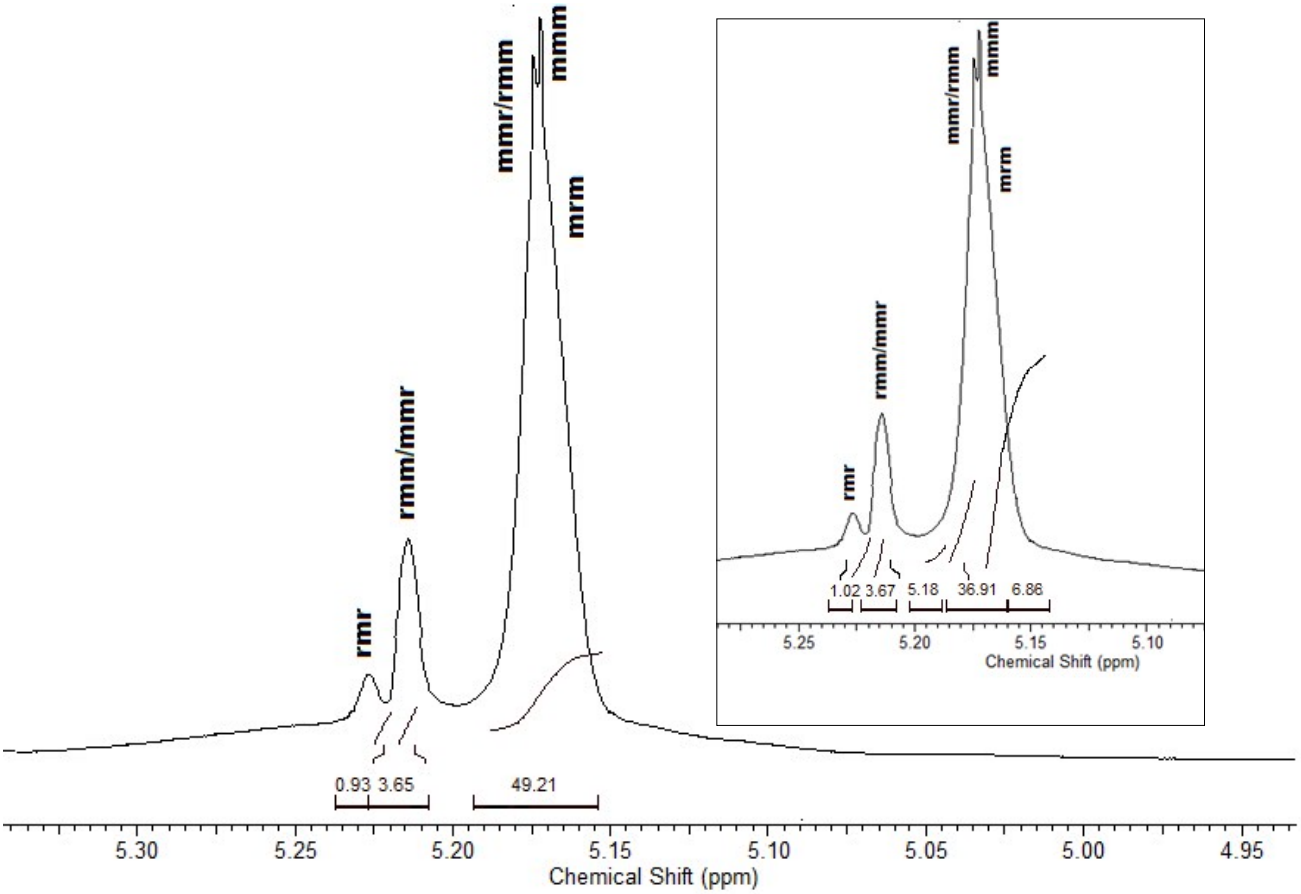

Figure FS 57. $^{1}H\{^{1}H\}$ NMR spectra ($CDCl_3$, 25 °C) of methine regions for ROP of rac-LA.

Analysis

Peak	Integration	Pm

[mmm] = Pm(Pm+1)/2
[mmr] = Pm(1 - Pm)/2
[rmm] = Pm (1 - Pm)/2
[rmr] = $(1 - Pm)^2/2$
[mrm] = (1 - Pm)/2

[mmm]	**0.68**	**0.77**
[mmr]	**0.096**	**0.74**
[rmm]	**0.067**	**0.84**
[rmr]	**0.0185**	**0.80**
[mrm]	**0.127**	**0.75**
Avarage		**0.78**

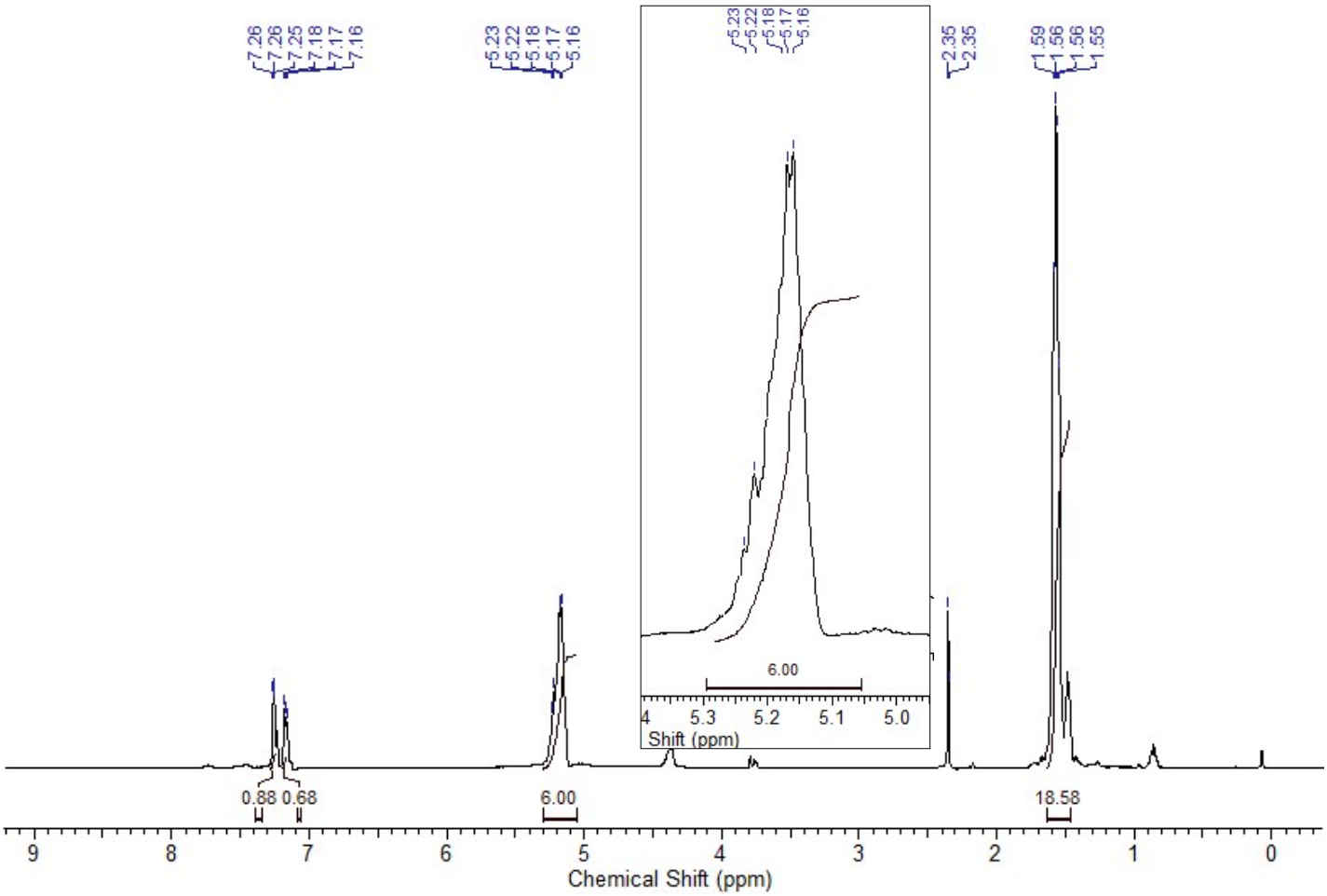

Figure FS58. ^{1}H NMR spectra ($CDCl_3$, 25 °C) of methine regions for ROP of rac-LA.

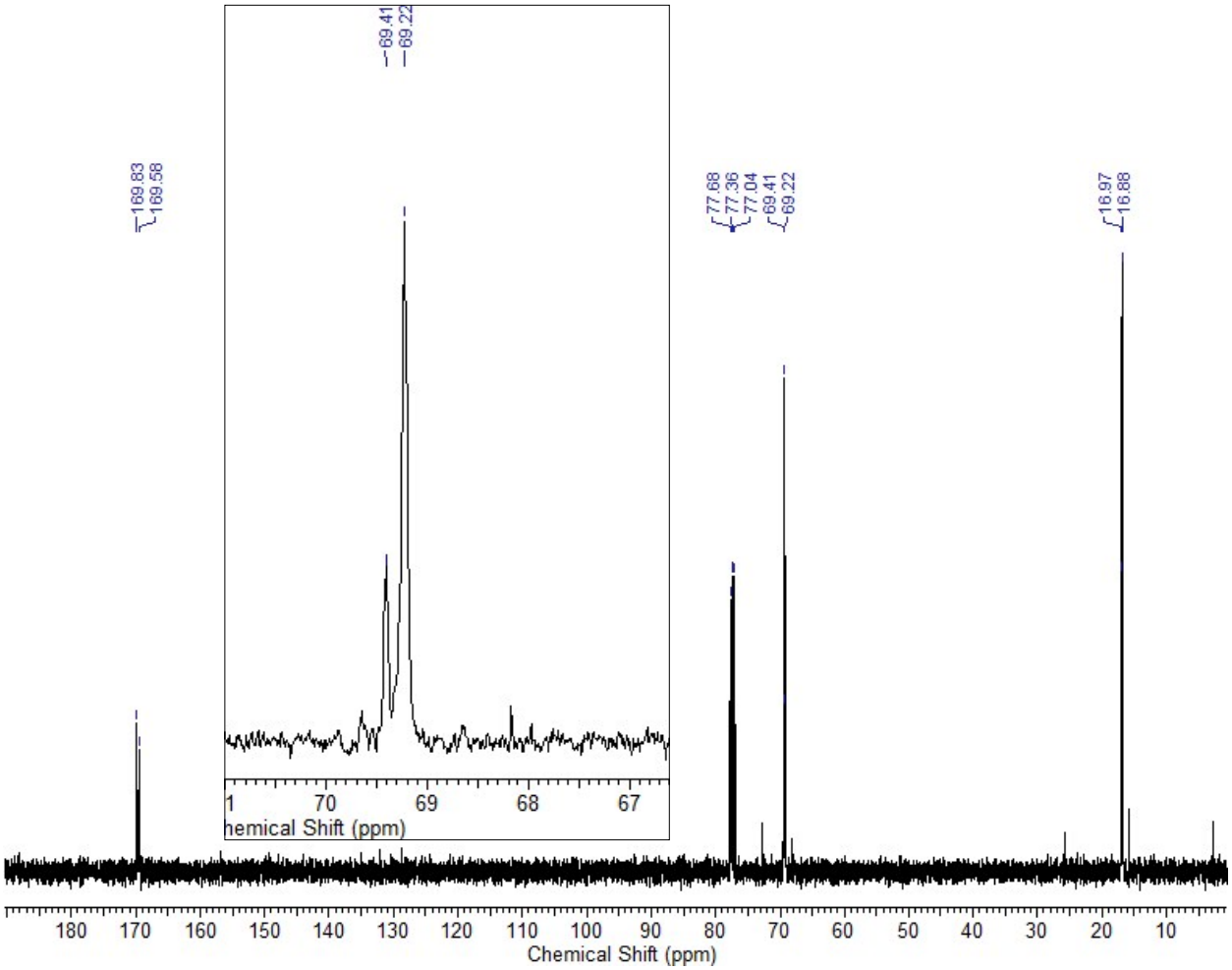

Figure FS59. Homocoupling ^{13}C NMR spectrum for ROP of rac-LA.

Details characterization data of Isotatic PLA formed by catalyst by (4a) at 88% conversion at 25 °C in toluene. (PLA: 4a = 100: 0.01 having Mn = 11.3 KDa, Mw = 15.6 KDa and PDI = 1.31).

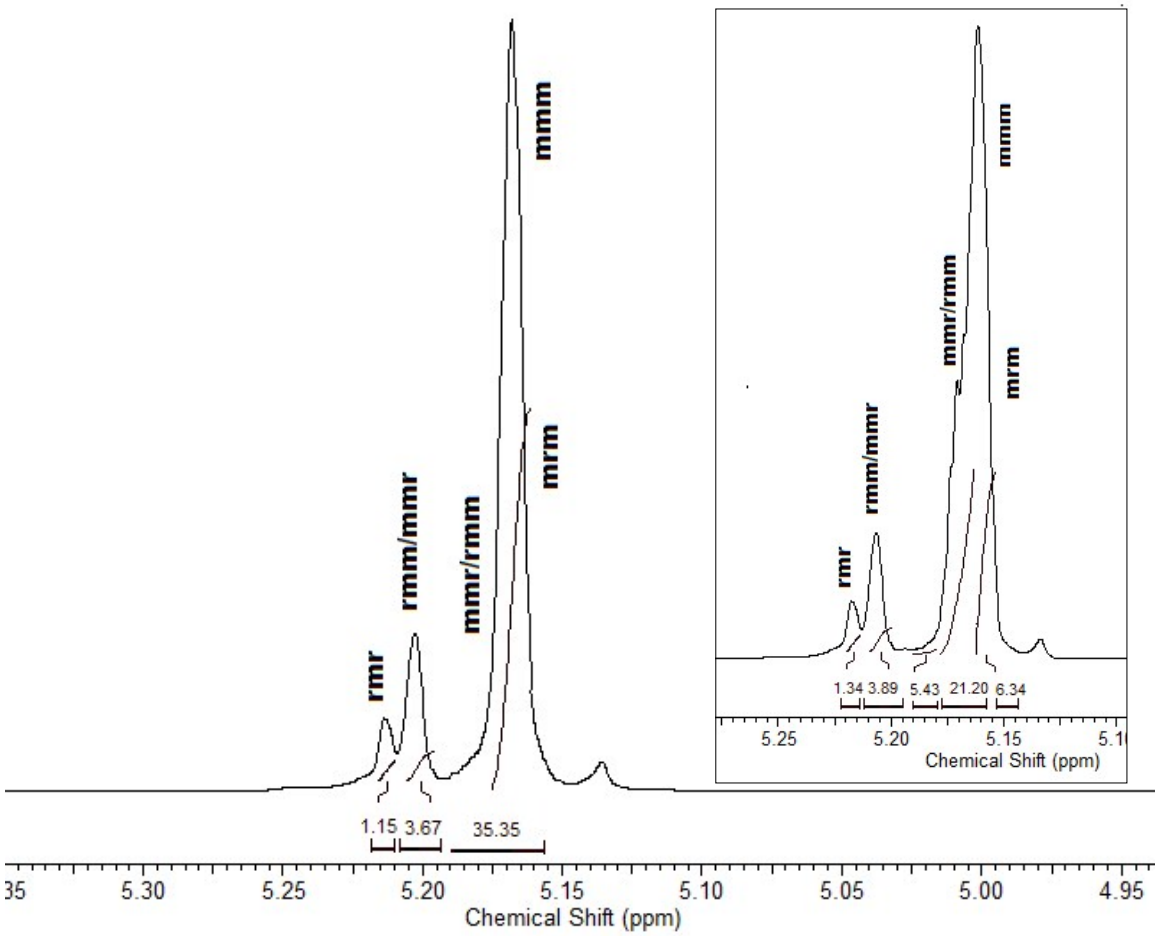

Figure FS60. $^{1}H\{^{1}H\}$ NMR spectra ($CDCl_3$, 25 °C) of methine regions for ROP of rac-LA

Analysis

[mmm] = Pm(Pm+1)/2
[mmr] = Pm(1 - Pm)/2
[rmm] = Pm (1 - Pm)/2
[rmr] = $(1 - Pm)^2/2$
[mrm] = (1 - Pm)/2

Peak	Integration	Pm
[mmm]	**0.56**	**0.67**
[mmr]	**0.140**	**0.71**
[rmm]	**0.105**	**0.69**
[rmr]	**0.0353**	**0.73**
[mrm]	**0.167**	**0.67**
Avarage		**0.70**

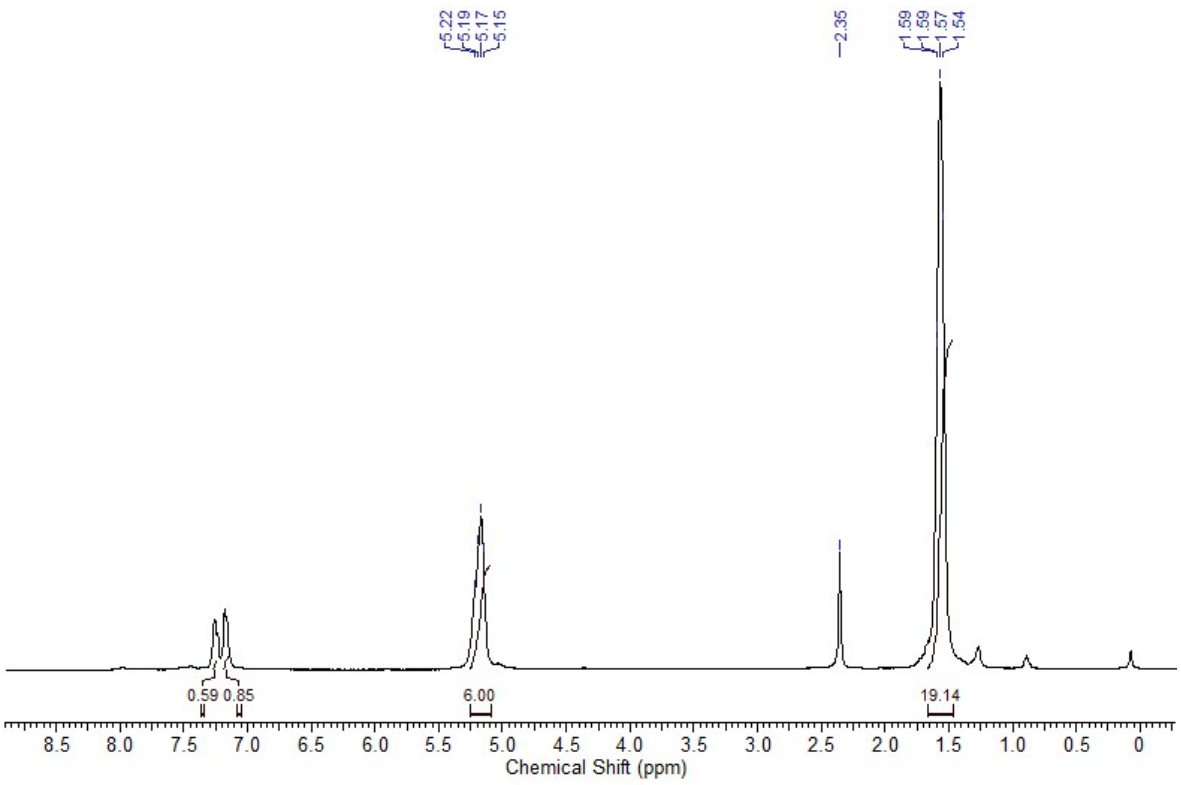

Figure FS61. ^{1}H NMR spectra ($CDCl_3$, 25 °C) of methine regions for ROP of rac-LA.

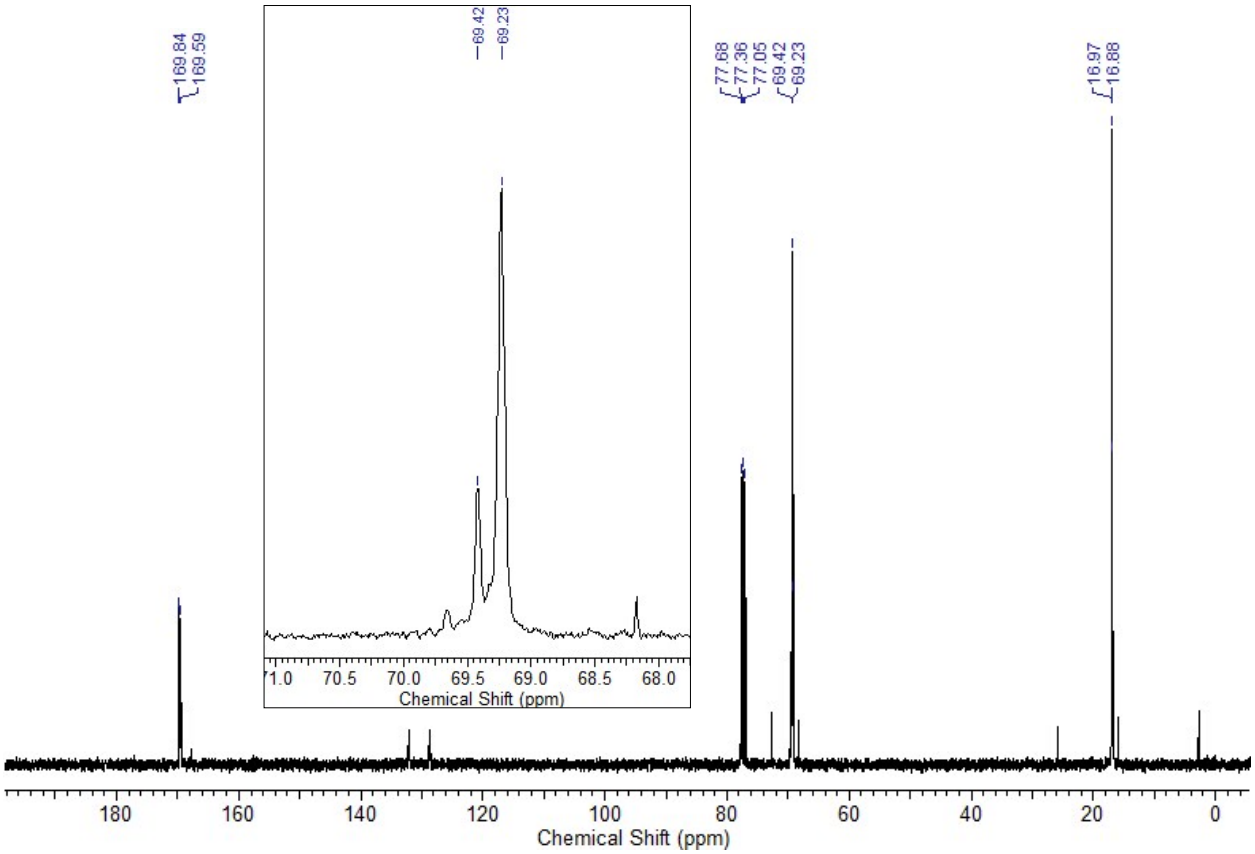

Figure FS62. Homocoupling ^{13}C NMR spectrum for ROP of rac-LA.

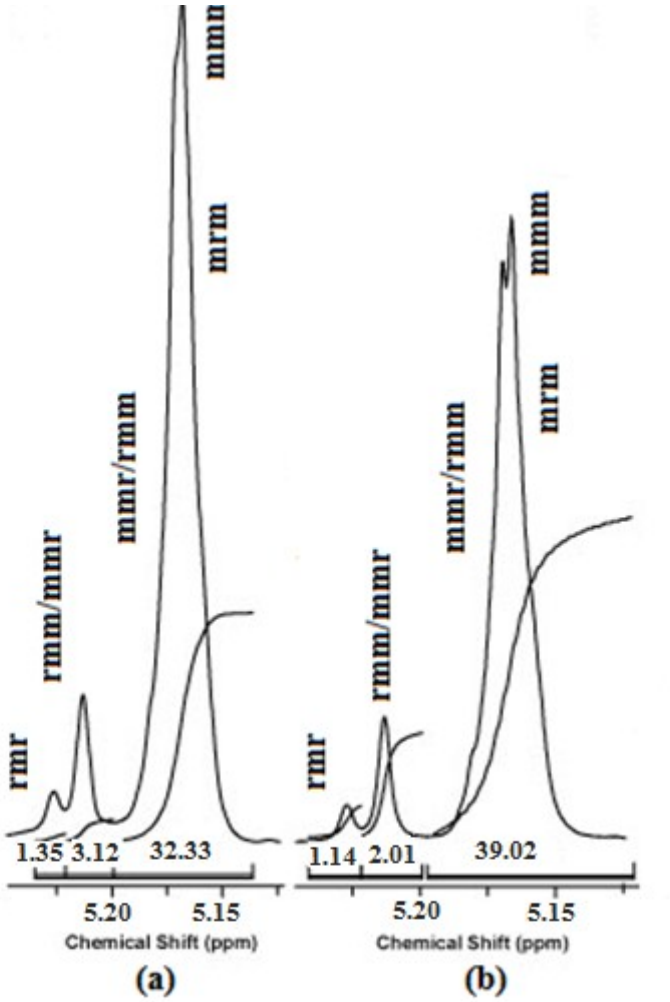

Figure FS63. $^{1}H\{^{1}H\}$ NMR spectra ($CDCl_3$, 25 °C) of methine regions for ROP of rac-LA catalyzed by (**5b**) at 91% conversion and 93% conversion at 25 °C in toluene.

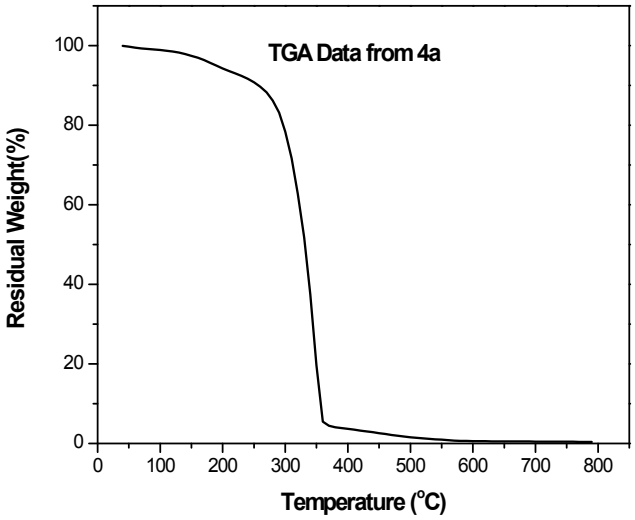

Figure FS64. Representative TGA trace and derivative plot of PLA catalysed by **4a**.

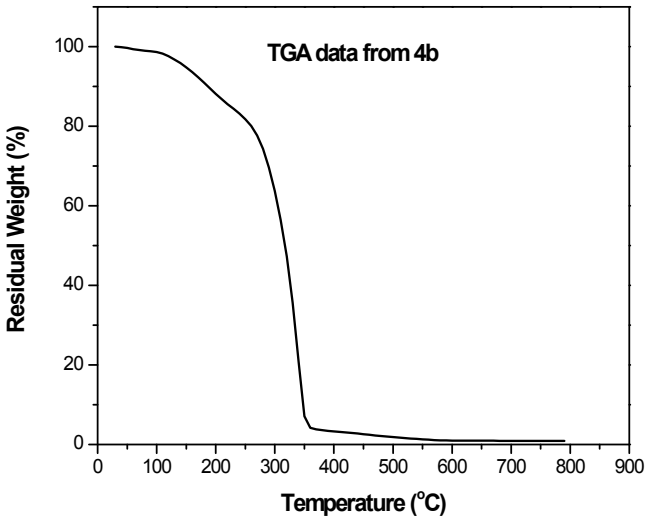

Figure FS65. Representative TGA trace and derivative plot of PLA catalysed by **4b**.

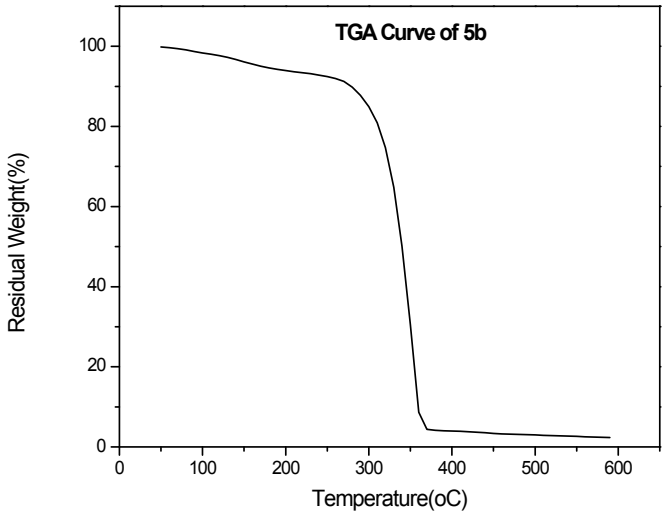

Figure FS66. Representative TGA trace and derivative plot of PLA catalysed by **5b**.

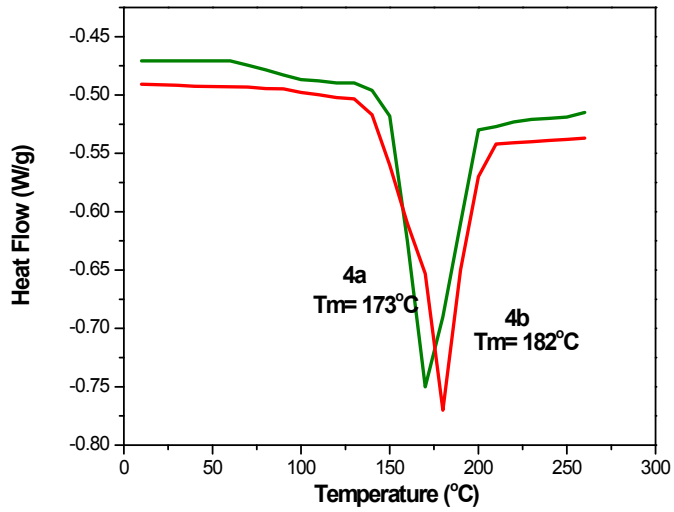

Figure FS67. DSC trace of PLA catalyzed by (**4a** and **4b**), Pi = 0.75, Mn = 26.2 KDa for **4a** and Pi = 0.78, Mn = 13.4 KDa for **4b**. Second heating curve shown, cooling curves omitted for clarity.

Two samples were measured, PlA having different molecular weight also catalyze by two different initiator taken for measurement. DSC samples were heated to 270°C and then cooled at various rates (quenched cooling 0.1, 0.5, 1, 5, 10 °C/min). The measurement was done using DSC6220 Differential Scanning Calorimeter. For the DSC measurement 10 mg of the sample was heated from 10°C up to 270°C at 10oC/min in a nitrogen atmosphere.

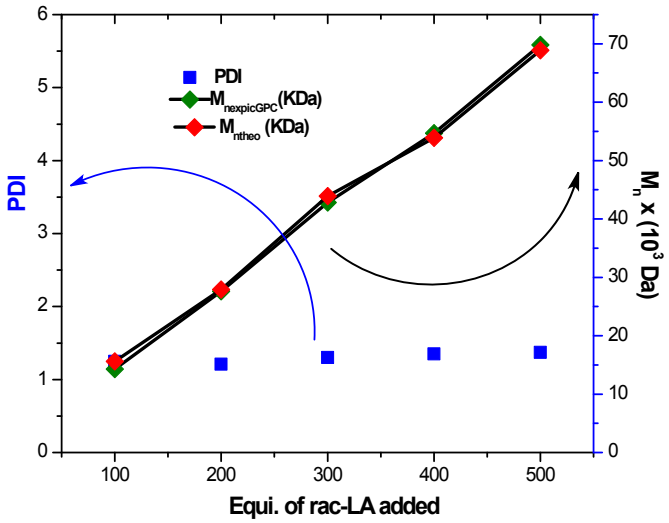

Figure FS68. Plot of observed Mn and molecular weight distribution of PLA as functions of added rac-LA with respect to catalyst **5a** (Mn = number averaged molecular weight, PDI = polydispersity index). The line indicates calculated Mn values based on the LA: initiator ratio. All reactions were carried out at room temperature in toluene, and conversion to polymer samples was >90%.

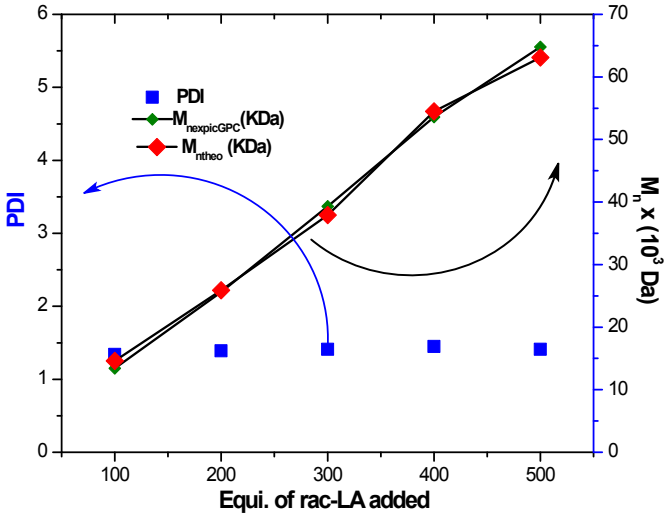

Figure FS69. Plot of observed Mn and molecular weight distribution of PLA as functions of added rac-LA with respect to catalyst **4b** (Mn = number averaged molecular weight, PDI = polydispersity index). The line indicates calculated Mn values based on the LA: initiator ratio. All reactions were carried out at room temperature in toluene, and conversion to polymer samples was >90%.

Caprolactone Polymerization

A typical polymerization procedure is exemplified by the synthesis of poly(ε-Caprolactone) at room temperature (TableTS15,). ε-Caprolactone (0.114 g, 1.0 mmol) was added to a solution of **4a,b**-**5a,b** (0.01 mmol) in toluene (5 mL). Immediately the monomer become converted into polymer, so the reaction was then quenched by the addition of a drop of 2(N) HCl and methanol. Then the solution was concentrated under vacuum, and the polymer was washed from hexane. The final polymer was dried under vacuum to constant weight.

Table TS15. ε-caprolactone Polymerization in the presence of alkali metal complexes bearing phosphinamine selenoid ligand.(**4a,b-5a,b**).

Entry	Catalyst	[ε-CL]0/ [M]0	Time (min:s)	conversion[b]	Mn (theo) [(KDa)]	Mn (GPC) [(KDa)]	Mw (GPC) [(KDa)]	PDI
1	4a	100	02:00	99	11.3	13.1	14.9	1.13
2	4a	200	01:00	98	22.3	21.5	27.5	1.28
3	4a	300	01:00	95	32.5	33.2	43.8	1.32
4	4a	400	01:00	96	43.7	45.9	61.0	1.33
5	4a	500	01:00	98	55.8	57.4	67.7	1.18
6	4b	100	01:00	99	11.3	11.4	15.2	1.33
7	4b	200	01:00	99	22.6	20.4	23.3	1.14
8	4b	300	01:00	96	32.8	35	41.3	1.31
9	4b	400	01:00	97	44.2	50.3	65.8	1.22
10	4b	500	01:00	98	55.8	56.4	59.2	1.05
11	5a	100	00.30	99	11.3	12.5	13.1	1.04
12	5a	200	00.30	98	22.3	25	32	1.28
13	5a	300	00.30	98	33.5	32	40	1.25
14	5a	400	00.30	97	45.6	43.5	51.3	1.18
15	5a	500	00.30	98	55.8	57	64.9	1.14
16	5b	100	00.30	98	11.1	12.7	13.0	1.03
17	5b	200	00.30	99	22.5	24	28.8	1.20
18	5b	300	00.30	97	33.1	32.5	39.6	1.22
19	5b	400	00.30	98	44.6	44.5	51.1	1.15
20	5b	500	00.30	98	55.8	58	63.8	1.10
21	5b	1000	00.30	95	108.3	110.9	138.9	1.25
22	3a	100	1400:00	49	5.58	13.1	21.3	3.81
23	3b	100	1400:00	47	5.24	13.1	20.1	3.84

In toluene at 25ºC, [Catalyst] = 1 mM. [b] Conversions were determined by ^{1}H NMR spectroscopy. $M_n$theo = molecular weight of chain-end + 114 gmol^{-1} ×(M:1) × conversion. [c] In THF (2 mg mL^{-1}) and molecular weights were determined by GPC-LLS (flow rate ¼ 0.5 mL min^{-1}). Universal calibration was carried out with polystyrene standards, laser light scattering detector data, and concentration detector. Each experiment is duplicated to ensure pracision.

.

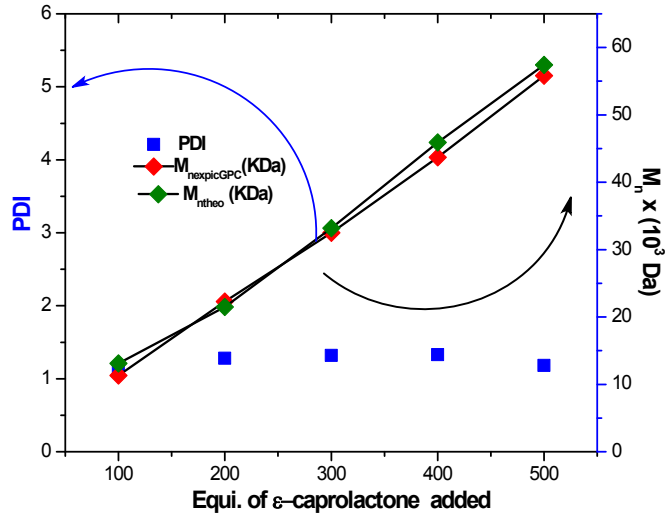

Figure FS70. Plot of observed PLA M_{ntheo} and M_{nexpi} (■) with molecular weight distribution (PDI) (◆) as functions of ε-CL : **4a** in (25°C, Tol, 99% conv.) The line indicates calculated Mn values based on the ε-CL : 4a ratio.

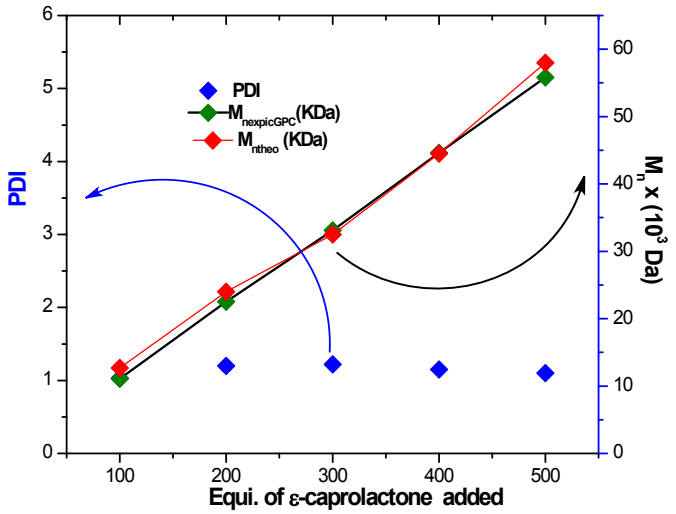

Figure FS71. Plot of observed PLA M_{ntheo} and M_{nexpi} (■) with molecular weight distribution (PDI) (◆) as functions of ε-CL : **5b** in (25°C, Tol, 99% conv.) The line indicates calculated Mn values based on the ε-CL : 5b ratio.

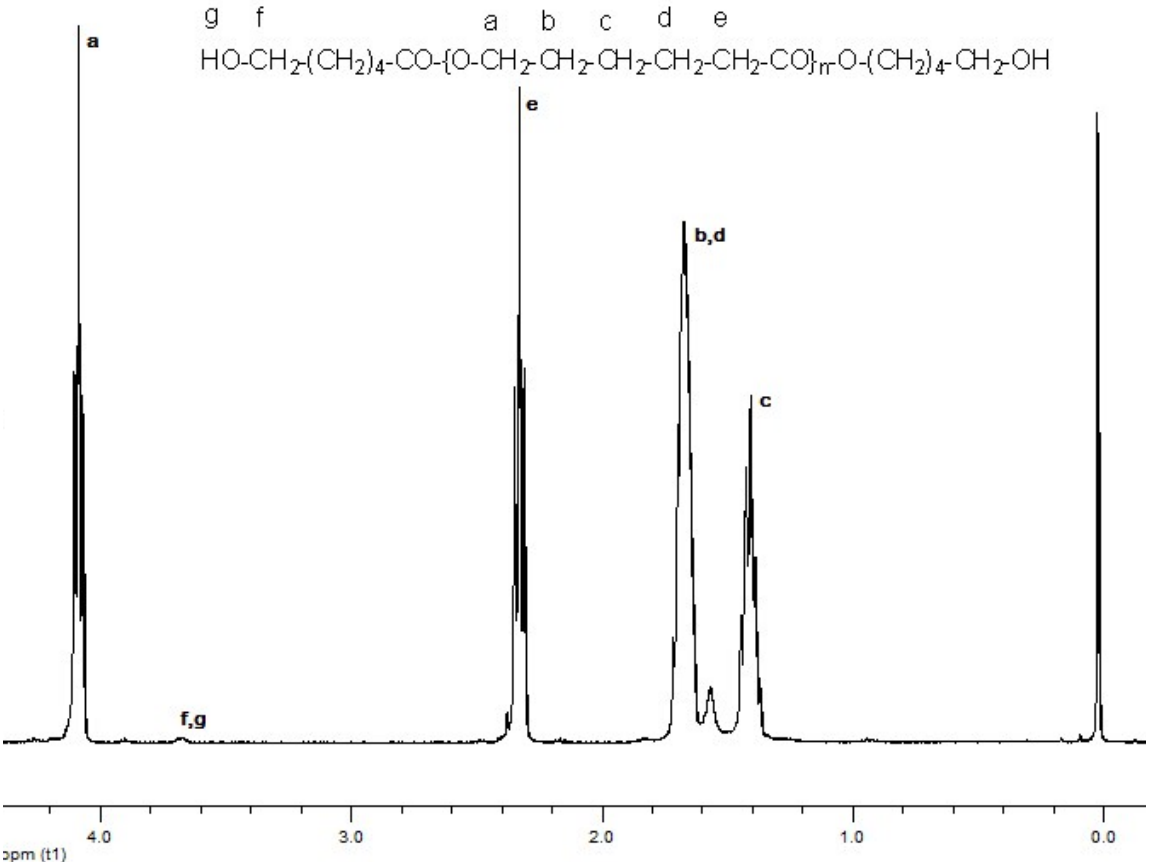

Figure FS72. ^{1}HNMR spectrum (400 MHz, 25°C, $CDCl_3$) of Poly(Ɛ-Caprolactone).

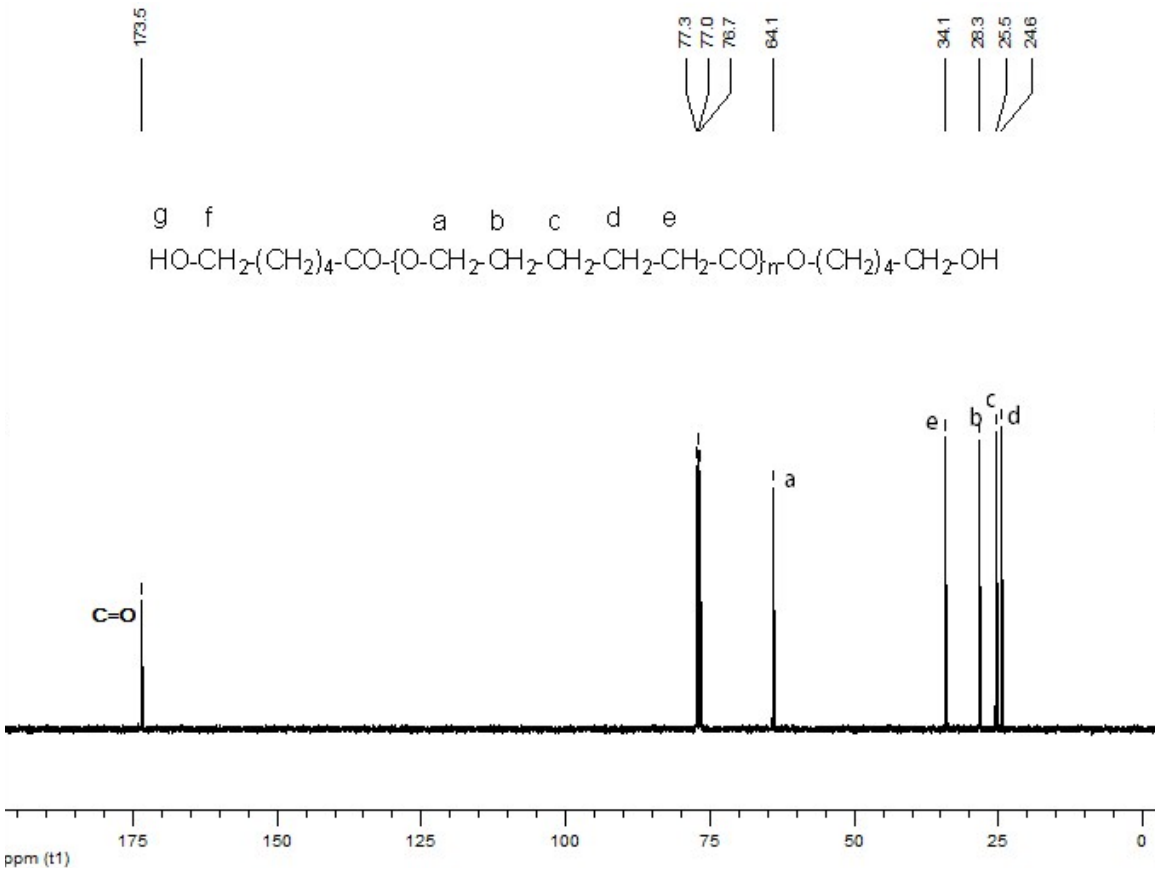

Figure FS73. ^{13}C NMR spectrum (100 MHz, 25°C, $CDCl_3$) of Poly(Ɛ-Caprolactone**).**

valerolactone Polymerization

A typical polymerization procedure is exemplified by the synthesis of δ-valerolacton at room temperature (TableTS16). δ-valerolacton (0.114 g, 1.0 mmol) was added to a solution of **4a,b-5a,b** (0.01 mmol) in toluene (5 mL). Immediately the monomer become converted into polymer, so the reaction was then quenched by the addition of a drop of 2(N) HCl and methanol. Then the solution was concentrated under vacuum, and the polymer was washed from hexane. The final polymer was dried under vacuum to constant weight.

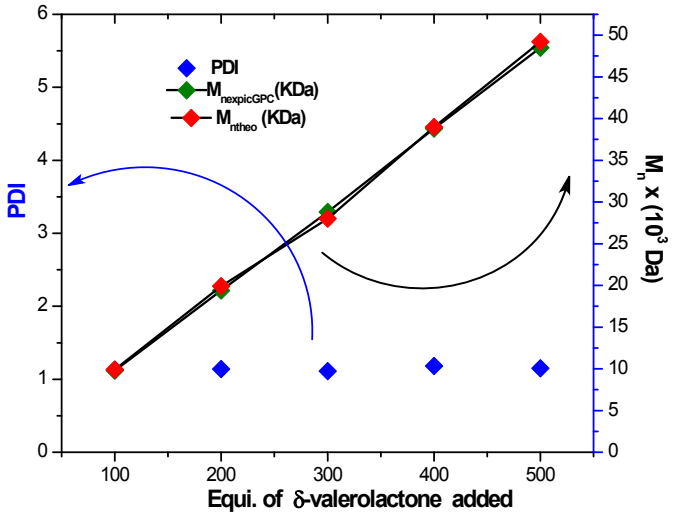

Figure FS74. Plot of observed PLA M_{ntheo} and M_{nexpi} (■) with molecular weight distribution (PDI) (◆) as functions of δ-VL: **4b** in (25°C, Tol, 99% conv.) The line indicates calculated Mn values based on the δ-VL: 4b ratio.

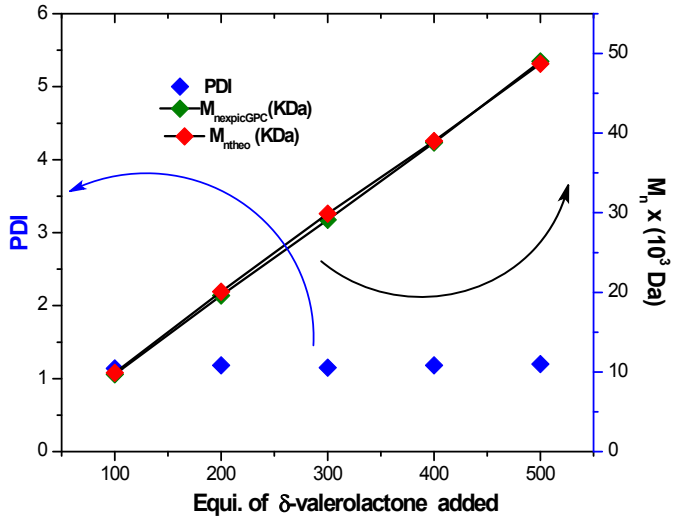

Figure FS75. Plot of observed PLA M_{ntheo} and M_{nexpi} (■) with molecular weight distribution (PDI)

(◆) as functions of δ-VL: **5a** in (25°C, Tol, 99% conv.) The line indicates calculated Mn values based on the δ-VL: 5a ratio.

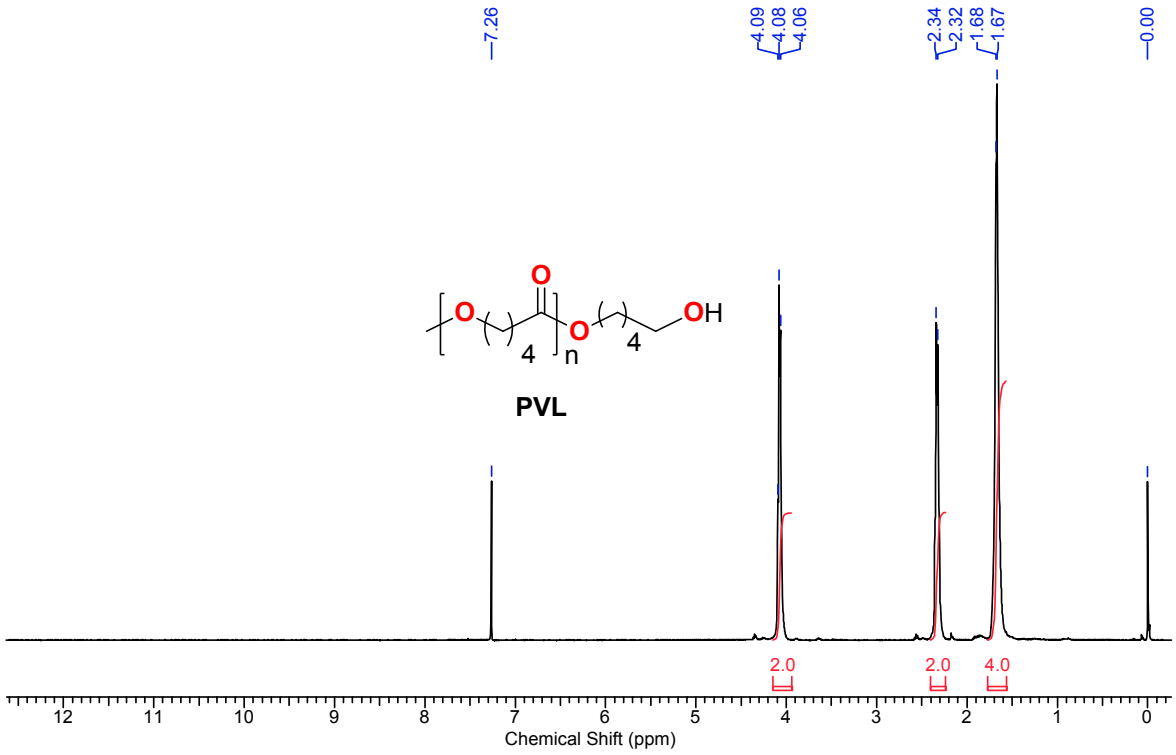

Figure FS76. ^{1}HNMR spectrum (400 MHz, 25°C, $CDCl_3$) of Poly(δ- valrolactone).

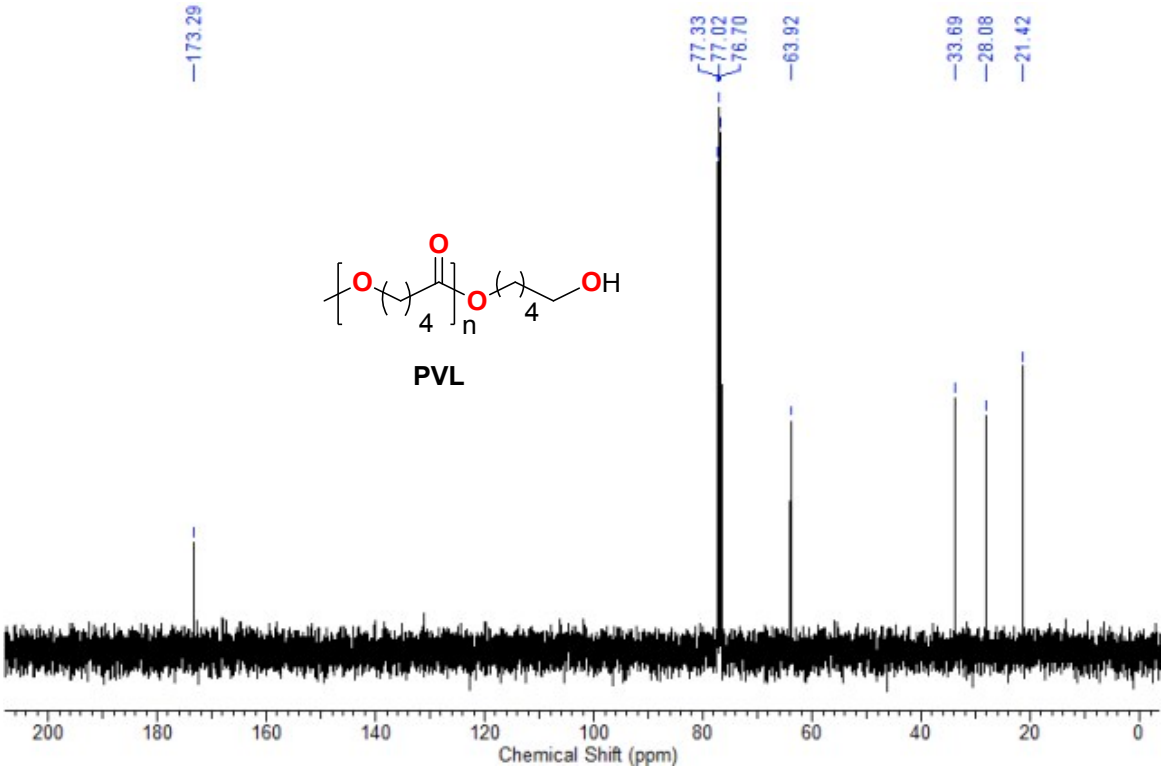

Figure FS77. ^{13}CNMR spectrum (100 MHz, 25°C, $CDCl_3$) of Poly(δ- valrolactone).

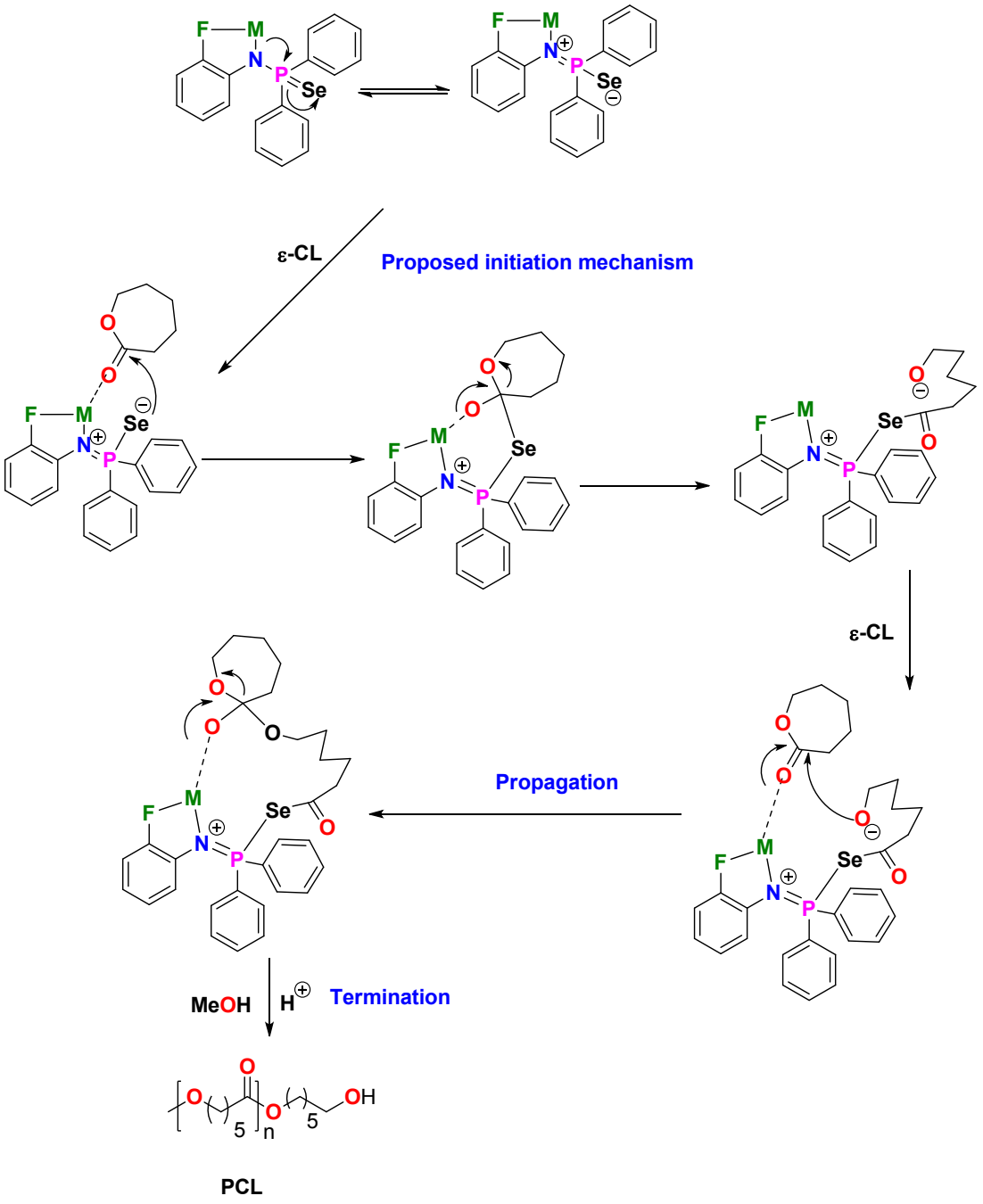

Figure FS78. Pluasible machanism for ring-opening polymerisation of ε-Caprolactone initiated by Alkali metal complex.

Reference.

1. Bhattacharjee. J.; Harinath, A.; Nayek, H. P.; Sarkar A.; Panda, T. K. *Chem Eur. J*, **2017**, *23*, 9319 – 9331.
2. Harinath, A.; Bhattacharjee. J.; Nayek, H. P.; Sarkar A.; Panda, T. K, *Inorg. Chem*. **2018,** *57*, 2503−2516.

3. Douglas, A. F.; Patrick, B. O.; Mehrkhodavandi, P. *Angew. Chem.* Int. Ed. **2008**, *120*, 2322-2325.
4. Yu, I.; Acosta-Ramírez, A.; *J. Am. Chem. Soc.* **2012**, *134*, 12758-12773;